Fabrication of Complex Oral Drug Delivery Forms by Three Dimensional Printing™

by

Wendy E. Katstra

B.S. Ceramics Science and Engineering
Rutgers University, 1997

Submitted to the Department of Materials Science and Engineering
In partial fulfillment of the requirements for the degree of

DOCTOR OF PHILOSOPHY
in Ceramics Engineering

at the
MASSACHUSETTS INSTITUTE OF TECHNOLOGY

June 2001

Signature of Author: _____
Department of Materials Science and Engineering
April 30, 2001

Certified by: _____
Michael J. Cima
Sumitomo Electric Industries Professor of Materials Science and Engineering
Thesis Supervisor

Accepted by: _____
Harry L. Tuller
Professor of Ceramics and Electronic Materials
Chair, Departmental Committee on Graduate Students

Fabrication of Complex Oral Drug Delivery Forms by Three Dimensional Printing™

by

Wendy E. Katstra

Submitted to the Department of Materials Science and Engineering
On April 30, 2001 in partial fulfillment of the
Requirements for the Degree of Doctor of Philosophy in
Ceramics Engineering

ABSTRACT

Three Dimensional Printing 3DP™ is a novel solid freeform fabrication technology that has been applied to the fabrication of complex pharmaceutical drug devices. Limitations of the technology as relating to pharmaceuticals have been addressed and prototype dosage forms have been fabricated.

The resolution of the 3DP tablets was found to depend on particle size and liquid migration during printing and drying. The surface finish of 3DP tablets was enhanced by uniaxial pressing. Migration inhibiting additives were effective in limiting transport. Both aqueous and ethanol-based solutions showed a decrease in migration on the order of 20% when appropriate powder bed additives were introduced. Migration was also decreased by pre-printing barriers to confine secondary printed drug solutions.

Low dosage forms were fabricated with as little as 2.3 nanograms. Lower dosages are expected upon dilution of the initial drug solution. Printing forms with high dosage is limited by powder void volume, filling efficiency, and drug solubility limits. Multiple print passes increased the dosage per tablet volume, δ, at the expense of process time. The use of drug suspensions to overcome solubility limits and uniaxial compression to reduce tablet volume was shown to significantly increase δ. The highest δ achieved was 427 mg/cc for pressed suspension-printed tablets, representing 74% of the theoretical limit.

Complex oral dosage forms were fabricated with 3DP to show lagged-release, extended-release, double-release, and zero-order-release. Release properties, such as lag time and release rate, were manipulated by varying the printing parameters.

Dual-release and zero-order-release forms were fabricated using a surface degradation/erosion system based on HPMC, lactose, and Eudragit® L100. Erosion rate constants were used to model release from tablets with non-uniform drug distributions. Diclofenac and chlorpheniramine dual-release tablets were designed with 3 drug regions, and dissolution of the tablets followed the model closely, exhibiting 2 onsets. Two types of zero-order tablets were invented and fabricated by 3DP. These contained drug concentration gradients designed to complement the volumetric non-uniformity of eroding shells. Three formulations showed constant release of diclofenac sodium over 1-7 hours (9.6mg/hr), 1-15 hours (6.8mg/hr), and 1-36 hours (2.5mg/hr).

Thesis Supervisor: Professor Michael J. Cima
Title: Sumitomo Electric Industries Professor of Materials Science Engineering

Acknowledgements

I would first like to thank my thesis advisor, Michael Cima, for his ideas and motivation throughout my years here at MIT. My thesis committee, Craig Carter, Charles Cooney, and Robert Langer, has been an excellent resource and very valuable to me. Many, many thanks to them.

My entire project was sponsored by Therics, Inc., Princeton NJ. I'd like to thank everyone there for their support and interest in my research. It has really been a pleasure to work with Therics and to see some of my research efforts being employed in the "real" world!

There are many individuals I need to thank. Much of the work done in the CPRL is a group effort, and I could not have finished without the help of my lab-mates!

First and foremost, I would like to express my most sincere gratitude to my friend and co-worker, Dr. William C. Rowe, a.k.a. "Bill". Bill and I have worked as a team on most of research topics, and I could not have finished without his contributions and motivation. Thanks again and again, Bill.

Thanks to Barbara, John, and Lenny, our gallant staff, for running the lab so smoothly, and for making our little basement cheerful!

All of the students, post-docs, and visiting scientists, past and present, have helped to unify our lab and make it a fun place to frolic. Special thanks to my "senior" mentors, Lynn, Scott, Jason, and Ben who introduced me to the ways of the lab, and who provided much-needed early emotional support and particular thanks to my first-year cronies, Richard and Mindy, who have sympathized and supported me throughout the entire PhD procedure. Thanks to everyone at the CPRL – there are too many to thank individually, but I wanted to say that you have all meant very much to me.

I want to thank my high school chemistry teacher, Mr. Hodge, for inspiring me to go into science and research, and my mentor Suhas Bhandarkar from Lucent for convincing me to go for the PhD.

Thank you Jesus for all that you have done in my life, the opportunities that you have laid down in front of me, and the wonderful experiences that you made possible. Thanks for keeping me at peace, even when things got tough. I *can* do all things *though you* which strengthen me.

Finally, I would not be here today without the loving support of my family. Thanks Mom! Thanks Dad! Thanks Jeff! Thanks Grandma! Thanks for supporting my decision to come to grad school, and always making sure I had everything I could ever need to succeed. Thanks as well to my *new* family from across the seas – The Pryce Lewis's – who have accepted me with open arms and have sent their prayers and loving support consistently.

And to Hilton, my husband and best friend and fellow *recent* doctor....
I'm just so thankful to have had someone to share my experiences with, to laugh with, to cry with, and to write a thesis with!! The lord strategically put us together- who else could have arranged "us": a New Jersey girl and a South African guy with a mutual respect for *The Boss*? Thanks for all you have given to me, and all you have *put-up* with! –urwb

Table of Contents

List of Figures

3.23 Mercury porosimetry low pressure incremental infiltration, Volume vs. pore diameter for 3 volume fractions of L100 polymer

3.24 Design of sandwich structures

3.25 Micrographs of the 4 sandwich structures (without layer drying)

3.26 Scanning images for green pixel distribution

3.27 Green pixel intensity vs. intended placement for 2wt%E100/ethanol binder printed into 80wt% lactose / 20wt% E100 fines powder

3.28 Red and green droplets show that saturation occurs preferentially in un-saturated powder of higher capillary suction

3.29 a) Procedure for printing pre-saturated walls
b) radial green pixel density c) cross-section

4.1 Microdose salicylic acid tablets{R4.1}

4.2 Fluorescence tablets – number of droplets deposited in each tablet

4.3 Detected fluorescein loading in the 9 samples of varying droplet number vs. the calculated loading based on printing parameters.

4.4 Iso-dosage lines in drug concentration vs. saturation
Assumptions: cylindrical shape device of radius 5mm and height mm, solution density = 1g/cc, packing fraction = 0.5

4.5 Iso-δ lines and their dependency on drug concentration and apparent saturation. Assumptions: p_f=0.5, ρ_{sol} =1g/cc.

4.6 δ (mg/cc) measured vs. predicted for un-pressed samples

4.7 δ Values achieved in this study

5.1 Breakaway Tablet design

5.2 Enteric Dual Pulsatory Tablet design

5.3 Two Phase Dual Pulsatory Tablet design

5.4 E100 placebo tablet during dissolution testing{R2.12}

5.5 Change in diameter of E100 placebo tablets

5.6 Dissolution profiles for varying Vol% E100{R2.12}

5.7 Swollen 3DP matrix of RLPO and cellulose

5.8 Dissolution of RLPO Extended Release Tablets with varying Vol% of RLPO

5.9 Higuchi plot of release vs. $t^{1/2}$

5.10 Break-away Tablets

5.11 Dissolution profile for the Enteric Dual Release Tablet

5.12 Dissolution profile for the Two-Phase Dual Release Tablets

6.1 Glass slide assembly

6.2 Tablet at 30 minutes with gel barrier

6.3 Solid/hydration front movement as measured by the solid radius

6.4 Dissolution profiles of diclofenac tablets with varying ratios of Lactose:HPMC

6.5 Dissolution profile for 70:30 Lactose:HPMC with diclofenac sodium fit to equation 6.7 using erosion rate constants of k_r = 13.902 and k_h = 5.227 mg/hr·cm^2

6.6 Schematic of Dual Release Design: a) Diclofenac sodium tablet b) Chlorpheniramine maleate tablet

6.7 Theoretical release plots for Chlorpheniramine Maleate Dual Release Tablets

6.8 Incremental release over time of the diclofenac sodium dual release tablets

6.9 Cumulative release profile of the Diclofenac Sodium Dual Release Tablets

6.10 Incremental release over time of the Chlorpheniramine Maleate Dual Release Tablets

6.11 Cumulative dissolution profile for the Chlorpheniramine maleate Dual Release Tablets

6.12 Drug concentration as a function of distance and 5 concentration zones

List of Tables

Introduction and Motivation

Three Dimensional Printing (3DP™) is a novel solid freeform fabrication (SFF) technology that has been studied for application in the fabrication of pharmaceutical drug delivery forms. 3DP is unique in comparison to other SFF techniques[1,2] as it offers selective spatial deposition of nanoliter quantities of multiple materials, and consequently can control local composition and microstructure. 3DP's design flexibility has been applied to the unprecedented spatial control of multiple drugs, actives, excipients, adjuvants, and other matrix modifiers. This unparalleled versatility has been especially important in the fabrication of complex controlled release forms and precision dosage forms.

1.1 Controlled Release

Controlled release is defined as the release of chemicals, specifically drug compounds, in a controlled manner. This includes controlling the release time, release rate, release location, or all of these. The method of release can have a significant effect on the drug's therapeutic efficiency.[3] There is an optimal therapeutic range of concentration in the body for some drugs.

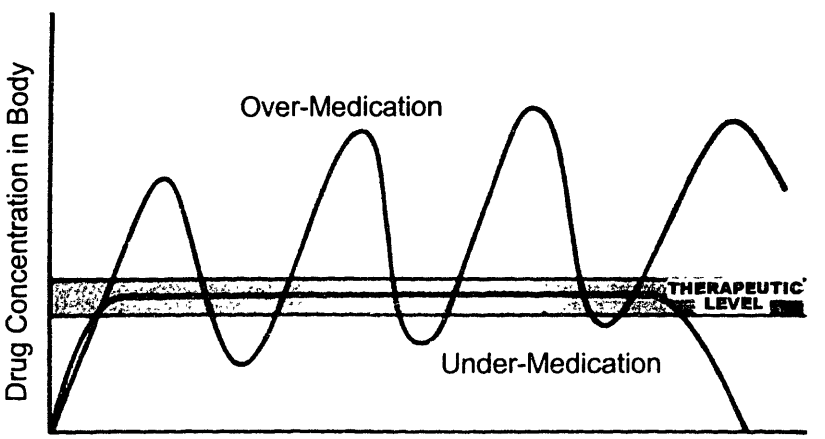

Figure 1.1 Peak-and-trough drug concentration pattern typically resulting from drug administration in conventional dosage forms.[4]

Delivery forms such as conventional tablets or injections may release drug rapidly at first, thereby peaking above a desired therapeutic range, and toxic effects and/or side effects may occur. Drug release that occurs below a critical range of concentration will provide little or no effect. Much research activity is currently centered around finding a way to release drug at a constant rate providing zero-order release and a way to maximize time within the optimal therapeutic range.[5,6]

The optimal therapeutic range can also change over time, even during a 24-hour cycle. "Evidence suggests the treatment of disease could be improved by giving drugs at carefully selected times of the day", William Hrushesky (1994). The field of chronopharmacology is concerned with how biological rhythmic phenomena influence the kinetics and effects of medication.[7] The ultimate goal of chronopharmacology is chronotherapeutics, or the timing of drug deliveries to biological rhythms to optimize their desired effects and/or to minimize undesired side-effects.[7] It has been shown, for example, that the daily chronobiological blood pressure pattern effects the efficacy of anti-hypertensive drugs.[8] The average systolic and diastolic blood pressure remains relatively constant during the day, but then declines during the night when sleeping, and rises again in the morning.[6] Other time-dependent variables have been determined during the 24-hour period including airway flow in obstructive lung disease, gastric pH in ulcer disease, pain, stiffness and inflammation in arthritic disease, etc.[7] Medications to treat these variables are best delivered not at constant rates, but with time-varying release rates and lag times to best match the circadian drug requirement and to help to prevent drug tolerance and side effects.[6] This requires quick-slow release, pulses of release, extended release, and combinations of these.

Diseases are also often treated with multiple medications delivered several times during a 24-hour period. Circadian timing-stipulated, multi-drug regiments are used for treatment of immunodeficiency syndromes (including

AIDS)[9], and those required for hypertension[8]. The strict dosing regimens have spurred discussions about adherence, and have motivated drug company R&D teams to try to design drugs and delivery forms that may be taken less frequently or less strictly.[10]

1.2 Conventional Dosage Form Processing and Fabrication

The technology surrounding the processing and fabrication of oral drug delivery forms (ODFs) or tablets, is well-known and has been described in many pharmaceutical reference books.[11,12,13] The process steps generally involve the granulation of components, weighing, mixing, transporting, tableting, and then sampling and statistically determining drug content. Several stages of these processes, however, are problematic, especially during the fabrication of low dosage forms of high potency actives[11]. The micronization of actives is difficult given electrostatic interactions,[14,15] and the dust generated in the process can pose serious health and safety hazards. Weighing the appropriate amount of components can also be a problem given the powder electrostatics, but can be lessened by the use of larger batches. One of the main problems encountered in traditional processing is achieving a homogeneous and uniform drug distribution within a mixture of other dilutents. The mixing technique can be ineffective or segregation can occur during the mixing stage or later during transportation and prior to tablet compression. The measurement of the degree of mixing is ultimately dependent upon the determination of the composition of a number of samples in the mixture using a sampling thief probe[16], although other non-invasive sampling techniques have recently been developed by researchers at MIT.[17]. The ultimate determination of dosage per tablet is done by sampling, dissolution, and statistical means.[11]

1.3 The Three Dimensional Printing™ Fabrication Technique

3DP™ has the unique ability to spatially control placement of polymeric binder fluid and drug active into excipient material to construct tablets layer by layer. The technology is similar to ink jet printing such that a motion-controlled printhead deposits fluid selectively into a two-dimensional pattern. The printing surface is a thin layer of powder, and the fluids range from liquid binders to active solutions. The general process is depicted in Figure 1.2.

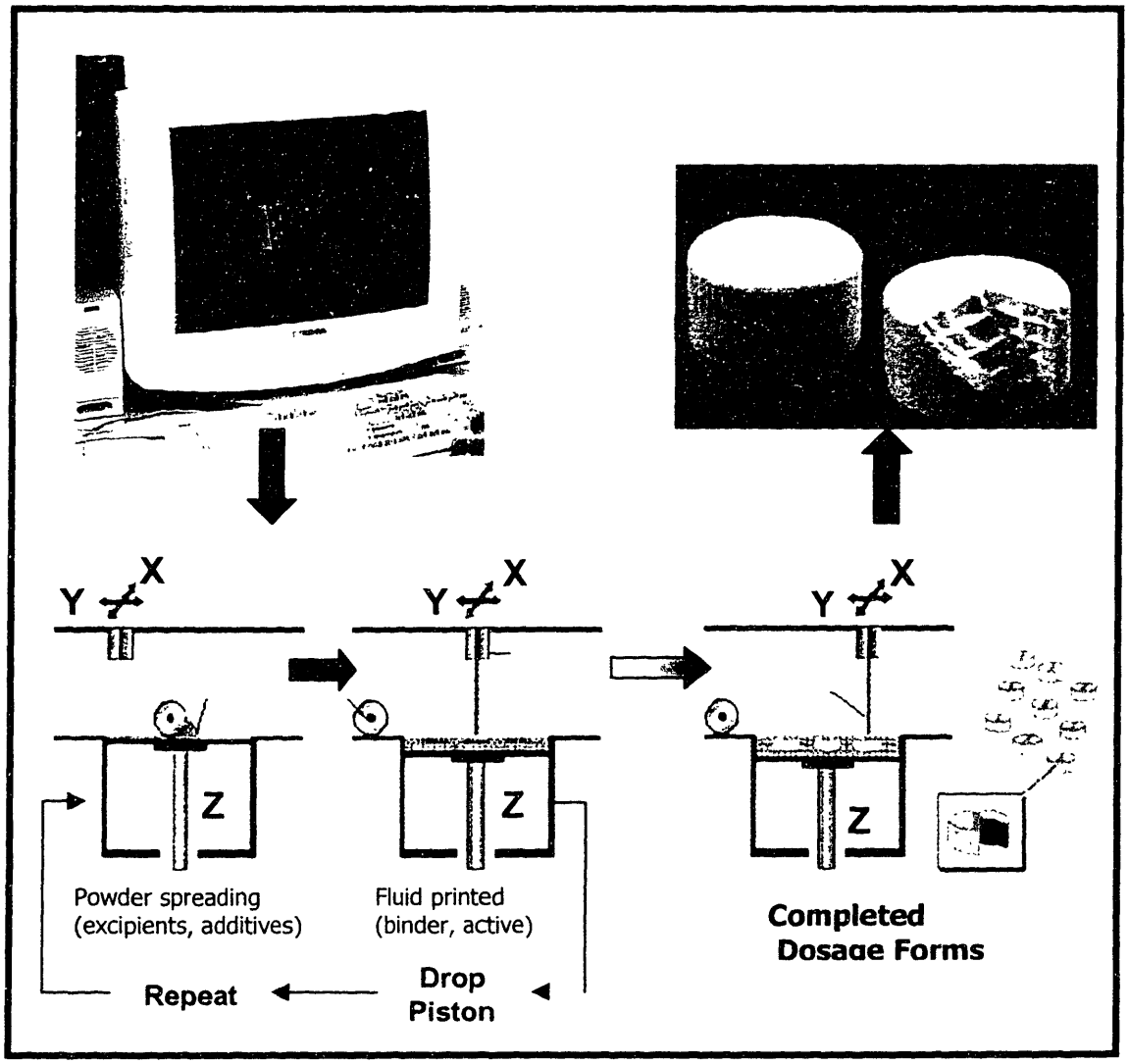

Figure 1.2 The Three Dimensional Printing™ (3DP™) Process

Three-dimensional devices are first designed and split into a series of two-dimensional slices depending on the layer height to be used. Complex structures, such as the multi-compartment tablet shown in Figure 1.2, are designed using computer aided design and drafting. (CADD). Powder is first spread into a thin layer on a smooth build plate atop a vertical (Z) piston. The two-dimensional shapes are then printed into the powder bed by rastering a printhead along a fast axis (Y) and stepping along a slow axis (X). The build plate is then lowered and more powder is spread. Subsequent layers are printed until the forms reach completion. They are then allowed to dry, and are removed easily from the un-printed loose supporting powder of the bed. No additional processing is needed, although the forms may be spray-coated, tumble-polished, or compressed to achieve enhanced surface detail.

1.4 3DP™ as a Pharmaceutical Fabrication Technique

3DP was originally used as a fabrication tool for processing metal and ceramic prototypes. It is able to control local composition and porosity in many materials systems, and is currently used to fabricate molds[18], tooling[18], electronic components[2], plastic prototypes[18], bio-medical implants.[1], and other functionally graded components.[19]

3DP has been used in this research to fabricate oral drug delivery forms from conventional pharmaceutical-grade powders and actives. Multiple materials and actives can be readily incorporated into the computer designed dosage forms. Functionality is achieved by printing several functional polymers, controlling the position and combination of such polymers, and by controlling the porosity, or diffusivity, of the matrices. Dosing the delivery forms is achieved by printing precise amounts of drug solution or suspension into each. Each tablet's dosage can be calculated with accuracy from the number of droplets printed. Pilot scale printers have been recently constructed[20], incorporating optical droplet

monitoring for validation, multiple jets for high throughput, and semi-continuous production feasibility.

These aspects of the 3DP process offer new possibilities for the direct fabrication of drug delivery systems. The ability to spatially control the deposition of multiple drugs and the strategic positioning of matrix modifiers will be important in designing the next generation of controlled release drug delivery systems. 3DP has the ability to fabricate oral dosage forms for sustained release, targeted release, pulsed release, cyclical release, or any combination of these. More precise spatial and temporal placement of drug into the body will reduce the size and number of doses, and this will thereby increase the therapeutic efficiency and safety of drugs, and help assist patient compliance.

1.5 Thesis Objectives and Organization

The specific objectives of this thesis are:

1) To apply a wide new sub-set of pharmaceutical materials to the 3DP process, and develop a printhead and printing strategies for pharmaceutical solutions and suspensions, many of which are based on organic solvents. Printing spaces have been identified in Chapter 2 for four general fluid systems for printing with a continuous jet charge and deflection printhead.
2) To increase the overall resolution of tablets fabricated by dry powder spreading – based 3DP. Several strategies for decreasing the surface roughness and decreasing migration within printed tablets are given in Chapter 3. The minimum layer height for pharmaceutical powders is found, and uniaxial pressing is used to enhance surface characteristics of 3DP tablets. Migration-inhibiting powder additives were also used to arrest migration occurring during and after the printing process.
3) To explore the lower and upper limits of dosages attainable with 3DP, thus helping to define its applicability. The accuracy and precision of printing very low dosages and strategies to increase the loading per unit tablet volume in high dosage forms is discussed in Chapter 4.
4) To use printing parameters to modulate release parameters such as lag time and release rate. Chapter 5 gives some examples of tablets fabricated by 3DP with varying release properties.
5) To design, model, predict, fabricate, and characterize complex dosage forms including double release forms and zero-order release forms. Chapter 6 acts to summarize the entire 3DP process from conception to characterization for these two complex controlled release formulations.

Printing of Pharmaceutical Materials

Three Dimensional Printing™ is a solid free form fabrication technique in which liquid binder droplets interact with a powder bed to selectively bind particles into three-dimensional structures. This chapter will define the parameters of the technology as it relates to the printing of pharmaceutical materials. The process steps, specific techniques, pharmaceutical materials, powder characterization and fluids characterization will be discussed.

2.1 Three Dimensional Printing Techniques

Several researchers have documented the general Three Dimensional Printing Process.[21, 22, 1] It is only briefly described here for reference purposes.

Figure 1.2 shows the general Three Dimensional Printing process. The first step in the process is the fabrication of the surface onto which fluids will be printed. This surface, also called the powder bed, can be fabricated using one of several techniques as discussed below in 2.1.1. Fabrication of pharmaceutical tablets begins with the spreading of powder into a thin horizontal layer on a smooth build plate. This build plate is part of a vertical piston with resolution of 5μm in the z-axis. One powder layer is spread and fluid is printed into that layer from a printhead which rasters along a fast y-axis with speeds up to 150cm/sec, and steps along a perpendicular slow x axis with a resolution of 1μm. The fluid is deposited from the printhead (see section 2.2) at a fixed flow rate and velocity into the powder bed below. Droplets merge together along the fast axis direction forming lines, or primitives, and the lines are separated by the parameter Δx, or the *line spacing*.[22] The piston plate is then lowered by one layer thickness, more powder is evenly spread across the surface, and the process is repeated until the three dimensional shape is completely formed.

2.1.1 Powder Bed Fabrication

The 3DP™ technology can first be divided into two main techniques based on the character of the printed surface or powder bed. The first is the solid powder bed fabrication technique, involving printing fluids onto pre-solidified surfaces that have been fabricated by one of many secondary techniques including tape casting[23], slurry printing[22], slip casting[2]. The advantages of pre-solidifying powder beds by these techniques include little or no powder bed displacement upon droplet interaction, and fine resolution due to the fine particles used in slurries. Part resolution has been shown to be limited mostly by droplet dynamics and size.[2] Parts are then later be retrieved by sonication techniques and other osmotically driven chemical processes to redisperse the solid powder bed.[2] This solid powder bed fabrication technique is currently employed in the printing of ceramics and metal parts and other materials systems where insoluble materials can be made into aqueous based slurries.

Most pharmaceutical materials are, however, either completely or partially soluble in water and/or most solvents. The pharmaceutical material classes used include sugars, starches, hydrophilic polymers, and several water soluble or water-reactive drug compounds. This limits the use of slurry based powder bed deposition techniques with these materials. The second powder bed fabrication technique, useful in fabricating pharmaceutical forms, involves dry powder spreading. Dry powder spreading requires powders be flowable, and easily spreadable into thin layers of uniform density near the tap density of the powder. The advantage of dry powder spreading is the easy removal of parts upon completion by removing the loose unbound powder.

Figure 2.1 shows the dry powder spreading technique. Powder is spread by a cylindrical smooth rod that rotates in a direction opposite that of the spreading direction to avoid powder compaction. The thickness of the powder

layer deposited in this technique is defined as the layer thickness. It can vary from 50um to 300 um based on the powder used.

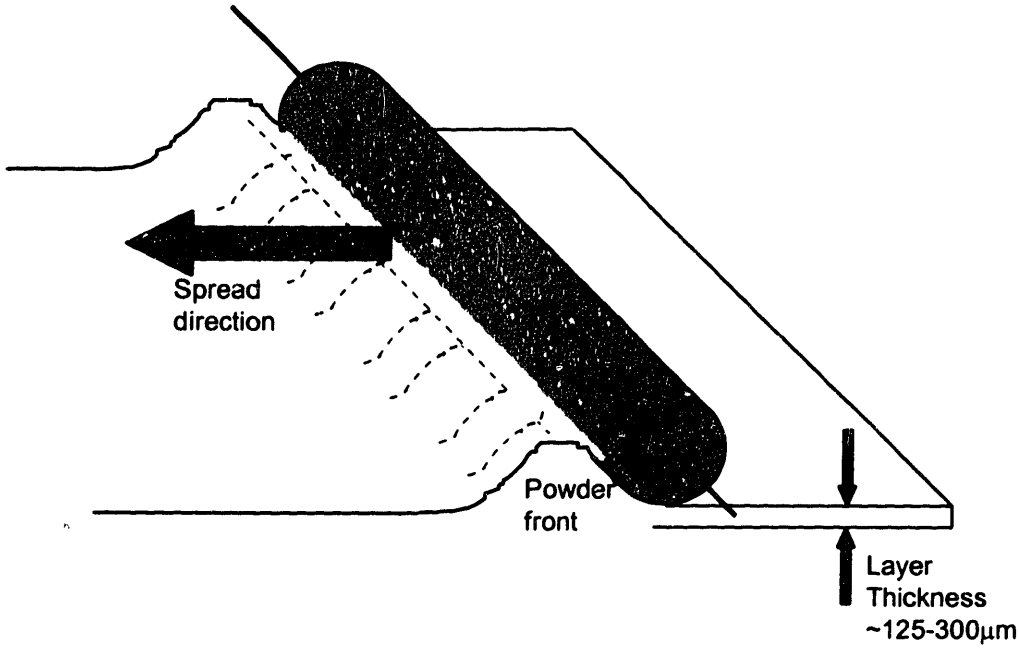

Figure 2.1 Dry powder spreading technique

2.2 Jetting Techniques

The Three Dimensional Printing technology can further be divided into printing techniques based on how fluid droplets are dispensed and directed to the powder bed surface. The two main printing techniques are 1) drop-on-demand and 2) continuous jet-based techniques.

2.2.1 Solenoid Valve Jet Drop-on-Demand (DOD) Printing

This first printing technique is called Drop-on-Demand printing, or DOD. The DOD printhead ejects discrete droplets when activated. A mechanically driven solenoid valve produces droplets by placing a fluid within the valve under pressure, and then opening and closing the valve for short durations to eject

discrete volumes.[24] This printing technique does; however, have problems printing organic solvents and small droplets. Organic solvents have been shown to swell the valve's interior polymeric components such as the valve seat, thus causing the volume inside the valve to change over time.[24] Furthermore, the mechanical modulation is low frequency, on the order of 800Hz, and large droplets are formed in the range of 270 to 310μm.[24] Large droplets such as these have been observed to cause detrimental ballistic impact due to their increased kinetic energy upon interacting with a loose dry powder bed.

2.2.2 Piezoelectric Drop-on-Demand (DOD) Printing

The piezoelectric DOD printing also forms discrete droplets when activated electrically. Fluid inside the nozzle head is under a slight negative pressure to prevent bleeding. Fluid enters a piezoelectric tube where it is squeezed into droplets at the orifice surface. Droplet velocity for this technique is fairly low, on the order of 3 m/sec. One advantage of this technique is the ability to form small droplets on the order of ~70μm.[25]

2.2.3 Continuous Jet (CJ) based printing

Continuous jet printing involves printing with an uninterrupted stream of fluid emerging from a round nozzle orifice. Printing fluid is pressurized and forced through in-line filters and out of the orifice at constant velocity throughout the print run. The pressure and the orifice size determine this velocity, and consequently the flow rate, which in return remains constant. The flow rate and velocity can be related through the radius of the orifice by the expression:

$$q = \pi \rho v r_o^2 \qquad 2.1$$

where q is the flow rate in mass/time, ρ is the fluid density, v is the stream velocity, and r_o is the radius of the orifice.

2.2.3.1 Continuous Jet Breakup

The nozzle orifices used in CJ printing have been selected based on laminar flow characteristics. The continuous jet of fluid breaks up into individual droplets after a fixed distance upon exiting the orifice. This is because the surface energy of a collection of individual spheres has less surface energy than a long cylinder of equal radius and volume.[26] Rayleigh's analysis of a fluid jet shows that oscillations develop and increase in amplitude upon exiting an orifice.[27] The oscillation frequency is related to a growth factor θ, and the wavelength, λ_{max}, with the largest growth factor dominates. For the inviscid case,

$$\theta = 0.97\sqrt{\frac{\sigma}{\rho d_o^{\,3}}} \qquad 2.2^{27,\,1}$$

where σ is the surface tension of the printed solution and d_o is the orifice diameter, and

$$\lambda_{max} = 4.51 d_o \qquad 2.3^{27,\,1}$$

It can further be shown by mass balance that the diameter of a single droplet upon breakoff be related to the flow rate, q, and the droplet frequency:

$$d = \left(\frac{6q}{\pi \rho f}\right)^{1/3} \qquad 2.4^{1}$$

where f is the natural droplet frequency given by:

$$f = \frac{v}{\lambda_{max}} \qquad 2.5^{1}$$

and v is the jet velocity given by:

$$v = \frac{4q}{\pi d_o^{\,2}} \qquad 2.6^{1}$$

Combining the above expressions 2.1 – 2.6 shows that the droplet radius for natural Rayleigh breakoff depends only on the orifice diameter:

$$d = 1.89 d_o \qquad 2.7$$

A jet of water exiting an orifice of 50μm in diameter with a flow rate of 1gram/minute travels at a downward speed of 8.48m/sec and breaks up into droplets of 94.5μm in diameter. This droplet size is considerable smaller than the size achievable with solenoid valve DOD printing. Natural Rayleigh frequency of breakoff is 37.6 KHz and the wavelength is 225.5μm. The jet breaks into individual droplets at a fixed distance below the orifice depending on the orifice size, velocity, and fluid properties. This distance, the breakoff length, L, is given by:

$$L = d \ln\left(\frac{d_o}{2\xi_o}\right) We^{0.5}(1 + 3Z) \qquad 2.7^{1}$$

where

- ξ_o is the estimated jet disturbance (~1.1 x $10^{-6} \cdot d$ Wu^{1})
- $We = \frac{\rho v^2 d}{\sigma}$ is the Weber number of the jet with surface tension σ and density ρ
- $Z = \frac{\sqrt{We}}{\mathrm{Re}}$ is the Ohnesborge number of the jet
- $\mathrm{Re} = \frac{dv\rho}{\eta}$ is the Reynolds number with viscosity η

The breakoff length for a given nozzle design depends greatly on fluid properties. Organic solvents, such as ethanol, methanol, and acetone, have much longer

breakoff lengths than water because the surface tensions of these solvents (σ_{eth}~ 22mN/m) are much lower than water (σ_{water}~ 72mN/m). The breakoff lengths for several common 3DP solvents are given in Table 2.1.

Table 2.1 Fluid properties for some common 3DP solvents (25°C, 1cc/min, 45μm orifice)

Solvent	Density ρ (g/cc)	Viscosity η (cP)	Surface Tension σ (dyne/cm)	Weber *We*	Reynolds *Re*	Ohnesorge *Z*	Breakoff Length *L* (mm)
Water	1.00	1.00	73.05	67.7	471.8	1.7E-02	5.1
Ethanol	0.79	0.55	22.75	171.6	676.8	1.9E-02	8.1
Methanol	0.79	0.55	22.07	176.9	677.4	2.0E-02	8.2
Acetone	0.79	0.30	23.70	164.5	1239.3	1.0E-02	7.8
Chloroform	1.47	0.54	26.53	274.8	1298.2	1.3E-02	10.0

2.2.3.2 Mask Printing with Continuous Jet Unmodulated Natural Breakoff

Mask Printing is one technique that is employed to fabricate 3DP parts by physically masking off sections of the powder bed and exposing only the sections that are to be saturated by the printed fluid. Un-modulated continuous fluid jets are passed over the mask during the fabrication of one layer. The mask is then removed and cleaned, more powder is spread, the mask is replaced, and the process continues. The same mask can be used in every layer to create extruded two-dimensional shaped parts, or different shaped masks can be used in each printed layer to generate complicated overall three-dimensional geometries. The mask itself is formed from 0.020 inch thick tempered steel that has been laser cut. (Rache Corp., Camarillo, CA). Wu[1] has shown that masks like this can provide resolution down to 5μm. An example mask is shown in Figure 2.2.

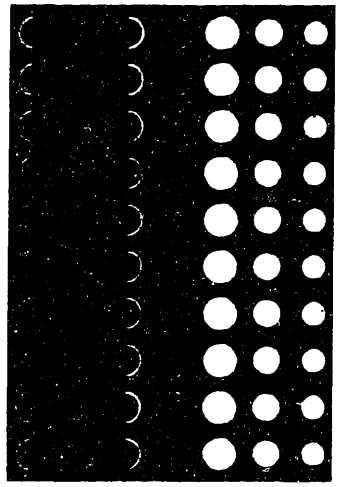

Figure 2.2 Example mask used in CJ Mask Printing

Mask printing is especially useful when testing new materials systems as it is simple to set up and implement. However, it does suffer several disadvantages.

- The complexity of a printed structure is limited by the mask shapes entirely. New masks must be made for every new desired geometry.
- Masks cannot easily create shapes with interior tunnels or interconnects
- Much material is wasted by this technique as fluid is dispensed over the entire region, and not just into the desired regions.
- The mask needs to be cleaned of this excess fluid between build layers.
- If the mask is not placed back into exactly the same location every layer, the part resolution can suffer drastically.

2.2.3.3 The CJ/CD printing technique

The second type of continuous jet printing used in fabricating pharmaceutical forms is called CJ Charge and Deflection Printing, or CJ/CD. A continuous stream is modulated using an in-line polycrystalline tube actuator located close to the orifice, and a more controlled droplet breakoff results. Individual droplets are either allowed to fall to the powder bed below, or are instead "caught" by an electronic printhead that applies a charge to droplets and

then deflects them selectively into a vacuum containment system to be recycled. This technique is far more complicated than CJ mask printing as it relies heavily on the fluid characteristics and fluid dynamics of a jet. The results presented in this thesis represent the first time this technique has been introduced to printing pharmaceutical materials. Pharmaceutical solvents such as ethanol and methanol are more difficult to print in this manner because of their low surface tension, σ. Pharmaceutical solutes such as polymeric matrix forming materials also present difficulties when printing in high concentrations due to viscoelastic jet properties.[1] This technique is however much more flexible as many geometries can be printed without the use of masks, and expensive drugs and other pharmaceutical materials can be recycled and printed only where needed. The CJ/CD technique as applied to pharmaceutical materials, and specifically organic solvents, is illustrated and described in the following sections.

The CJ/CD technique can be divided into 3 steps. These three steps are illustrated in Figure 2.3 below.

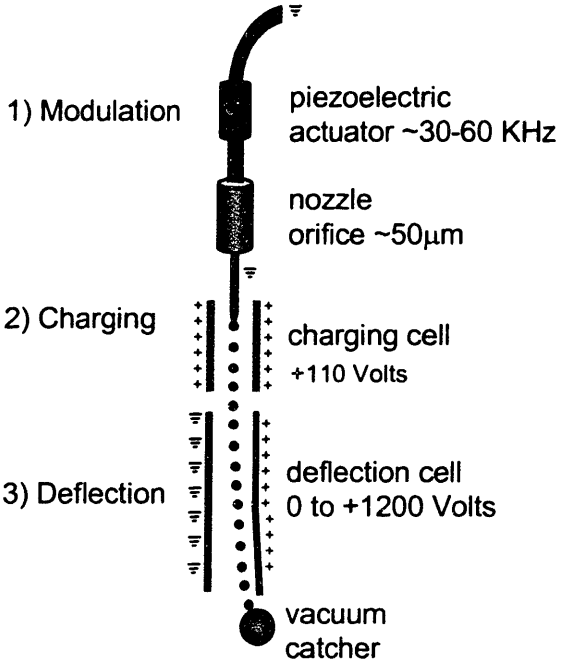

Figure 2.3 Schematic 1) modulation 2) charging 3) deflecting

2.2.3.3.1 Stream Modulation

The first of these steps is stream modulation. The fluid is forced through a piezoelectric tube actuator (Morgan Electro Ceramics) that is connected to a function generator. (Lodestar Electronics Corp.) Square waves of frequencies of ~30 to ~60 KHz are used to modulate jets during normal operation. The mechanical vibration introduced into the fluid stream is larger than the spontaneous instability of natural un-modulated jet breakoff, [1] and can be used to control droplet break off upon exiting the orifice. Frequency is tuned to obtain clean breakoff of spherical droplets of equal size and spacing.

2.2.3.3.2 Droplet Charging

In order for droplets to be controlled using computer design, the droplets must be charged electrostatically. The jet is continuous up until breakoff, and is thus in contact with the grounded printhead and machine. Below the point of which droplets break up, they are isolated from one another. The stream is passed between two parallel charging plates breakoff occurs between the plates.

The two charging plates can be charged or uncharged. The charging cell is "on" when the plates are charged positively. Droplets take on a negative charge upon breakoff between the plates when the charging cell is "on". The stream is grounded, and the droplets become negatively charged upon breakoff as the positive field in the cell attracts the negative ions down stream. The charging cell is "off" when the plates are neutral or uncharged. Droplets remain neutral in this state.

The charging cell carries a low variable voltage of 0-110 Volts in the "on" state, and is discharged in <20 msecs. This ability to charge and discharge the charging cell plates leads to fine printing accuracy. An "on-off-on" command takes a minimum of ~1 millisecond to implement on the current machine, and this

corresponds to ~40 drops at 40KHz, or ~15nL of volume given 90μm diameter droplets. This is the minimum volume of fluid that can be printed given the above assumptions and the current machine capabilities.

The charging plates have been designed to accommodate the longer breakoff lengths that correspond to organic solvents, as well as the traditional aqueous based binder fluids for the purposes of printing pharmaceutically relevant solutions and suspensions.

The capacitance of a centered jet between two parallel plates has been treated by Milner[28]:

$$C = \frac{2\pi\varepsilon_o}{0.216 + \ln\left(w/d_{drop}\right)} \qquad 2.6$$

where ε_o is the permittivity of free space, 8.84 pF/m, w represents the distance between the two charging plates and d_{drop} is the droplet diameter. The smaller the distance between the two charging plates, the larger the capacitance. The charge/mass ratio is also an important parameter that determines the later deflection path of the droplets. This ratio is given by:

$$\frac{q}{m} = \frac{4CV}{\pi d_o \rho} \qquad 2.7[28]$$

where V is the potential at the charging plate, d_o is the orifice diameter and ρ is the density of the fluid. This assumes that a fluid is conductive and readily takes on charge. Note that the charge to mass ratio is independent of flow rate, but can be increased significantly by reducing the spacing between the charging plates. The flow rate does affect the deflection path of the droplets downstream as discussed below.

2.2.3.3.3 Droplet Deflection and Catching

Droplets exiting the charging plates then travel between two parallel deflection plates. One deflection plate carries a variable net positive charge of up to 1200 volts. The opposite plate is grounded and is therefore neutral. Droplets exiting the charging cells that have not been charged, i.e. when the charging cell is "off", pass through this asymmetric charge field and continue straight to the powder bed to be printed. Thus, when the charging cell is "off", the printhead is dispensing fluid to the powder bed below. Droplets exiting the charging cells with a negative charge, i.e. the charging cell is "on", will be deflected towards the positive deflection plate. A cylindrical vacuum catcher is located below the positive plate and directly in the path of a deflected stream. A deflected stream of droplets wets this cylindrical vacuum catcher and is vacuumed into a containment unit for later recycling.

The acceleration of negatively charged droplets in the deflection direction, x, perpendicular to the original direction of the stream is shown in Figure 2.4. Milner[28] has shown that this acceleration is found from:

$$a_x = \frac{q \cdot V_d}{m w_d} \qquad 2.8$$

where V_d is the voltage between the deflection plates, m is the mass of a droplet, and w_d is the distance between the deflection plates. Assuming that there is no drag force acting upon the droplets in flight, the overall deflection in the x direction as a function of vertical distance, z, parallel to the original jet, can be given as:

$$x_{defl}(z) = \frac{a_x}{v_{zo}^{\,2}}\left(\frac{l_d^{\,2}}{2} + l_d z\right) \qquad 2.9[28]$$

where v_{zo} is the original jet velocity in the z direction and l_d is the length of the deflection plate.

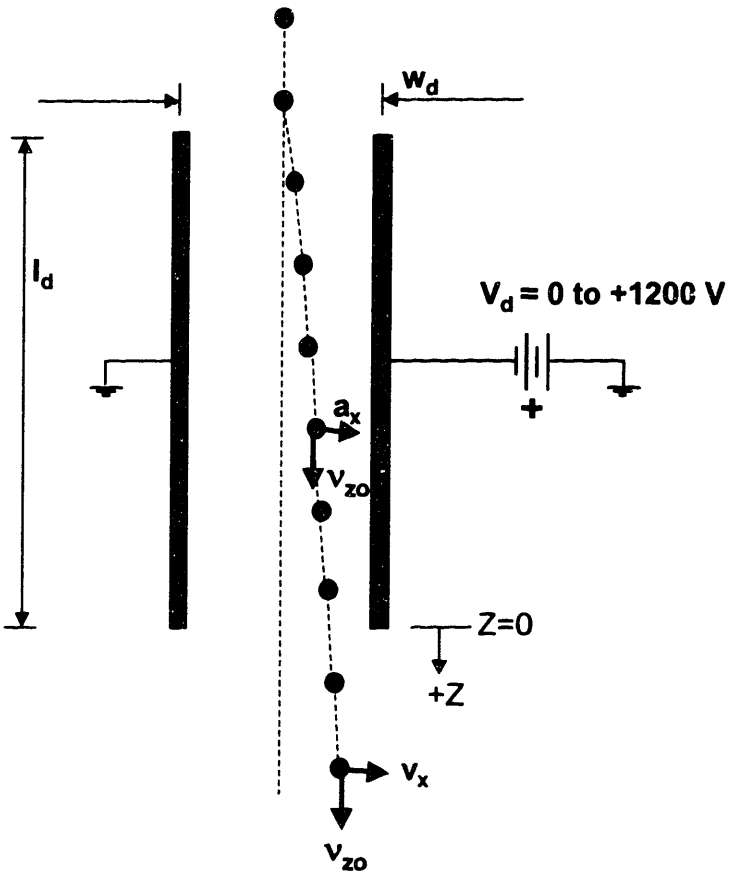

Figure 2.4 Deflection path within deflection cell

2.3 Design of Continuous Jet CD Organic Solvent Printhead (CJ CD OSP)

A new printhead has been designed for printing pharmaceutical solvents such as ethanol, methanol, acetone and water. It is based on another CJ CD design presented by Milner.[28] for printing aqueous based solutions. It was designed with the capability of CJ CD printing this wide range of solvents, and therefore it has been called the CJ CD Organic Solvent Printhead (OSP). Many of these solvents have poor conductivities and therefore do not obtain normal charge-to-mass ratios as compared to conductive solvents. The low charge to mass ratio decreases the acceleration of the droplets in the x-direction as shown in eq. 2.8, and thus decreases the x deflection. It can be seen from eq. 2.9 that the horizontal deflection distance can be improved by 1) increasing the capacitance by decreasing the distance between the charging plates, 2) increasing the length of the deflection plate, and 3) by moving the vacuum catcher closer to the center of stream. The voltage of the deflection plate could be increased as well, but it is more desirable to make the above 3 adjustments given the low flash point of organic solvents such as methanol, and the breakdown voltage of air. The new design takes these adjustments into account. The charging cell plate separation has been decreased to 0.6 mm, which translates into 26.9 pF given a droplet size of 94.5μm. The charging cell length has been increased to 2mm to allow for the longer breakoff length caused by the lower surface tensions and viscoelastic nature of organic solvent based solutions. It also has a longer deflection plate of 11mm. The Teflon and stainless steel printhead has also been designed for individual operation of 4 fluid jets, and allows for individual fluid recycling which is important when simultaneously printing and recycling various binder solutions, excipients, and drugs. Figure 2.5 shows the CJ CD OSP.

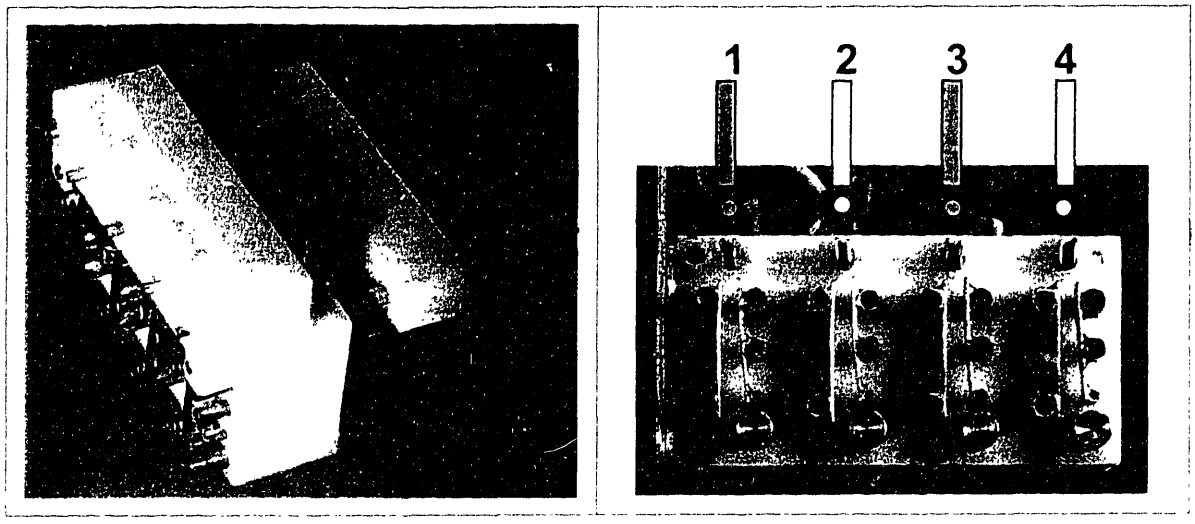

Figure 2.5 The CJ/CD OSP –Continuous Jet Charge/ Defection Organic Solvent Printhead

Additional drawings and electronic circuitry diagrams for the CJ/CD OSP are given in Appendix 2.

2.4 Fluids Characterization

The printed fluids in 3DP are subject to many constraints. Fluids, whether they be present as solvents, solutions, or suspensions, must print with stability and reproducibility. It is necessary to fully characterize all fluid systems in order to print with accuracy. Factors that often limit the reliable fluid range include rheology, such as viscosity and viscoelasticity, solubility limit, and conductivity.

2.4.1 Rheology

2.4.1.1 Viscosity of Newtonian Fluids

The viscosity is the first constraint that limits the range of fluids applicable to 3DP. Viscosity is used as the first selection criterion for all printing techniques, including DOD and CJ techniques. High viscosities cause the stress required to shear the fluid and force a plug of fluid through the orifice to become too high and the pressure drop to become large. The jet breakoff length (eq. 2.7) becomes

smaller as viscosity is increased to this limit and the jet fails to break off below the orifice and falls into drip mode. It has been found empirically that 15cP (at 9000 1/s and 25°C) is the upper limit for printing Newtonian fluids through a nozzle of 50μm nozzle at 30 PSI. Above that limit, jetting problems occur. It is actually desirable to stay below 12cP to ensure jetting reliability, especially at typical pressures of <20psi. This has been shown using a wide range of aqueous based Newtonian solutions including sucrose solutions, cornstarch solutions, NaCl, etc. Organic solvent based solutions such as diclofenac sodium /methanol solutions up to 30wt% loading have also been shown to display Newtonian behavior, viscosities up to 12cP, and are readily jetted. This viscosity limit is used as the first fluid selection criterion.

2.4.1.2 Non-Newtonian fluids: Thixotropic Suspensions

Thixotropic, or shear thinning, solutions or suspensions work very well as long as the viscosity at rest is also manageable as solution remains inactive until being pressurized into the fluid lines and through the orifice. Suspensions often display thixotropic behavior, especially at high solids loadings.

Naproxen suspensions have been used in this research to fabricate tablets with high dosages (see chapter 6), and have been shown to exhibit this behavior. Suspensions of ~300-500nm naproxen in water, with a small percentage of dispersing agent of PVP, polyvinylpyrrolidone, (Nanosystems, Inc.) was tested for rheological behavior to establish the ability to be jetted at different solids loadings. The viscosity characteristics vs. shear rate was measured using a Paar Physica rheometer with 7.5cm parallel plates with 1mm gap at 25°C for various solids loadings. The viscosity vs. shear rate is shown in Figure 2.6.

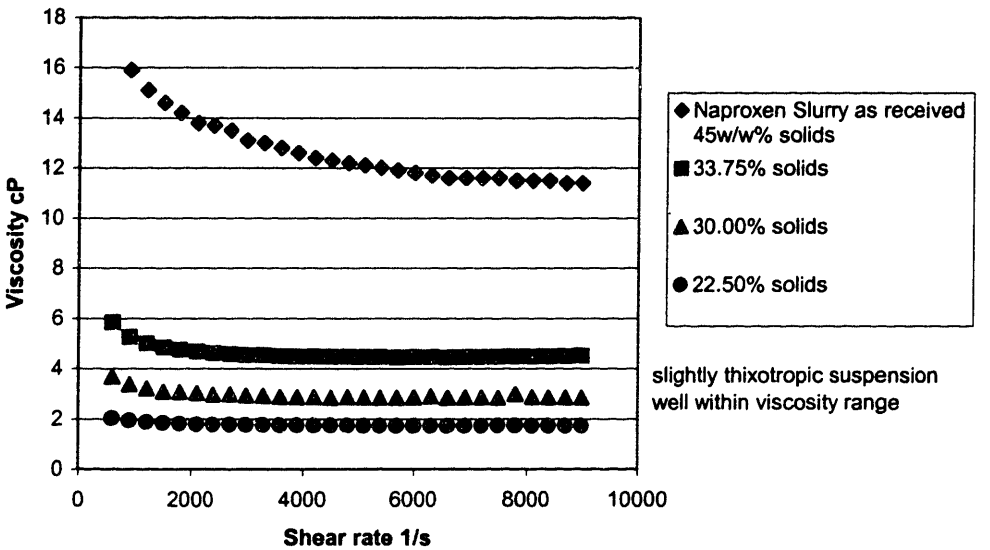

Figure 2.6 Viscosity vs. shear rate for aqueous naproxen suspensions

The viscosity decreases with shear rate, especially for the higher solids loadings of naproxen. At about 9000 1/s the viscosities level out and become constant. Figure 2.7 shows the viscosities of the different solids loadings of naproxen measured at 9000 1/s.

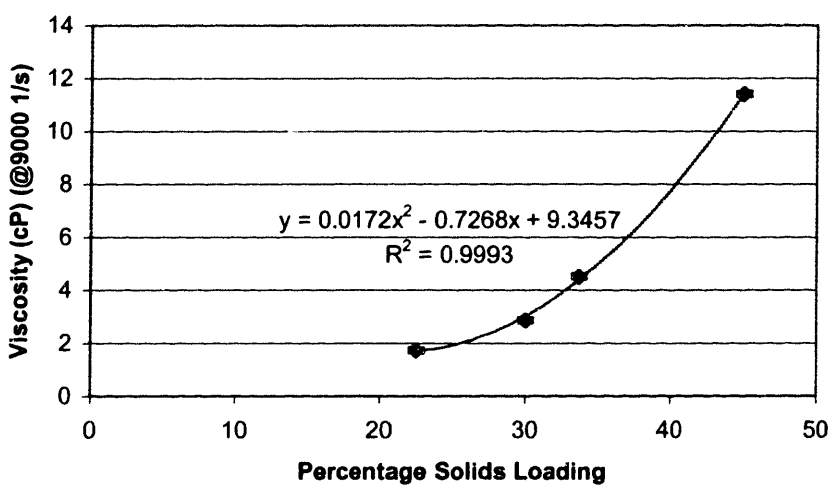

Figure 2.7 Viscosity vs. solids loading for aqueous naproxen suspensions

Given the viscosity limit of ~12cP, this indicates that solids loadings up to ~45wt% naproxen can be jetted. Solids loadings up to 41.5wt% have been subsequently printed reliably for more than 5 hours. This high solids loading capability and aqueous nature make these suspensions ideal for printing pharmaceutical forms. Attributes of drug suspensions are discussed further in Chapter 6.

2.4.1.3 Non-Newtonian fluids: Shear Thickening Polymer Solutions

The rheological properties of other types of fluids act to constrain the range of possibilities. Shear thickening solutions, for example, become more viscous when sheared through in line sintered element filters and small nozzle orifices. Many pharmaceutically relevant 3DP polymers, such as Eudragit L100 (Rohm America, Inc.), display this behavior when dissolved in solvents such as ethanol.

Solutions of L100 in ethanol were prepared containing 0 – 10wt%. The viscosities of the solutions were measured vs. shear rate on a rotary rheometer (Paar Physica) with parallel 7.5cm plates with a 0.5mm gap at 25°C adapted with a solvent trap to prevent evaporation. The viscosity profiles are shown in Figure 2.8 below.

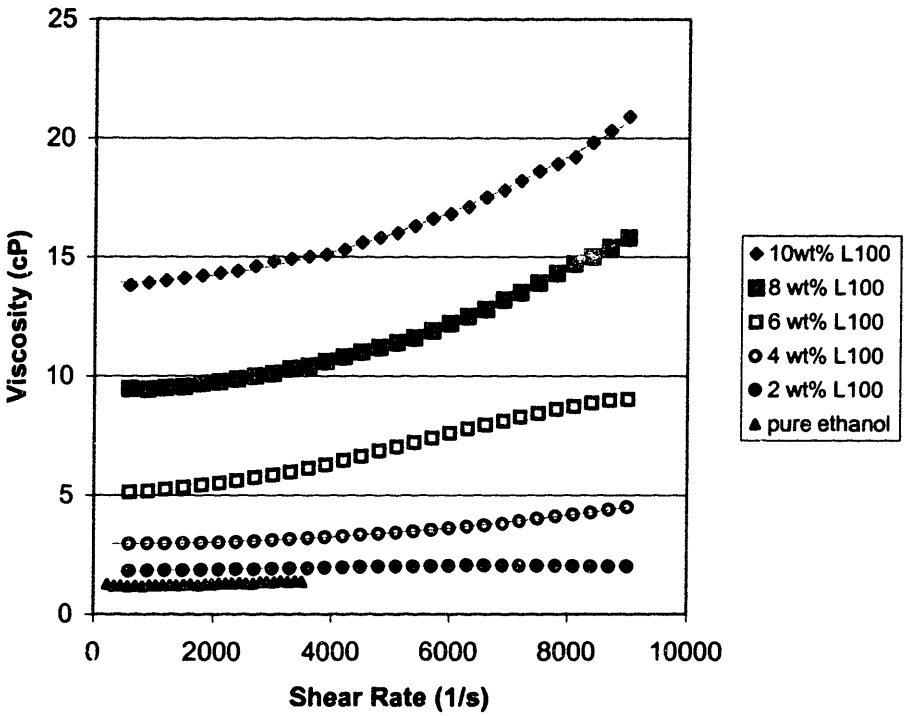

Figure 2.8 Viscosity vs. shear rate for L100/ethanol solutions

The polymer solutions of L100 exhibit increasing shear-thickening behavior with increasing solids loadings as represented by the upward curvatures. The solutions were also tested on the CJ CD OSP printhead, and solids loadings higher than 8wt% caused jetting failures.

2.4.1.4 Viscoelasticity and Jet Breakoff Characteristics

The viscoelastic properties of solutions, especially polymeric solutions, can also adversely affect the breakoff characteristics of a jet. Goldin[29] showed that jets of weakly viscoelastic fluids exhibit more rapid growth of axisymmetric wave disturbances than Newtonian fluids of the same viscosity. The disturbances appear as a series of droplets connected by random lengths of threads, which thin with distance and eventually lead to jet breakup at longer breakoff lengths.[29] These threads are also called "stringers" and are undesirable

especially during charge and deflection printing where electrically insulated droplets are necessary. Experiments conducted by Goldin[29] show that this non-linear phenomena dominates those fluids with pronounced elastic properties. Organic solvent-based solutions are especially at risk to developing threads during jetting because of their significantly lower surface tensions.

Fluids were tested for viscoelasticity, or non-linear stress-strain characteristics, on a rotary Rheometer (Paar Physica). Non-linearity was shown to increase with the polymer loading. The viscoelasticity of a 8wt% L100/ethanol solution is shown in Figure 2.9 which illustrates non-linear stress vs. shear rate.

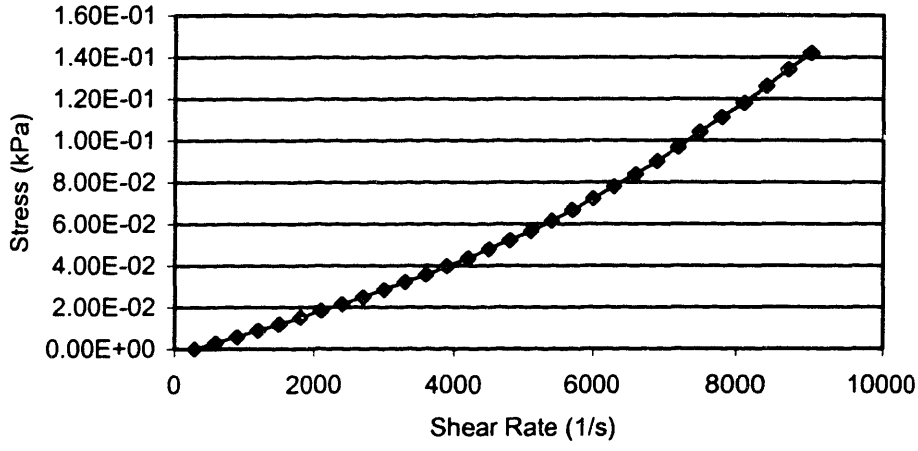

Figure 2.9 Non-linear stress vs. shear rate of 8wt% L100 in ethanol

Fluid jets were photographed under a wide range of parameters including modulation amplification and frequency. Regimes of clean breakoff were determined for several viscoelastic solutions of L100 in ethanol. Examples of clean breakoff and breakoff with threads are shown in Figure 2.10

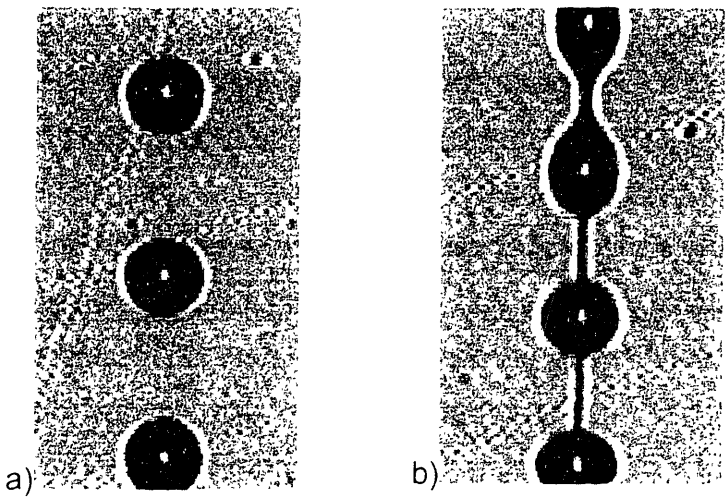

Figure 2.10 a) Clean breakoff, b) Threaded breakoff (stringers)

The jets consistently have thinner threads that persist for longer distances as polymer loading is increased. Jets in which the threads eventually break up and collapse back onto the droplets can be printed reliably as long as breakoff happens in the charging cell. Jets in which thread break up leads to the formation of secondary droplets, or satellites, cannot be printed reliably. The satellites and primary droplets traverse across the deflection field at different accelerations due to their different charge to mass ratios. (see eq. 2.9) The upper limit for polymer loading in the case of L100 in ethanol has been determined to be ~8 wt% as determined by this analysis, should the solution be printed by charge and deflection. The viscosity limit of 12cP gave a higher limit of ~10wt% for 50μm nozzles. This viscosity limit cannot be used in the case of charge and deflection printing, but it may still be used for the case of CJ with masks.

2.4.2 Conductivity

Equation 2.9 represents the deflection in the x-direction of a stream of conductive droplets under the influence of a deflecting field. Non-conductive or slightly conductive fluids do not obtain the same horizontal acceleration. Equation 2.8 shows that the horizontal acceleration decreases as the charge to mass term decreases. Organic solvents and even DI water alone are not very conductive, and often need additives to be charged. The new OSP printhead was built with this in mind; it has a longer deflection cell and smaller distance of 1.4mm between the center of the stream and the vacuum catcher. The x deflection must be at least 1.4 mm in order for the stream to be successfully turned "on" and "off", thus affording the ability to print shapes electrostatically. The deflection voltage can be increased to increase the horizontal acceleration, but is limited by the breakdown voltage of air. Additives can also be introduced to increase the conductivities to a point at which the deflection is at lease 1.4mm at the highest deflection voltage, approx. 1200V.

The ability to deflect a stream 1.4mm was tested with respect to conductivity in order to calibrate the printhead. Five conductivity standards of KCL in water were jetted and deflected to determine the x-deflection corresponding to conductivity. The deflection voltage used was 1200 V (V_{defl}), the distance between the charging plates was 0.6mm, the distance between the deflection plates was 2mm, the length of the deflection plate was 11mm, and the flow rate used was 0.6g/min. This represents a low flow rate and the highest deflecting voltage possible with the current settings. Using this low flow rate and high voltage allows the determination of the minimum conductivity requirement.

Conductivities were measured using a conductivity probe (Fisher Scientific Co.) accurate in the range 0.05 to 20,000 μS/cm. The deflections were measured between the discharged stream position and the deflected position at 12mm below the top of the deflection plate. Table 2.4 shows the conductivities and deflection distances for the five KCL solutions tested.

Table 2.2 Deflection vs. conductivity for KCL solutions

KCL concentration g/L	Conductivity μS/cm	x-Deflection μm	Stream caught?
$4.87x10^{-2}$	71	2000	yes
$5.17x10^{-3}$	7.54	1320	No
$5.20x10^{-4}$	.759	813	No
$3.41x10^{-5}$	.0497	499	No
0 (D.I. water)	~0	50	No

Figure 2.11 shows a plot of the conductivity measurements vs. x-deflection on the CJ/CD OSP using the above KCL calibration solutions.

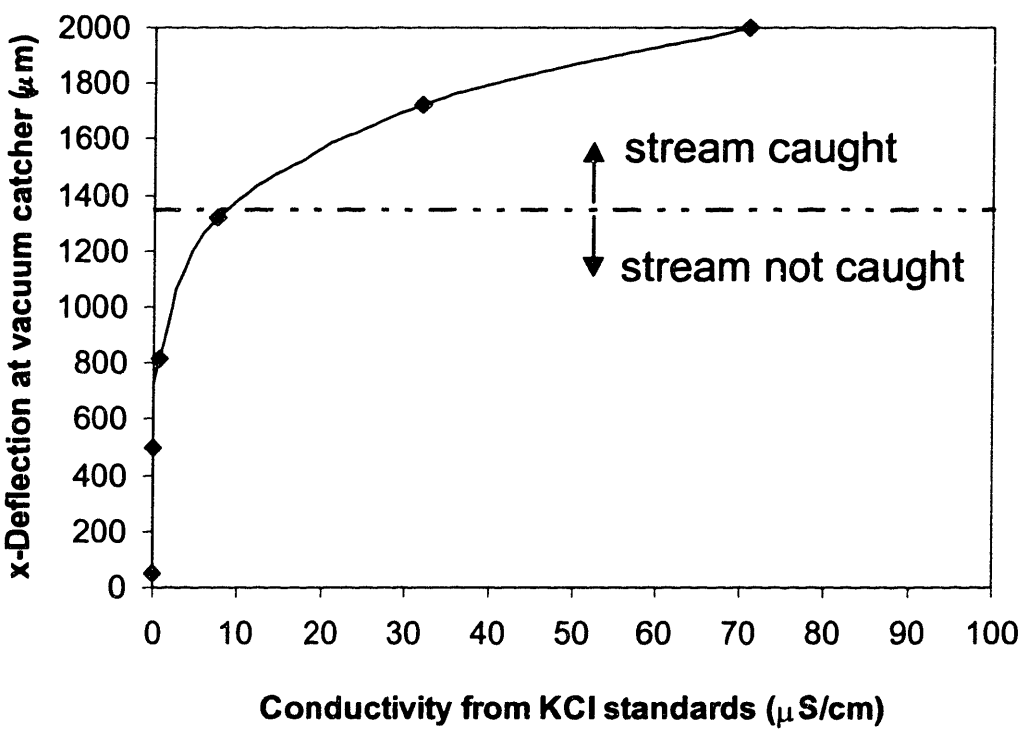

Figure 2.11 Conductivity vs. x-deflection

It can be concluded from this study that given the above conditions, the minimum printable conductivity for the CJ CD OSP is ~10 μm/cm. This is used as a selection criterion for fluids printed on the CJ CD OSP.

2.5 Printing Space for common 3DP fluids

The above characterizations serve to constrain the range of possible fluids suitable for the 3DP process. These constraints have been applied to the construction of 4 main printing spaces. Illustrated below are maps that serve as guides to fluid selection. They serve to represent 1) *aqueous Newtonian solutions;* examples from this research include, but are not limited to, chlorpheniramine maleate in water, sucrose in water, etc.; 2) *Newtonian organic solvent-based solutions* such as diclofenac sodium in methanol; 3) *viscoelastic polymer solutions*; examples include L100 in ethanol, RLPO in acetone, etc.; and 4) *aqueous suspensions* such as naproxen dispersed in water.

2.5.1 Aqueous Newtonian Solutions

The printing space for aqueous Newtonian solutions is straightforward. It is bounded by the limits for conductivity, viscosity, and solubility limit. The map for chlorpheniramine maleate dissolved in water is given in Figure 2.12. This map can be easily generalized for any solute given the viscosity/concentration relationship, the conductivity/concentration relationship and the solubility limit of the solute.

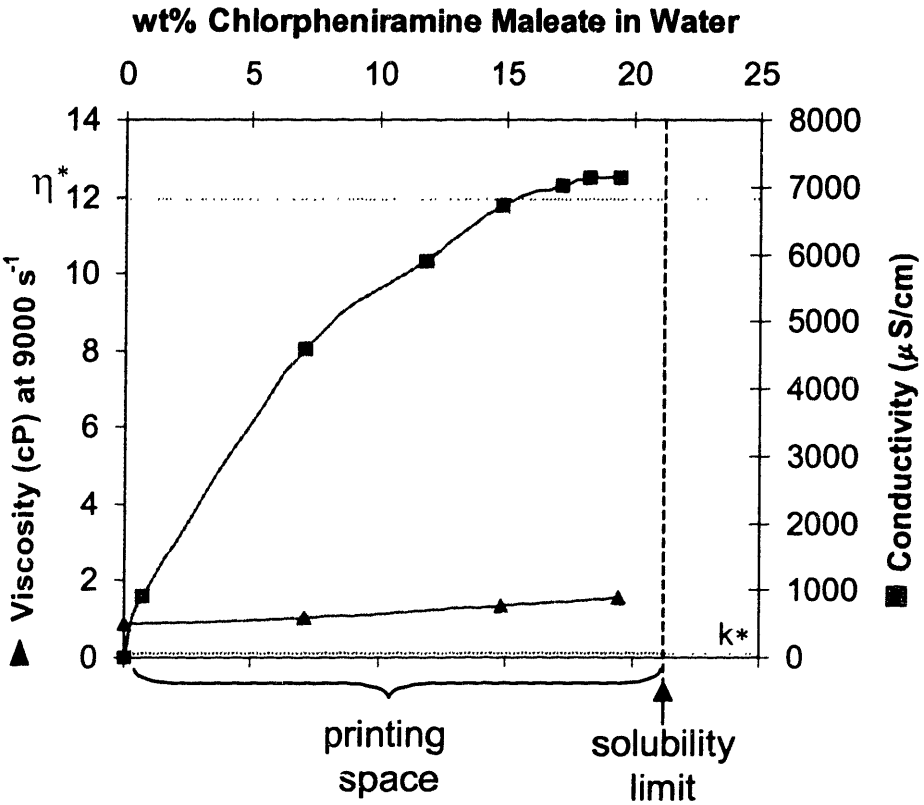

Figure 2.12 Printing space for chlorpheniramine maleate/ D.I. water

2.5.2 Newtonian Organic Solvent-based Solutions

The printing space for Newtonian organic solvent-based solutions is very similar to the aqueous case. The bounds are again conductivity, solubility and viscosity limits. It is, however, not desirable to print near the solubility limit. The vapor pressures of organic solvents are much higher than water (numbers..), and therefore evaporation at the orifice can result in crystallization and adversely affect the jet. The empirical limit for diclofenac sodium has been found to be ~20wt% in methanol at flow rates of 1 g/min. Higher loadings caused jets to fail in less than 5 hours in the absence of any cleaning procedure. 5 hours is the standard reliability time used because it generally takes on the order of 5 hours

to complete a print run on the prototype machine. It is plausible that should a cleaning procedure be incorporated into the process, much the same way the ink jet printheads are automatically cleaned between print jobs to avoid build up, higher solids loadings may be possible. This empirical limit has been included in the printing space for diclofenac sodium in methanol, as shown below.

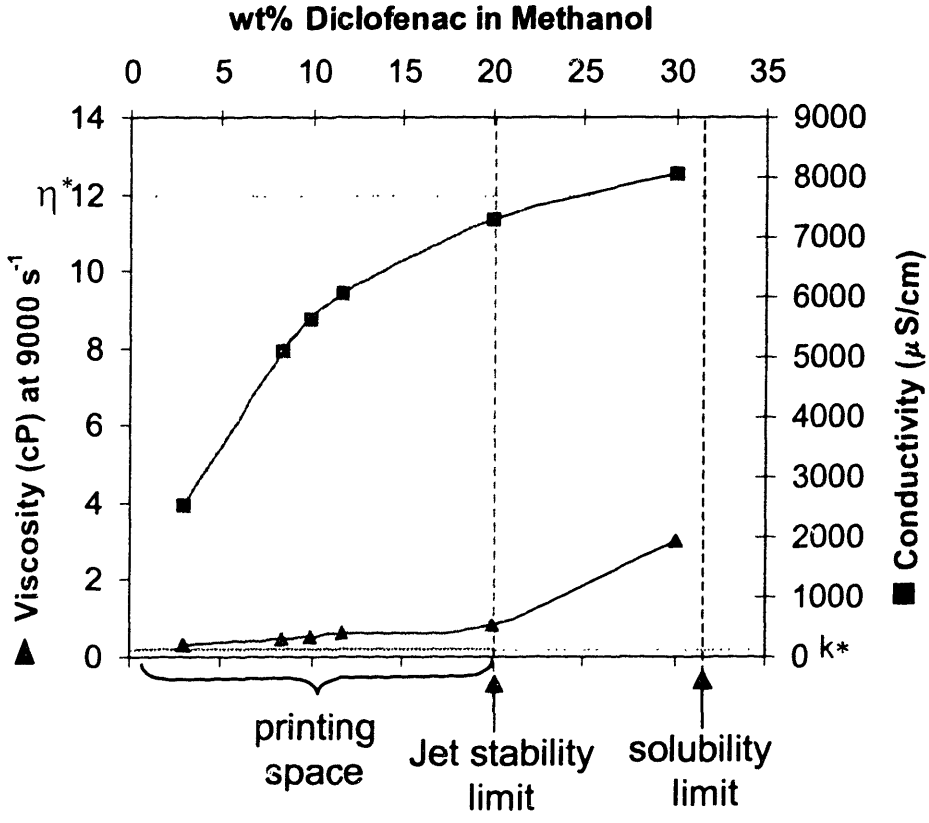

Figure 2.13 Printing space for diclofenac sodium / methanol

2.5.3 Viscoelastic Polymer Solutions

Viscoelastic polymer solutions have the additional constraint of needing to be printed at concentrations lower than the point where threads inhibit clean breakoff as described in section 2.4.2.1.4 for CJ CD printing. The printing space for L100 in ethanol is given in Figure 2.14.

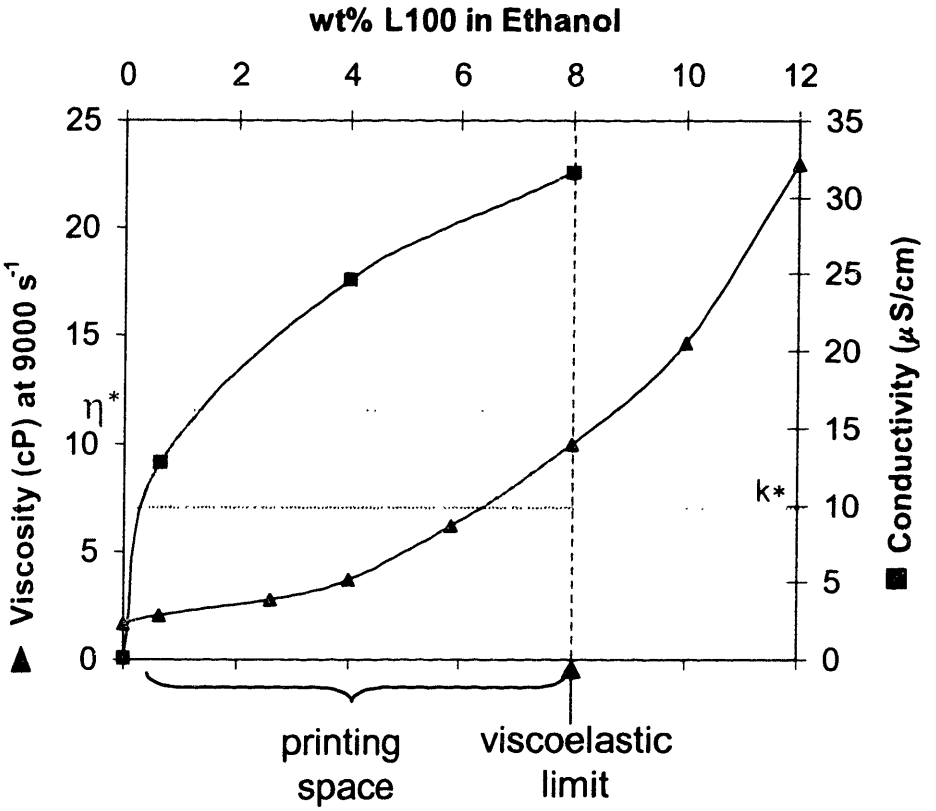

Figure 2.14 Printing space for L100 / ethanol

2.5.4 Aqueous Suspensions

The last class of fluids considered is aqueous-based suspensions. These suspensions are limited by viscosity and conductivity, but are also limited by dispersion physics. The maximum solids loading is therefore limited by the loading obtainable in a stable suspension. The printing space for the aqueous suspension of naproxen (300-500nm) (Nanosystems, Inc.) is given in Figure 2.15. The dispersion limit for this system is approximately 45 wt%.

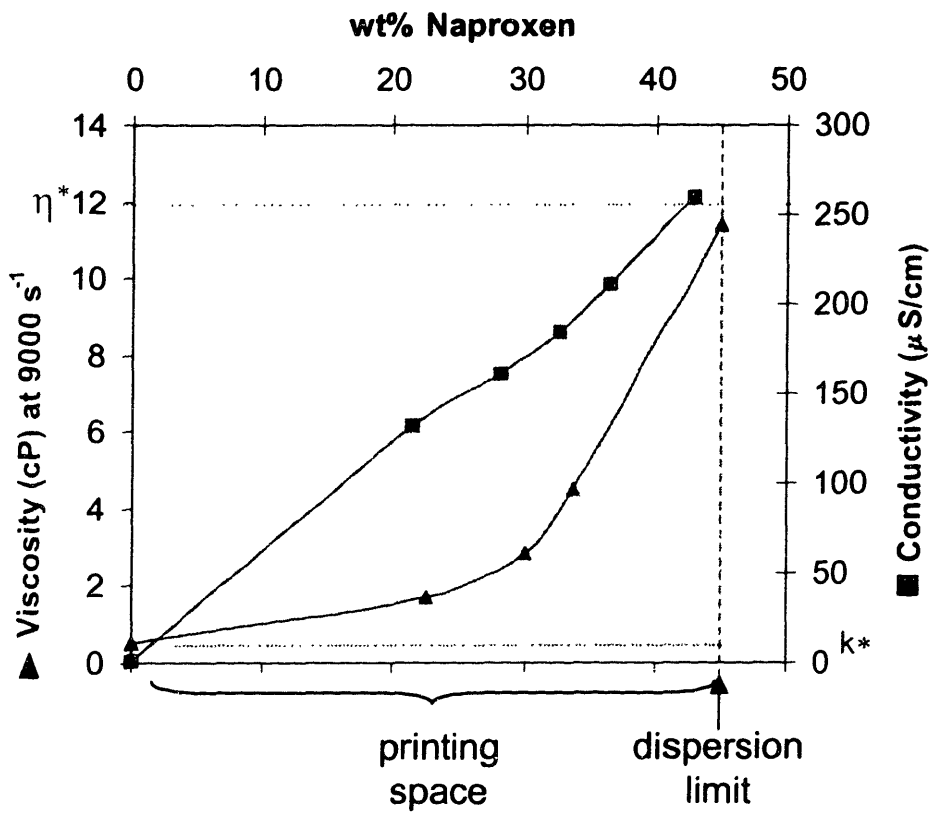

Figure 2.15 Printing space for naproxen aqueous suspension

2.6 Summary for Chapter 2

One main limitation to printing by continuous jet or drop-on-demand is viscosity. Viscosities lower than 12cP are generally used to ensure jet reliability. Charging and deflecting droplets in the CJ/CD technology requires that fluids be somewhat conductive and able to break off into clean, electrically isolated, and equally sized droplets. It has been determined that fluids must have conductivities of at least ~10μS/cm to be caught and re-cycled on the CJ/CD OSP. The printing spaces based on viscosity, conductivity, and other limitations have been determined for 4 common 3DP fluids. These spaces can be easily generalized for use in other fluid systems.

CHAPTER THREE

Tablet Resolution

A major objective of this research is the enhancement of resolution by decreasing the printed feature size. This will allow the ability to design devices with better functionality and appearance. 3DP has always been limited by the feature size and surface roughness of parts, especially in dry powder spreading operations. Either the powder size or the migration of printed fluid within the powder limits the size scale. The printing of pharmaceutical materials introduces even more challenges. Many researchers have attempted to find ways to decrease feature size in other systems,[1, 2, 22, 30] but more research has been necessary to enhance resolution in the specialized materials systems used for pharmaceuticals, many of which are based on polymeric powders, sugars, and aqueous and alcohol binder fluids.

The size scale or resolution is important in printing pharmaceutical oral dosage forms for a few reasons. The most obvious reason to improve resolution is for desirable aesthetic properties. Tablets will need to be swallowed by the end user, and must be smooth and ordinary, or else compliance will be problematic. More important is the overall mechanical properties and functionality of the device. Tablets with rough surface finish are friable, and their mechanical properties are poor as a result.[31] Furthermore, tablets with poor internal resolution will not release drug in the way originally intended. This is illustrated by Figure 3.1 in which three hypothetical right hand circular cylinders containing central cylindrical drug containing regions of equal original concentration are allowed to bleed outward. Moderate bleeding is defined as migration to 125% of the original drug region volume, and severe bleeding is defined as migration to 160% of the original volume. The hypothetical release curves shown in Figure 3.1 assume perfect erosion, and were obtained by stepped integration.

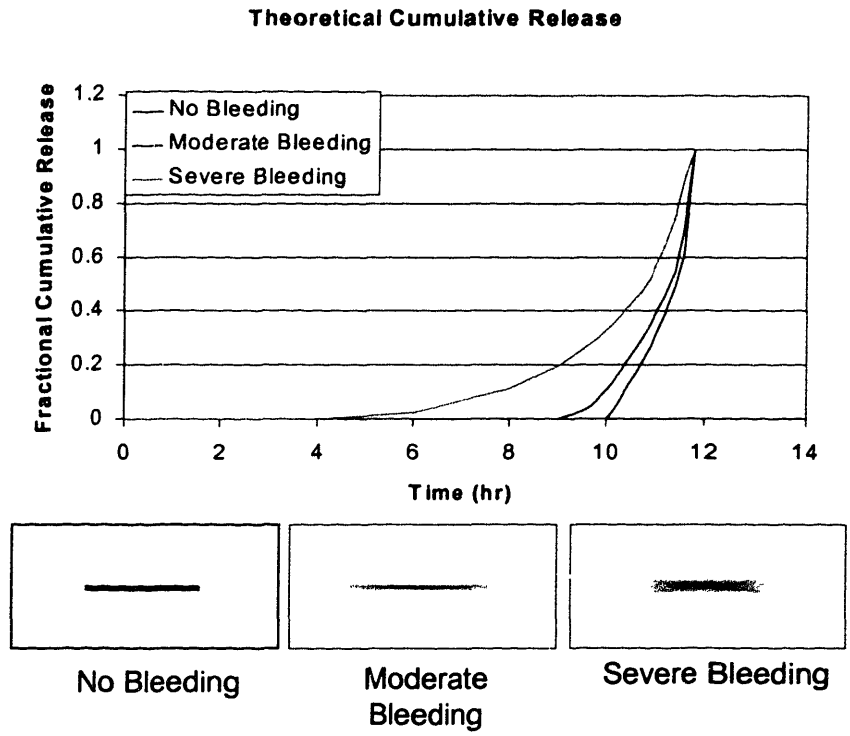

Figure 3.1 Hypothetical erosion-type release profiles of three drug distributions a) no bleeding from a central drug region, b) moderate bleeding, c) severe bleeding

A drug region that is designed with sharp boundaries for a pulsatile-type release upon erosion may lose its pulsatile nature if the fluid is allowed to migrate out of its original intended region. Figure 3.1 shows that as migration occurs from an interior region, the release profile begins sooner and is less pulsatile. The inability to precisely control the drug placement results in the inability to control the ultimate release profile. Means of controlling this type of migration will be important in the ultimate utility of the technology.

It should be noted that the first improvement in feature size was achieved by switching from CJ mask printing to CJ CD printing. (see sections 2.2.2.2 and 2.2.2.3) In many cases it was found that the use of a mechanical stop in re-positioning a mask over the printed surface led to poor layer to layer alignment. This is apparent in Figure 3.2 which shows the side walls of a printed cylinder

with the CJ mask technique versus a cylinder printed with CJ CD. The CJ CD technique allows cleaner cutoff and alignment in the formation of shapes.

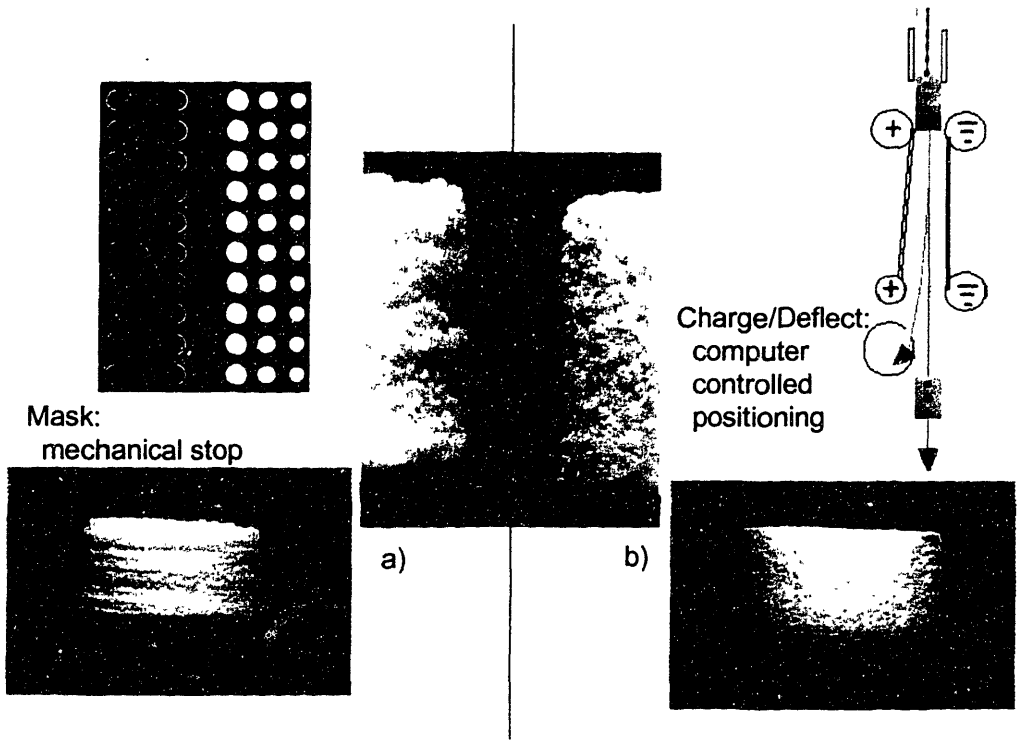

Figure 3.2 Side walls printed with a) CJ mask technique
b) CJ charge/deflect technique

Further enhancement of both external and internal resolution has been approached from two main directions: 1)the improvement of powder characteristics to allow for smaller particle size and smaller step size and 2) the incorporation of post processing techniques to improve surface characteristics. These will be discussed in section 3.1. The second section, 3.2, discusses the process of fluid interaction and then provides novel techniques to arrest fluid migration within the powder bed by introducing migration inhibiting additives to the powder and by pre-printing migration barriers.

3.1 Step Size and Post fabrication techniques

Increasing the resolution of 3DP pharmaceutical structures ultimately allows for greater design flexibility, better mechanical properties, and better control over the release characteristics. This section discusses the reduction of step size, an important first step for better resolution. Post processing techniques such as spray coating and uniaxial die pressing will also be considered as means to better surface finish and mechanical integrity of the tablets.

Decreasing the step size or layer height used in the fabrication of tablets first requires that the powder size be decreased. Once the powder size has been decreased below a critical limit, however, electrostatic attractive forces become large and aggregation occurs. This aggregation or clumping decreases the flow properties of the powder, and therefore makes uniform spreading more difficult. For ceramic alumina powder, Fan[32] reports that the lowest particle size that is spreadable is 10μm. This lower limit corresponds with the particle size at which the gravitational force on two particles becomes less than the Hamaker attractive interaction. The Hamaker potential between two spherical particles is given as:

$$V_A = \frac{-Aa}{12h} \qquad 3.1^{33}$$

where A is the Hamaker constant in joules, *a* is the particle radius, and *h* is the distance between the two particles. The Hamaker attractive force in Newtons is given as the derivative of the potential over the distance:

$$F_{Hamaker} = \frac{\partial V_A}{\partial h} = \frac{Aa}{12h^2} \qquad 3.2^{33}$$

Figure 3.1 shows how the gravitational force on one particle changes with diameter, and how the attractive Hamaker force changes with diameter for both a

ceramic material (alumina, A=1.75x10^{-20}J [34]) and for polymeric materials, such as methacrylates, acrylics, and Eudragits™ where the Hamaker constant is much larger. (~7x10^{-20}J[33]).

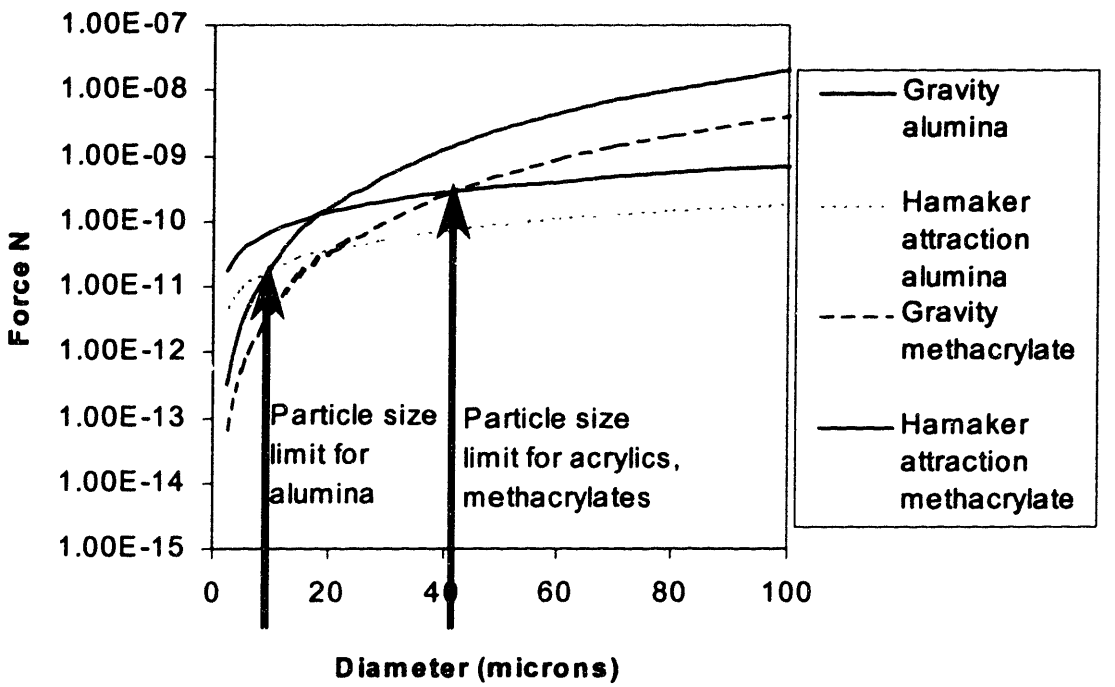

Figure 3.3 Hamaker force vs. gravitational force for alumina powder and polymeric powders

Figure 3.3 shows that the cross-over diameter where attractive forces begin to dominate occurs at a larger diameter for polymeric materials. The smallest acrylic powder that can be used is ~40μm, which is also the size below which spreading becomes difficult given qualitative observations. The lower limit for lactose powder has been determined to be approximately 40 microns as well, and this lower limit is greatly dependent on humidity given the hygroscopic nature of lactose. The smallest particle size range for most 3DP pharmaceutical powders (see Appendix 1) has been determined to be 38-53μm for low humidity

environments, although greater particle sizes (i.e. 53-74) are often used for consistency and reliability.

Layer thickness not only limits the ability to fabricate curved surfaces with good resolution, it also has been shown to affect the ballistic interaction of a droplets hitting the powder surface. The droplet decelerates, deforms, mixes with powder particles, displaces material causing a crater to be formed, and finally comes to rest. This ballistic impact in dry powder systems has been fully characterized by Lauder[35] and Fan.[32] Crater dimensions have been reported to be about 300μm in diameter and 200μm in depth for 90μm water droplets traveling at 10m/sec interacting with 10-25μm alumina powder with 40%packing.[32] Similar crater dimensions have been reported for polymeric powders with lower density[1]. This effect can be detrimental for large droplets due to the increased kinetic energy available for displacement, such as those used in some current solenoid nozzles where droplets can range in size from 220 to 280μm.[36] The above crater depths are for droplet interaction with unprinted powder beds. The crater size has been reported to be significantly smaller in subsequent printed layers due to the cohesive strength of the underlying printed layers. Fan has shown that this phenomena is directly related to the layer thickness used. For dry powder, he has shown that the bearing capacity of the powder bed scales linearly with the depth of the powder bed. It has been demonstrated that decreasing layer height can help to decrease the ballistic impact and therefore greatly improve the surface finish of the printed structures.[32]

The following experimental section explores the lower limits of layer thickness based on powder properties and packing characteristics. Post fabrication techniques have also been introduced as a means to improve the surface finish of tablets while not drastically altering the internal geometries.

3.1.1 Experimental

3.1.1.1 Powder characterization:

As-received powder samples including lactose, microcrystalline cellulose, and other additives (see Appendix 1) were sieved using stainless steel sieves (Buehler) into size ranges of <38μm, 38-53μm, 53-74μm, 74-106μm, 106-150μm, and >150μm. These samples and mixtures of these samples were characterized for tap density and packing fraction. Tap density is defined as the weight of the powder occupying a unit of apparent volume at the powders most efficient state of packing. Tap density was measured by filling a 10mL glass graduated cylinder with powder, tapping the side of the cylinder until the powder stopped settling, and then recording the powder weight and apparent volume. The packing fraction of the powder samples was calculated as the tap density divided by the bulk density of the material used.

3.1.1.2 Spread Density

It is important to achieve uniform powder density across the entire spread surface; therefore, it is desirable that the powder within one layer be fluid, or flowable, and able to achieve tap density. Tap density describes a state of efficient packing in which powder occupies a minimum volume.

The spreading density is defined as the mass of powder that has been spread into a powder bed of given volume (bed height x area) during 3DP. A powder bed with a spread density equal to tap density is stable and will not deform or shrink if small drops of a non-solvent fluid is introduced. A powder bed at tap density therefore acts as a scaffold into which fluids can be printed and forms can be built layer by layer.

The spread density is not always at the tap density. This might be a result of poor flowability, as powders may not efficiently pack under the spread bar.

This results in layer non-uniformity and density differences from sample to sample within the powder bed.

Spread density has also been shown to change as the average powder size changes for a given layer thickness, or as the layer thickness is changed given an average powder size. Spray-dried spherical lactose powder was measured for spread density to show this phenomenon.

Lactose monohydrate powder (see Appendix 1) was first sieved to a particle size cut of 53 – 74μm. It was then spread onto a level build plate using a layer height of 75μm. Ten more layers were spread at 75μm layer height for a total bed height of 0.825mm. A sharp circular frame of area 43.01cm^2 was used to capture a circular sample of the powder bed, and thus define a volume of 3.55 cc. Excess powder around the frame was gently blown off the surface with an air gun. The powder was weighed to be 2.21g, giving a spread density of 2.21g/3.55cc or 0.623 g/cc. The tap density of this powder was measured by filling a 10cc tall glass graduated cylinder with powder and tapping the cylinder until the powder completely settled. The volume of powder in the cylinder was 8.33cc with a weight of 6.49g giving a tap density of 6.49g/8.33cc or 0.779g/cc.

Spread density measurements were repeated 5 times for the layer height of 75μm, and 5 times each using the same powder and layer heights of 125μm, 150μm, and 200μm. Figure 3.4 shows the spread densities for this powder system as the layer height is increased.

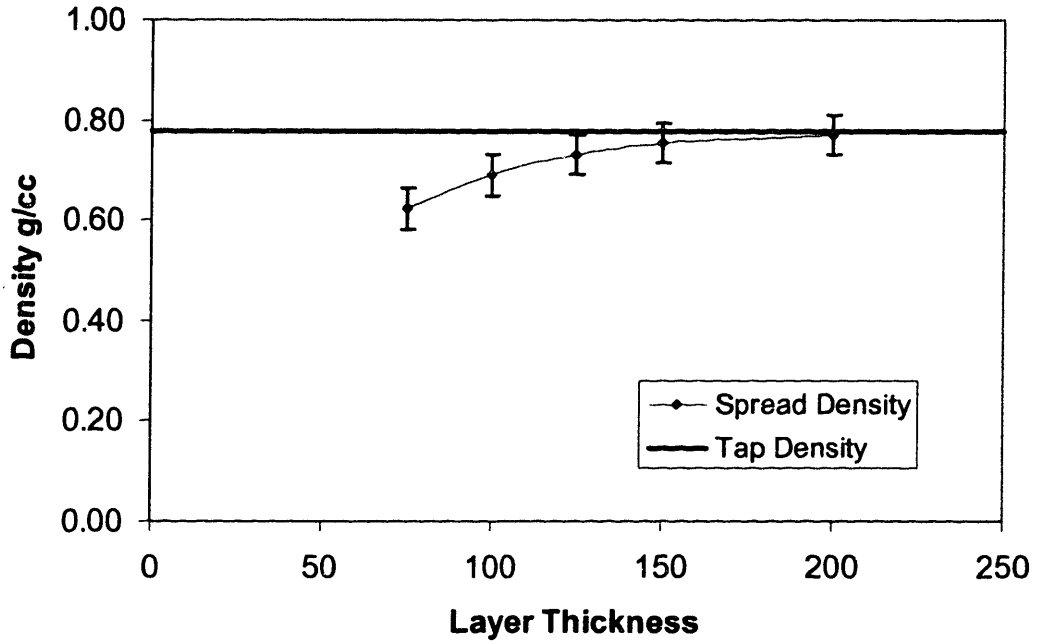

Figure 3.4 Spread density and tap density for varying layer heights of lactose monohydrate powder in size range 53-74μm

The spread density increases asymptotically towards the tap density of the powder. Increasing the layer height to ~150μm results in a spread density that is statistically insignificant from tap density. This result is shown in Table 3.1.

Spread densities were also obtained for other size ranges of lactose and powder systems of microcrystalline cellulose, and a mixture of 30wt% lactose/ 40wt% L100/ 30wt%cellulose. The spread densities for these systems also asymptotically approached their tap densities. The layer height at which the spread density is statistically equal to tap density for these powder systems is listed in Table 3.1. At this point, the powder bed is considered stable and well packed.

Table 3.1 Minimum layer heights to achieve tap density

Powder System	Particle size range	Minimum Layer Height
Lactose Monohydrate	38-53μm	~125μm
Lactose Monohydrate	53-74μm	~150μm
Lactose Monohydrate	53-106μm	~200μm
Lactose Monohydrate	74-106μm	~225μm
Microcrystalline Cellulose	38-53μm	~200μm
Microcrystalline Cellulose	53-74μm	~250μm
30:40:30 Lactose:L100:Cellulose	38-53μm	~200μm
30:40:30 Lactose:L100:Cellulose	53-74μm	~225μm

3.1.1.3 Contoured Sucrose Tablets

Two sets of placebo tablets were fabricated using the CJ CD 3DP technique. The first set of tablets was constructed from lactose with particle size 53-106μm and a layer height of 200μm, and the second set of tablets was constructed from lactose with particle size 38-53μm and a layer height of 125μm. For both sets the binder solution was 35wt% sucrose, 1wt% NaCl in D.I. H_2O printed with a line spacing of 120 μm, and saturated to 90% with volume fraction sucrose added $\theta_{sucrose}$= 0.17. Each of the tablets was printed into the shape of a tablet with a top curvature of r=1.32cm as shown below in Figure 3.5.

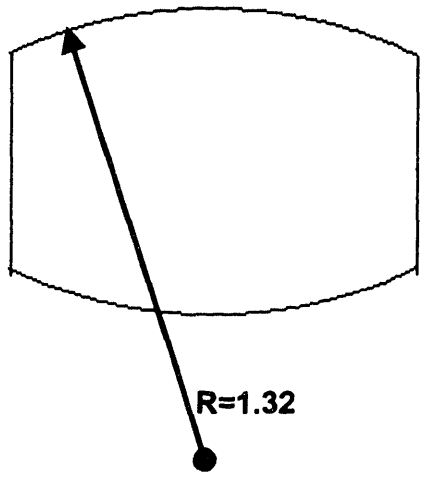

Figure 3.5 Tablet shape with contour curvature r = 1.32cm

The tablets were allowed to dry for two days in a nitrogen glove box at room temperature. Excess dry powder was then removed from the build plate with an air gun, and the samples were mounted in EpoThin™ (Buehler) low temperature low viscosity epoxy. The samples were then cross-sectioned through the center to illustrate the step-like approximation of the top contoured surface. Micrographs of backlit samples were taken to show the surface in high contrast. Figures 3.6 shows these samples and micrographs.

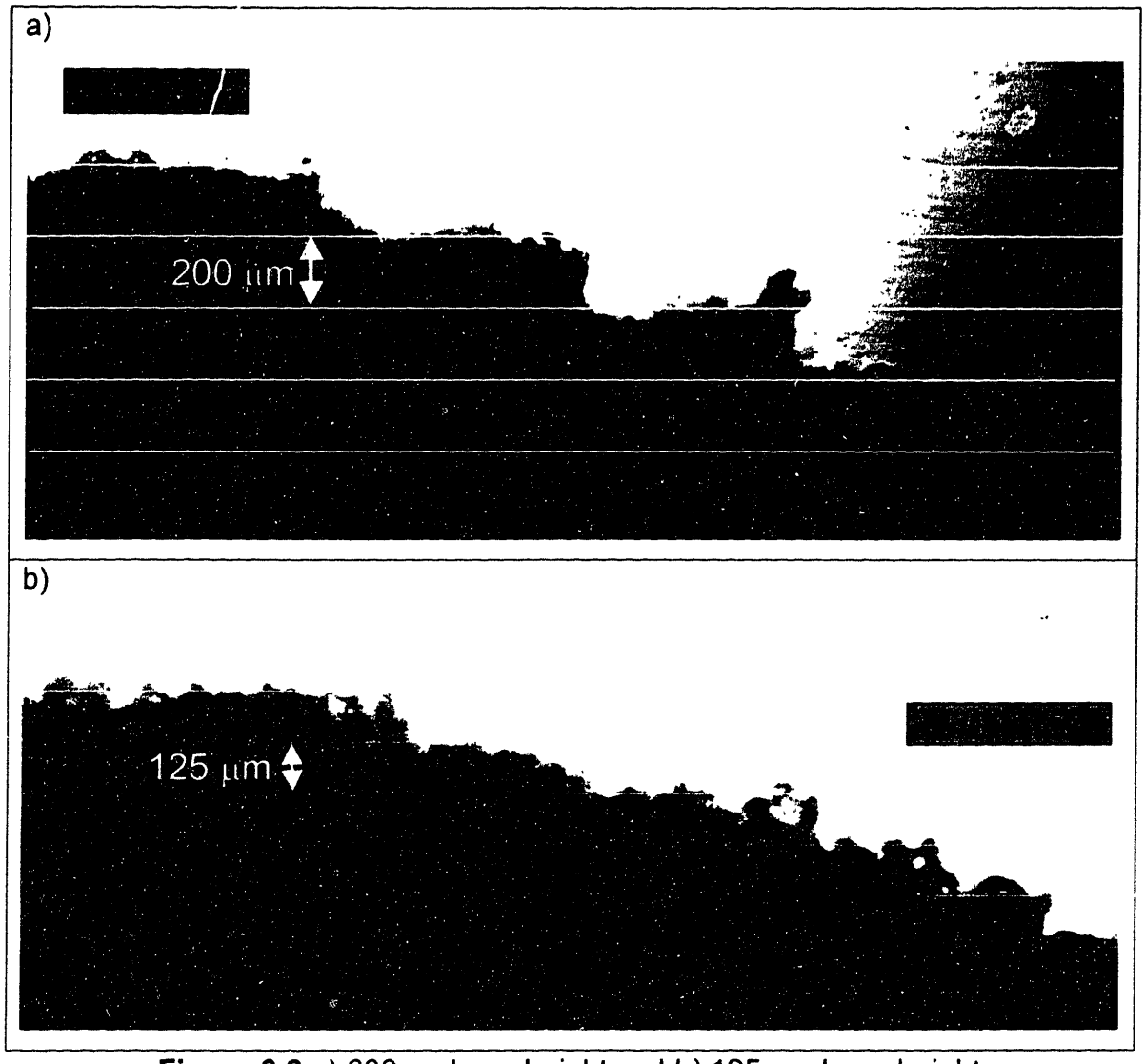

Figure 3.6 a) 200μm layer height and b) 125 μm layer height

The smaller steps of the second sample are the consequence of the smaller layer height used. The surface roughness in each is on the scale of the particle size used. This is especially illustrated at the ends of layers where the printed section is in contact with the dry build powder.

3.1.1.4 Spray-Coated Contour Sucrose Tablets

Tablets fabricated in the previous experiment (section 3.1.1.4) were then spray coated using a common Eudragit™ coating solution, 15wt% E100 in 50/50 isopropanol / acetone.{R3.9} The spray coating set up is shown in Figure 3.8. Samples were set up on a turntable 14 cm from the spray nozzle (Paasche Airbrush Co.) and 30 cm from a heat gun. The turntable rotated at 100RPM, and the air pressure into the unit was set to 35psi. The temperature at the sample was determined to be ~40°C. This resulted in a coating rate of ~4 microns/second as determined by weighing samples over time, and approximating the surface geometry as the top hemisphere of a circumscribed cylinder with diameter = 11mm, and height = 5mm, such that the coated surface area = $1/2\pi(dh+(d)^2/2)$. {R3.9} The actual coating rate for this procedure was not important as commercial spray coating machines operate with much different parameters.

One sample with a coating thickness of ~30μm is shown in Figure 3.7.

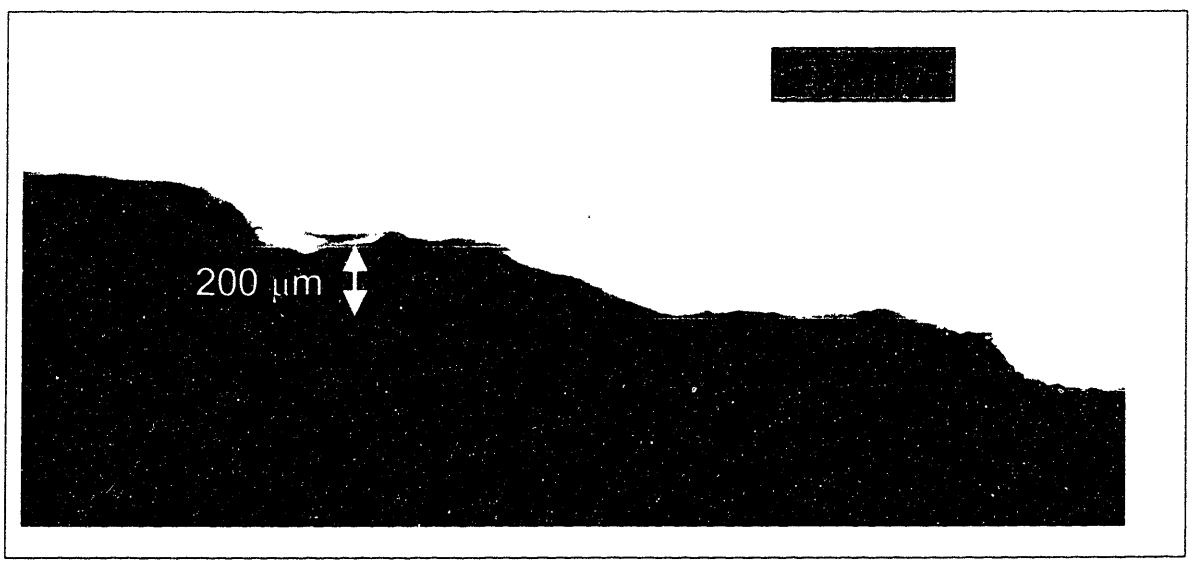

Figure 3.7 Spray-coated contoured surface

3.1.1.4 Contoured Naproxen Tablets

Contoured naproxen tablets were fabricated using the CJ CD OSP 3DP technique. These tablets have a contoured outer profile and an inner square drug region profile. The schematic design of these tablets is illustrated in Figure 3.8.

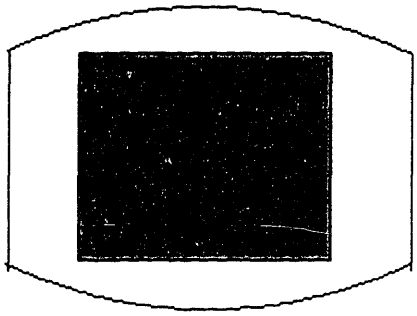

Figure 3.8 Design of contoured naproxen tablets

The powder used in fabricating these samples was 50wt% microcrystalline cellulose (38-53μm) and 50wt% lactose (53-74μm), with a packing fraction of 0.428, and using a layer height of 200 μm. Two fluids were printed to fabricate the two composition regions of the tablet. The interior drug region was printed with a suspension of 22wt% naproxen in water plus 0.05wt% fluorescein sodium salt (Sigma Chemical Co., see Appendix 1). A saturation of 1.0 was used to print this interior region, with a volume fraction naproxen of θ_{nap}= 0.107. Thus the void space or porosity remaining in this inner section was 1-0.428-0.107=0.465, meaning that the inner matrix is 46.5% porous. The outer region was printed with a solution of 5wt% L100 in ethanol. A saturation of 1.3 was achieved in this outer region, giving a volume fraction L100 of θ_{L100}= 0.024. Thus the void space or porosity remaining in this section is 1-0.428-0.024=0.548, meaning that the outer matrix is 54.8% porous. The tablets were constructed in a symmetrical

geometry with 9 layers making up the top curved surface, 9 layers making up the bottom curved surface, and 25 center layers making up the girdle of the shape for a total of 43 layers or 8.6mm in height. The center layers made up the outermost diameter or of 11mm, into which rings of the outer wall regions (O.D.=11mm, I.D.=7mm) were first printed, and circles of the drug region (O.D.= 7mm) were next printed.

The tablets were dried for two days in a nitrogen glove box, and then the excess powder was removed with an air de-duster. Two of the samples were then uniaxially pressed at 15000psi using a stainless steel tablet die with diameter of 11mm, and custom plungers with convex surfaces to match the contour of the tablet caps (radius of curvature = 1.32cm).

Pressed and un-pressed samples were measured with digital calipers. These measurements are given in Table 3.2 below.

Table 3.2 Average tablet dimensions before and after pressing

		Height	Diameter	Girdle
a	Un-Pressed	8.70mm +/- 0.1	11.22mm +/- 0.1	5.26mm +/- 0.1
b	Pressed	4.59mm +/- 0.01	11.16mm +/- 0.01	2.58mm +/- 0.01
	% (b/a)	**52.8%** +/- 0.8%	-	**49.0%** +/- 1.2%

The volume shrinkage incurred during uniaxial compression, approximately 50%, can be attributed to the removal of available void volume in the matrix, which was shown above to be 46.5% in the drug region (inner section) and 54.8% in the outer region.

The pressed and un-pressed tablets were then mounted in EpoThin™ (Buehler) epoxy and cross-sectioned to observe the internal detail and surface finish. Macro-photos were taken of the cross sections under UV light. The fluorescein in the drug section fluoresces and therefore makes it possible to distinguish between the two regions of the tablet. Figure 3.9 shows the cross

sections of the un-pressed and pressed tablets. Table 3.3 lists the internal measurements obtained by digital analysis of these cross sections.

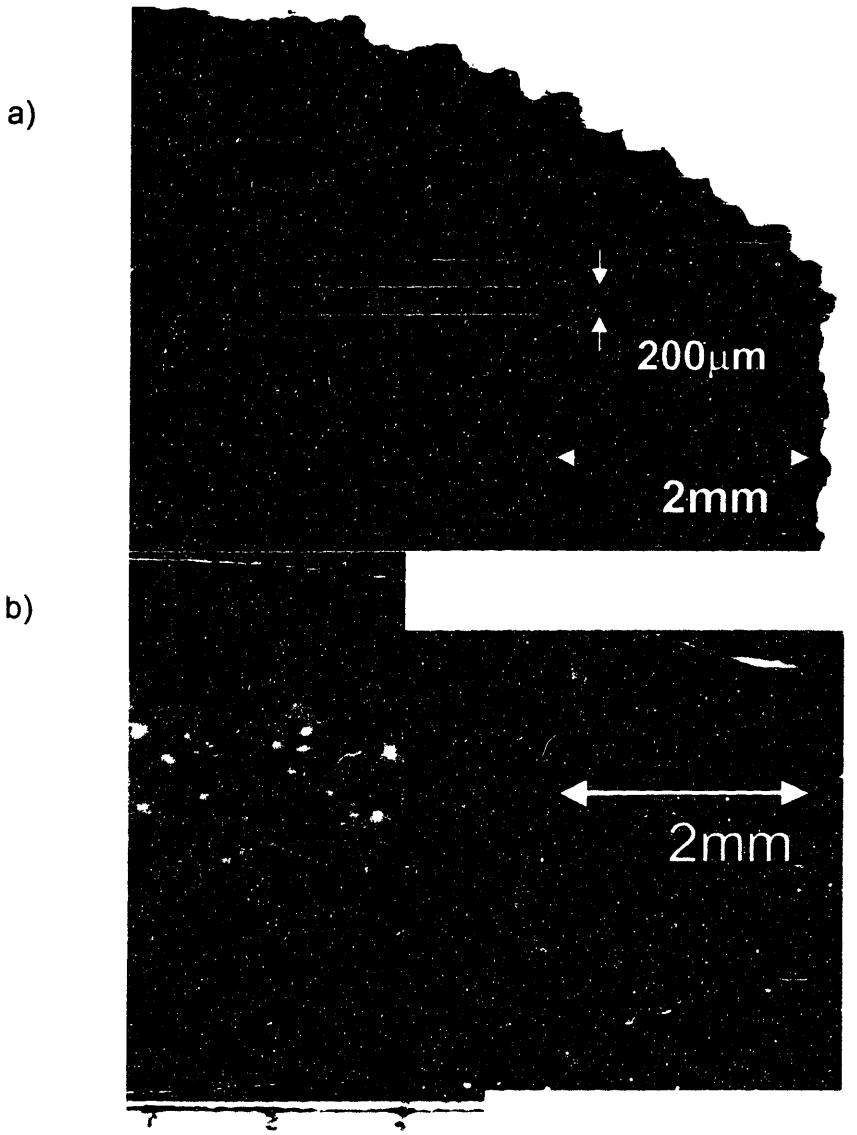

Figure 3.9 Photos of internal naproxen section under 510nm light
a) Un-pressed tablet section showing 200μm stepping b) Pressed tablet section

Table 3.3 Internal measurements of naproxen contour tablet un-pressed and pressed

		Height Drug Region mm	Diameter Drug Region mm	Wall Thickness mm
a	Un-Pressed	5.00 +/-0.1	7.1 +/-0.1	2.06 +/-0.1
b	Pressed	2.47+/- 0.12	8.16 +/- 0.16	1.50+/-0.08
	% (b/a)	**49.4%** +/-2.9%	**115%** +/-3.4%	**72.8%** +/-7%

Table 3.3 shows that there is rearrangement of the material in the pressing procedure. Material moves from a region of high density and low void fraction to regions of lower density and higher void fraction. Figure 3.10 shows the printed naproxen tablets after pressing.

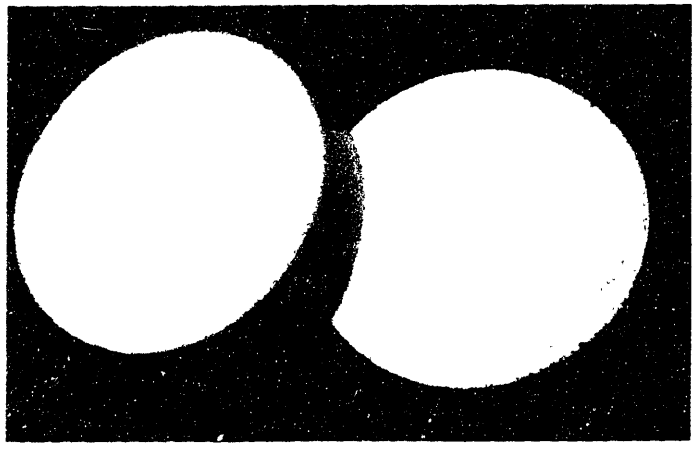

Figure 3.10 Photo of printed and pressed naproxen tablets

3.1.2 Observations and Discussion

The layer height, Δz, used in 3DP directly limits the resolution and ability to fabricate smooth contours. Figure 3.11 shows how decreasing the layer thickness decreased the step size of a curved surface, and increases the number of unit cells available for printing complex geometries.

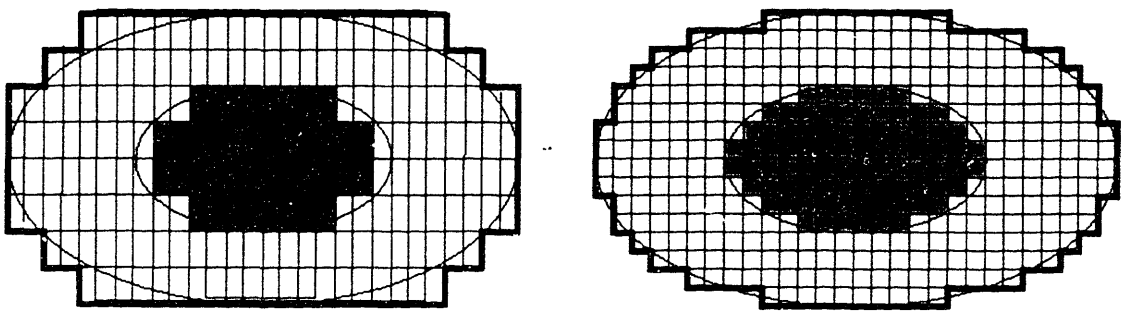

Figure 3.11 Stepping phenomena and unit cell dependency on layer height

A shape is better and better approximated when the layer thickness is decreased, but the time to fabricate a structure becomes correspondingly longer.

The decrease in layer thickness is also limited by the size of the powder used to build the layer. The powder size depends on the electrostatic forces that cause agglomeration and a decrease in flowability. The cross-over diameter between the gravitational force and the Hamaker attractive force was found to be ~40μm based on theoretical calculations for common 3DP polymeric powders, and confirmed through empirical spreading tests.

The surface roughness of each of the tablets, excluding layer to layer steps, is on the scale of the particle size used in fabrication. This is especially

illustrated at the ends of layers where the printed section is in contact with dry powder.

Layer height for spray-dried lactose is limited to higher than 125μm. This limit was found by measuring the spread density of various layer heights for 38-53μm lactose powder, and determining the lowest layer height where spread density equaled tap density. The results of these measurements show that below a minimum layer height, powder does not pack efficiently. Powder particles may be dragged in the spread direction leaving low density wakes behind them if the layer height is too small. It can be seen from Table 3.1 that the minimum layer heights are at least a factor of 2 larger than the largest particle size in the corresponding range.

Spray coating has been shown to decrease surface roughness, but does not eliminate stepping. Coating also increases the size of the tablets, thereby decreasing the dosage per unit tablet volume.

Uniaxial pressing greatly enhances the surface characteristics. It also enhances the interior vertical resolution, as the effective layer thickness is smaller after pressing. It does not, however, improve the resolution in the horizontal or radial direction. Compression eliminates the void volume of these forms, and shrinkage occurs up to the void volume. Material can transport out along a horizontal plane, perpendicular to the pressing axis, if there is a difference in void volume or density between two regions. Material will move from a region of high density and low void volume to a region of low density and high void volume. This transfer should be taken into account in tablet design if pressing is to be employed.

3.2 Migration Inhibition in Pharmaceutical Powder Systems

Excessive fluid migration is an undesirable effect after a volume of fluid has been printed into the powder bed. Some migration is needed, as the two dimensional patterns stitch together in the third dimension when fluid from one printed layer is able to migrate into the previous layer just enough for adhesion. Layer adhesion should take place as close to the boundary as possible. It has been shown that the coalesced line diameter changes about 20% in most cases[30]. This would lead to layer adhesion that occurs over a scale of ~30μm to 50μm for primitive diameters of 150μm to 250μm.

Figure 3.12a shows a tablet array in which extreme fluid migration or bleeding has occurred. These tablets were fabricated using a powder system of 74-106μm microcrystalline cellulose saturated to 90% by a binding solution of 35wt% sucrose in D.I. water. The tablets, spaced 2mm apart, have all been connected by the migrating binder fluid. Figure 3.12b shows the desired tablet separation.

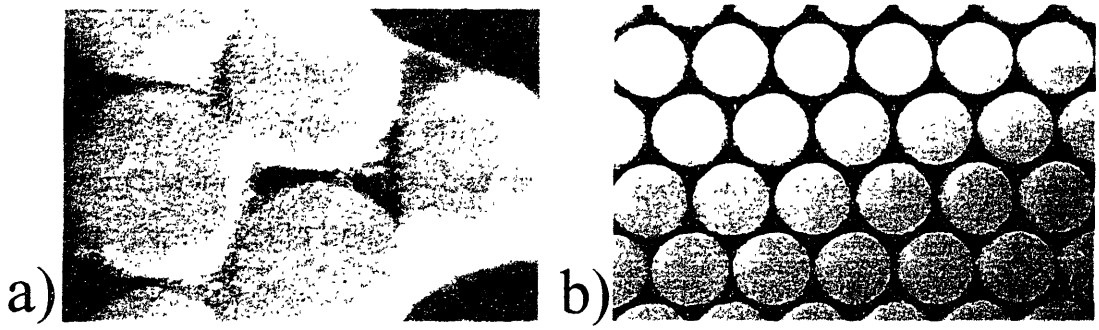

Figure 3.12 a) Undesirable fluid migration in a powder bed
b) Same samples with migration inhibition

Figure 3.12 illustrates the dire need for migration control in these systems. Two approaches to this problem have been taken. The first is based on using powder additives to either decrease the permeability of the powder by mechanism of polymer swelling, or increase the viscosity of the fluid and slow the

transport by additive dissolution and gelation. The second approach involves pre-printing barriers to migration. Such barriers or walls would limit the fluid to the printed regions due to the difference in capillary pressures in powders of different saturations.

The mechanics of fluid interaction within the powder bed will first be considered in section 3.2.1 to provide background. Section 3.2.2 outlines the experiments and techniques used to attempt migration inhibition and section 3.2.3 includes observations and discussion.

3.2.1 The four stages of droplet interaction

Several researchers have thoroughly characterized the process of droplet-powder bed interaction.[1, 30, 37] Wu has identified four main stages of droplet interaction during three dimensional printing. The four stages of droplet impact are ballistic impact, imbibition and drainage, dissolution and/or swelling of constituents in the powder bed, and finally evaporation and re-precipitation. These stages are illustrated in Figure 3.13.

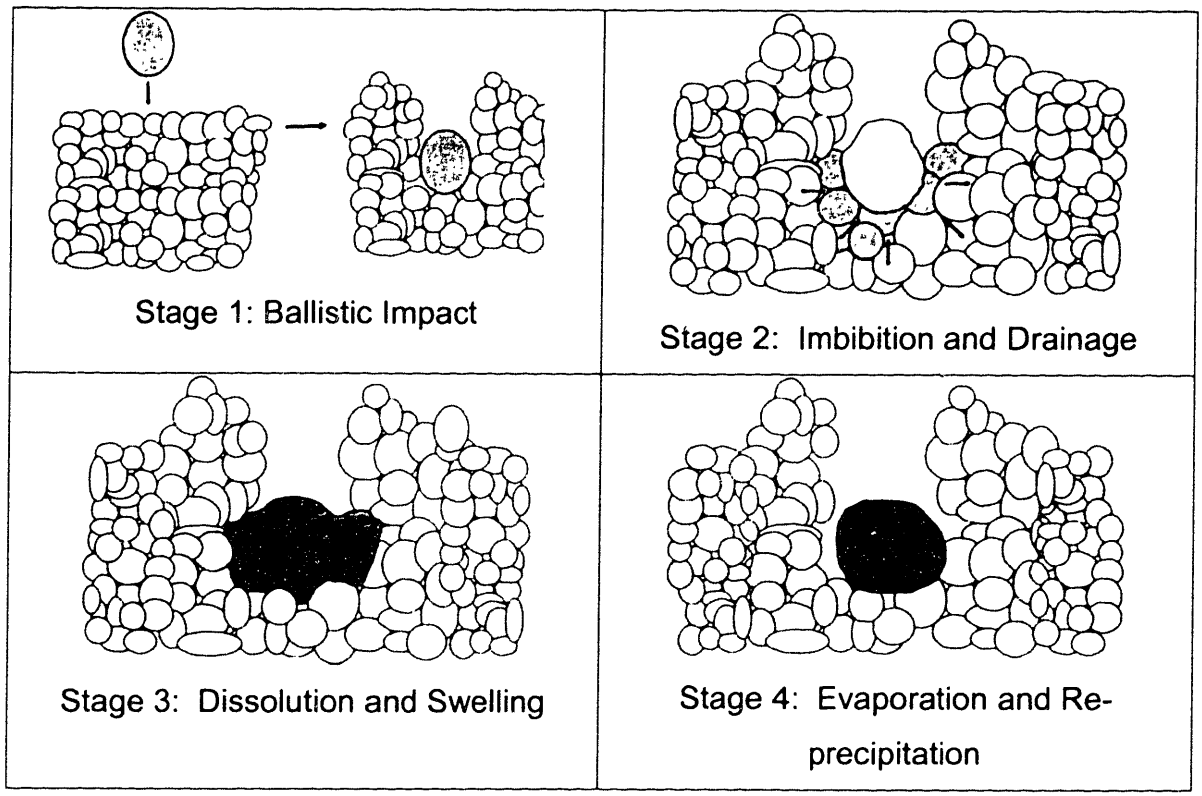

Figure 3.13 The four stages of droplet interaction[1].

3.2.1.1 Ballistic Impact

A printed droplet first interacts with the powder bed during the ballistic impact stage. This stage is described above in section 3.1. This initial stage has been shown to occur over a period of 10^{-4} seconds from the point of contact through complete deceleration based on an initial droplet velocity of 10 m/sec in 30μm particles of alumina with a packing fraction of 40%.[30] Fan[32] also measured this time to be less than 1 msec using high speed photography with droplets 90μm in diameter impacting alumina 10-23μm and 40% packing at 10 m/s. Similar time scales for ballistic impact are expected for polymer systems.

3.2.1.2 Imbibition and drainage – capillary equilibration

The second stage is that of imbibition and drainage. The initial powder-fluid mixture begins to migrate from the saturated core within the crater, and drains into neighboring pores. This drainage depends greatly on the saturation of the powder bed. The saturation parameter, or the fraction of void volume filled with printed fluid, should be below unity, or else fluid automatically spills over into unprinted regions and bleeding results. Figure 3.14 shows a diagram of a wetting fluid in a porous medium with a saturation less than one.

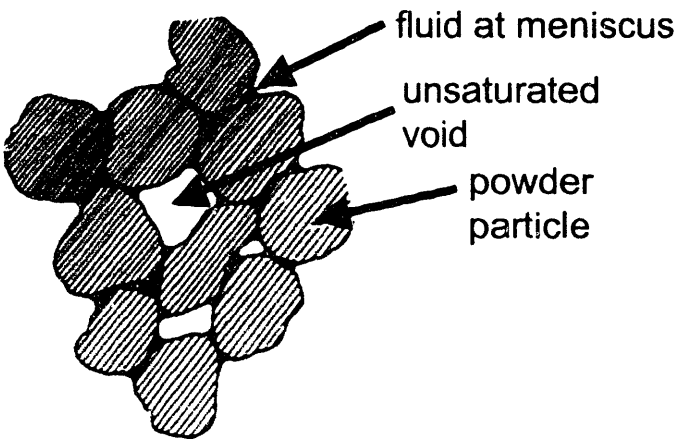

Figure 3.14 Saturation of a porous medium with a wetting fluid

A volume of packed powder can be saturated up to a saturation of unity during one print pass. The solvent can then be allowed to dry, and more solution may be printed into the same region. Printing several times into one region, and allowing for time for evaporation, is the only case in which saturations greater than unity can be achieved without automatic bleeding out of a region of powder. The saturation parameter, S, is given by

$$S = N \frac{q}{v_{fast} \rho_{sol} (1 - p_f) w} \qquad 3.3$$

where N is the number of print passes over one region, q is the mass flow rate, v_{fast} is the printhead velocity along the fast axis, ρ_{sol} is the density of the printed solution, p_f is the powder packing fraction, w is the individual layer height, and l is the spacing between adjacent printed lines. The volume fraction of printed solute (polymer, drug, other additive) can then be defined as

$$\text{Vol. fract. additive} = \theta = \frac{S(1-p_f)\rho_{sol}}{\rho_{add}} \qquad 3.4$$

where ρ_{add} is the bulk density of the additive, i.e. the polymer binder material, the drug, or other additive. The Vol. fract. polymer, for example, is an important parameter in determining the strength and diffusivity characteristics of the printed matrix (see chapter 5) as the printed material, present as a solute, often deposits at the necks between particles once the solvent evaporates.

The saturation of one print pass must be below unity to prevent automatic bleeding from occurring, but some fluid migration does occur even for saturations less than one. This is because small pores surrounding a saturated region exhibit large capillary forces and large pores tend to offer less resistance to fluid drainage. Consider the hydraulic element in Figure 3.15 below.

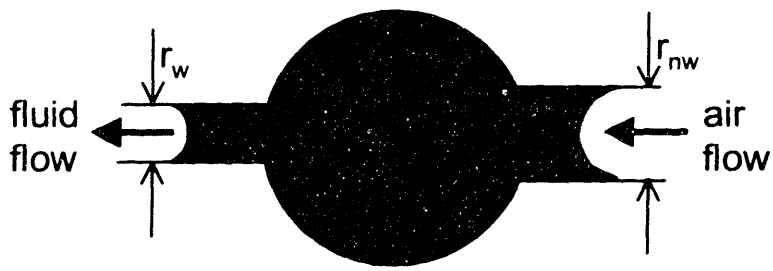

Figure 3.15 Fluid advancement between two pores

Fluid flows from right to left in Figure 3.15 as it is motivated by a capillary pressure difference. This capillary pressure difference is

$$\Delta P = 2\sigma_{LV}\left[\frac{\cos\theta_{adv}}{r_w} - \frac{\cos\theta_{rec}}{r_{nw}}\right] \qquad 3.5$$

Infiltration fronts in porous media can be fractal in nature in this case.[38] A fractal structure can be expected if fluid percolates outward along a network of larger pores, or ducts, as it is pulled along by the capillary suction of smaller pores along the way. This occurs until the lower limit of saturation in which the fluid in the ducts becomes discontinuous. Such percolation has observed especially for the case in which powder particles contain pores that are much smaller than the radius of curvature of the interparticle voids. Such voids act as ducts through which fluid drains en route to filling the smaller pores along the way. The time scale over which this percolation occurs depends greatly on the connectivity, the number of small pores available for infiltration at the fluid front, the available volume within the small pores, the viscosity of the fluid, etc.[38]

Bear has shown that capillary pressure motivating such transport is dependent on the packing fraction of the powder, the contact angle, the surface tension of the migrating fluid, and the saturation:

$$P_{cap} = P_{cap}(S, p_f, \sigma_{LV}, \theta) \qquad 3.6^{30}$$

Such dependence occurs over a length scale greater than the pore size since that is the scale over which saturation is defined. Still, such a dependency is important in considering average capillary pressures over adjacent regions of a powder bed. A typical curve of saturation dependent capillary pressure for saturation is given in Figure 3.16.

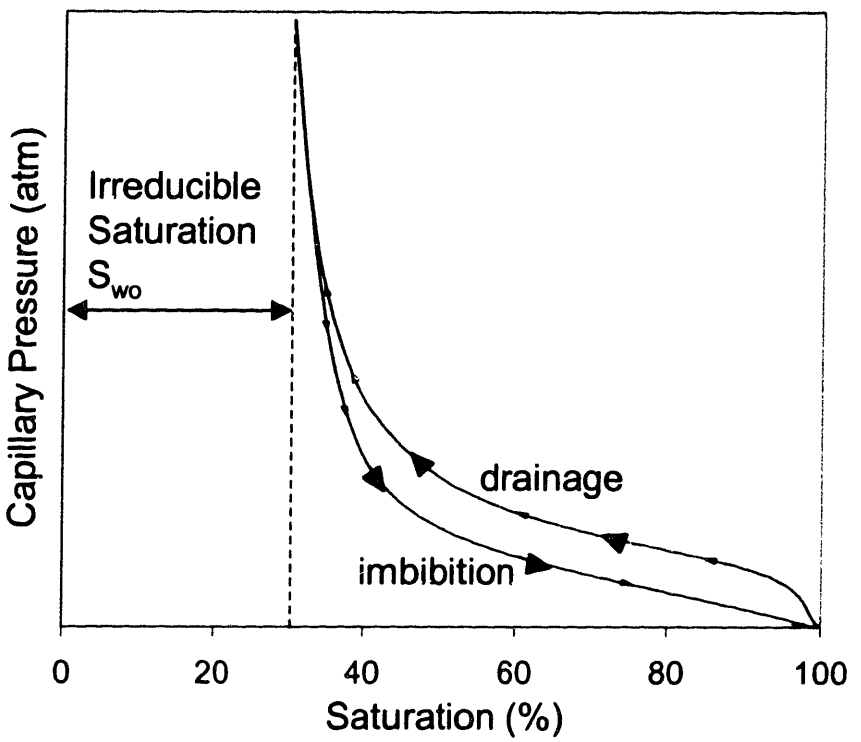

Figure 3.16 Typical saturation dependent capillary pressure [39]

The hysteretic relationship existing between capillary pressure and fluid saturation depends on the flow direction. The capillary pressure is higher for drainage than imbibition for a given saturation. Furthermore, it can be seen that upon drainage, an irreducible saturation of discontinuous fluid exists which is immobile and cannot reach from one pore to the next. This state is known as the pendular state when the fluid becomes confined at the menisci of high curvature.[39] The saturation at the transition to this state from the funicular state, where the fluid has finite mobility, is the irreducible wetting saturation, S_{wo}, or the non-wetting percolation threshold.[30] It has been shown that this transition occurs at saturations of approximately ~0.3 for several powder systems of varying packing fraction.[39]

Bredt reports that, in 3DP, fluid is delivered to one point on the powder surface that becomes fully saturated. This central saturated core is surrounded

by dry powder. As fluid migration progresses, the saturated regions drain and follow the drainage curve. The unsaturated regions imbibe and follow the imbibition curve. Equilibration was found to occur when the two regions reached equal capillary pressures, thus $\Delta P=0$. At this point, the two regions have different saturations in equilibration due to the hysteresis of the curve. The time for a saturated region to equilibrate with a dry powder region for alumina powder was found to be on the order of milliseconds.[30] It was found that the migration rate was sufficiently rapid to allow liquid binder to migrate as far as 1mm in alumina 30μm powder with line spacing of 200μm.[30] To explain this property of 3DP features, it is necessary to develop a percolation model for binder fluid through a network of pores in the porous powder bed.

Wu[1] reasoned that the above models consider fluid reservoirs that are infinite in nature, but the fluids printed during 3DP are finite in volume, and therefore the equilibration kinetics should be faster. Thermodynamic analysis and kinetic models have shown that the penetration of finite fluid volumes into porous capillary systems is different than that of an infinite reservoir. Such examples include ink jet printing, spray painting and other wicking involving infinite fluid volumes.[40, 41, 42] Thermodynamic analysis by Murmur shows that the finite dimensions of the medium and liquid reservoir or droplet are important in determining the phenomenon of penetration.[43] He considered two limiting regimes to account for the effect of geometry in radial spreading and a shrinking liquid reservoir. He concluded that the radius of penetration scaled with $t^{1/6}$. proportional to radius assuming unlimited surface area for penetration.

The total surface area available for drainage in 3DP depends on the position of the printed line. This is illustrated in Figure 3.17.

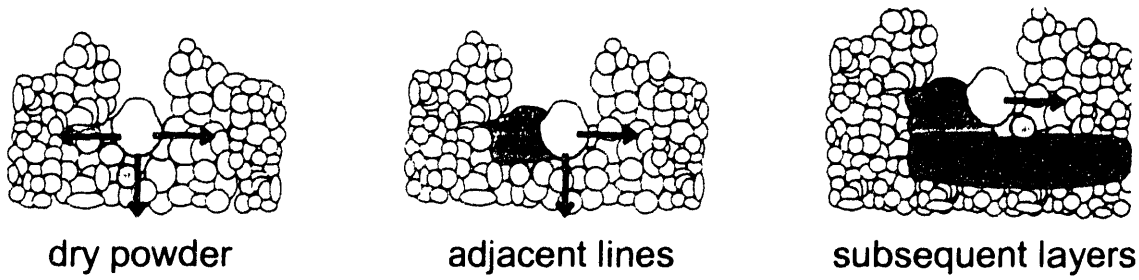

Figure 3.17 Directions available for capillary infiltration during printing[1]

Fluid lines printed into unprinted dry powder experience capillary suction in the 3 directions shown ignoring end effects. Adjacent lines only experience migration in two directions. Lines printed in subsequent layers may only experience migration in one direction.

3.2.1.3 Dissolution and Swelling

The third stage of droplet/powder interaction is that of dissolution and/or swelling. This stage only applies if constituents in the powder bed are capable of either dissolving or swelling in the printed fluid. The time for dissolution and swelling depends on the mechanism and materials properties of the substance. The dissolution or swelling of added constituents could become important to fluid migration from a printed region if the mechanism rapidly increases the viscosity of the fluid or decreases the permeability of the powder bed. This must occur over a time which fluid is migrating in order to help limit the ultimate migration distance.

Wu[1] has found that some polymer-solvent combinations require a minimum dissolution time which was found to be reptation limited and depend heavily on molecular weight.[1] It was found that PLGA particles (85:15 M_W=108,000) less than 75μm in diameter dissolve with a minimum time of 1.25 seconds. DeGennes[44] estimated the molecular weight dependence on minimum reptation time to scale with molecular weight to the third powder, $t_{rep} \alpha M_W^3$. Other researchers predict dependences between powers of 2.9 and 3.4.[45]

3.2.1.4 Evaporation and Re-precipitation

The fourth and last stage of interaction involves evaporation of solvent and reprecipitation. Recipitation can involve any solute originally dissolved into the binder fluid or any powder that was dissolved during stage 3. The process of evaporation directly competes with the process of dissolution and/or swelling because the time scales (seconds) are of the same order for the two events.

The drying of a packed powder bed saturated with fluid takes place over two regimes: the constant rate period, and the falling rate period assuming there is no particle rearrangement and the powder is initially packed to tap density. The schematic for these evaporation regimes is shown in Figure 3.18.

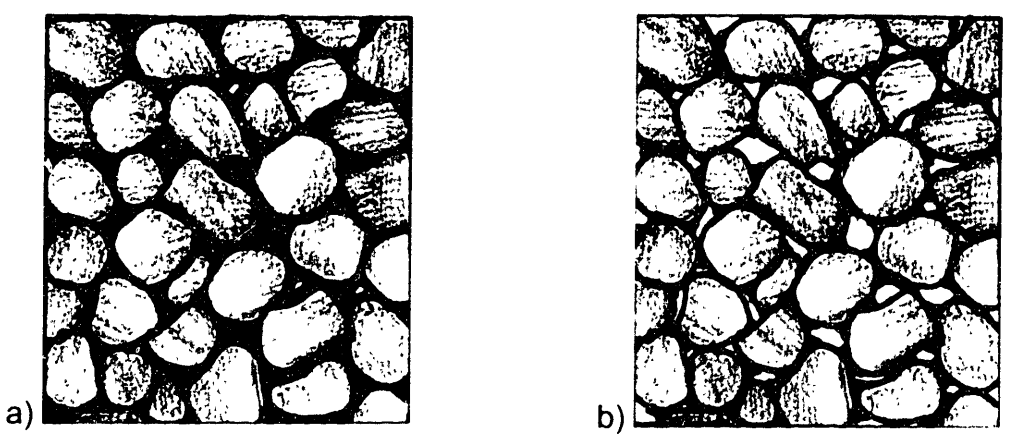

Figure 3.18 Evaporation from a powder bed a) Constant rate period, funicular state, b) Falling rate period, pendular state

Evaporation initially takes place from the external surface of the saturated region. Evaporated fluid at the surface is replenished by liquid transported to the surface from interparticle spaces by fast diffusion and capillary flow.[50] This flow to the surface may cause the transport of solutes such as drug solutes, or small dispersed colloidal particles, such as colloidal drug particles, away from a intended region. Adsorbed polymeric binders, polymers of higher molecular

weight, and gelled binder will resist migration with the fluid, but other constituents may not.[50]

Evaporation occurs with this constant rate from the constant surface area of the saturated region until the fluid in the pores becomes discontinuous in the pendular state. Bear showed that for a wide variety of packed particles, this pendular state occurs when the saturation is about 0.3.[39] Here evaporation begins to occur at the menisci of the pores when the rate of internal fluid transport is lower than the evaporation rate. When the pores begin to become unsaturated, the evaporation rate decreases and the falling rate period begins. During this period, the remaining solution is stationary in the regions of highest curvature. The solutes within the solution begin to precipitate out of solution and deposit at the necks between particles, or in small pores within the particles themselves where the fluid meniscus remains.

Fluid is usually printed near full saturation in the 3DP process, and is only allowed to dry over the period between printing passes in the print, spread, print cycle. A typical cycle can take between 2 and 15 minutes on a lab-scale machine depending on the complexity of the printed pattern. Commercial machines typically operate with cycle times on the order of 10 minutes.[51] A print cycle may or may not allow for sufficient time for drying within one layer. It is plausible for low volatility solvents like water that the saturation of a layer could remain above ~0.3, meaning the pores are still connected by fluid, before a new saturated layer is printed in the adjacent upper layer. The evaporation surface changes in this case and fluid from the first layer may still be able to transport by diffusion to the new surface. The evaporation rate of water during a constant rate period (constant surface area) is approximately 2.85×10^{-6} g/sec-cm^2 at room temperature without forced convection.[1] A typical printed layer of 1 cm x 1cm and 200μm in height printed to a saturation of 100% in a powder of packing fraction 0.5 could take up to ~60 minutes to completely dry or ~40 minutes to

decrease to a saturation of 0.3 using this evaporation rate and assuming evaporation from the top surface only in the absence of capillary forces.

The evaporation of water may also cause condensation in dry powder causing appearance of moist powder around part after sufficient time has elapsed. This phenomenon is different than bleeding, but if the moisture by condensation approaches a saturation of s_{wo}, this could affect the external feature resolution, especially in situations where the powder is hygroscopic, such as is the case with lactose and other pharmaceutical excipient powders. Care should be taken to remove excess powder shortly after the fabrication is completed to avoid this phenomenon, except perhaps in the case where overhangs or other features need the support of the powder bed before sufficient strength is achieved during drying.

3.2.2 Experimental

Transport effects during initial fluid imbibition and later upon migration during evaporation can have serious implications for the internal resolution of features printed with compositional gradients and boundaries, such as those in complex drug delivery forms. The experimental section below explores the transport effects in 4 different systems and the times over which such effects take place.

3.2.2.1 Dissolution of E100 and L100 grains, Swelling of Cornstarch Grains.

Fine particles (<38μm) have been added to some powder systems in attempt to arrest migration either during the initial drainage or during evaporation. The kinetics of dissolution of these particles have been observed using optical microscopy. Individual grains of both E100 (M_W = 150,000) and L100 (M_W= 135,000) were placed onto glass microscope slides and observed under 375X

magnification. Droplets of ethanol, a good solvent for these materials, were added to the glass slides in such a way that the wetting ethanol front would interact with the grain from the side, and then surround it. Dissolution times were estimated as the time between initial contact and the point at which the particle was no longer distinguishable from the surrounding transparent medium.

The dissolution of E100 and L100 grains, all less than 38μm in diameter, took place between 2 and 4 seconds. Fifteen grains were observed between 10 and 38μm, and nearly all of them dissolved in 3 seconds.

It was previously reported[1] that various viscosity grades of PLLA were dissolved in chloroform to give minimum reptation times that were proportional to $M_w^{2.6}$, such that $t_{rep}=kM_w^n$ with $k=\sim 1x10^{-13}$ and n=2.6. A PLLA with M_w=132,000 had a minimum repation time of 2.1 seconds, for example[1]. Other investigators have found similar relationships for a wide range of polymers reptating in good solvents with the power n ranging between 2.6 and 3.4. [44, 45, 46] This molecular weight dependence on dissolution time predicts minimum dissolution times of 3.0 seconds for E100 (M_w=150,000) grains, and 2.3 seconds for L100 (M_w= 135,000) grains if the same relationship and proportionality constant ($k=\sim 1x10^{-13}$ and n=2.6) is applied. These estimates are in good agreement with the observed dissolution times for these materials.

Fine particle grains of cornstarch (Argo) were also observed upon initial contact with D.I. water in the same manner as above. The cornstarch grains were observed to swell at least double in size in 10 seconds at room temperature. Figure 3.19 shows these grains before contact with D.I. water, and after 10 seconds immersed in D.I. water.

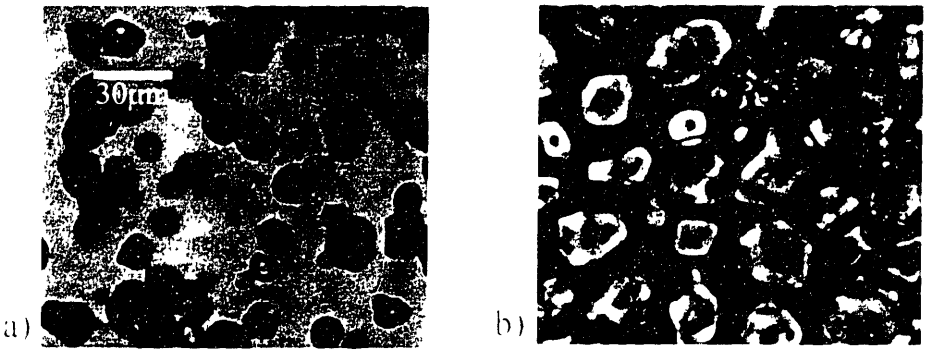

Figure 3.19 a) Cornstarch grains b) cornstarch grains in water at room temperature for 10 seconds

3 2 2 2 Viscosity of E100 in Ethanol

The viscosities of E100/ethanol solutions were measured at 150 1 sec on a parallel plate rheometer (Paar Physica) at 25 °C using a plate 7 5cm in diameter with a gap of 0 5mm and a solvent trap to prevent evaporation The viscosities for various concentrations are plotted in Figure 3 20

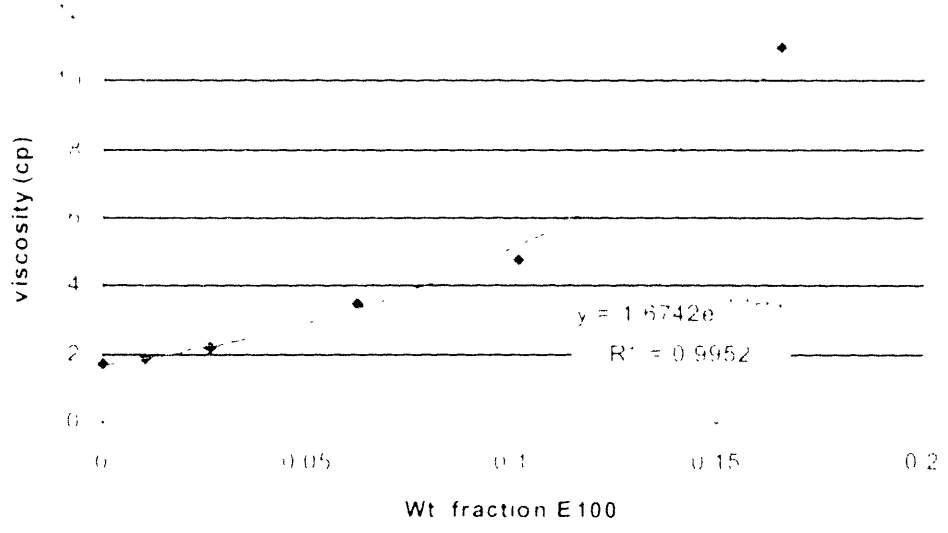

Figure 3.20 Viscosity vs concentration for E100 / ethanol solutions

The viscosity increases as the concentration increases. This can occur during printing from the evaporation of solvent or by the dissolution of distributed fine particles of E100.

Given the large increase in viscosity with E100 concentration in ethanol, an estimate of time dependent viscosity has been made during evaporation from the surface of a printed unit cell assuming constant surface area and an evaporation rate of -2.7×10^{-5}g/sec-cm^2. This evaporation rate was obtained by mass/time data for evaporation of ethanol in this solution from a constant surface area. This increase in viscosity over time is estimated for the evaporation of solvent only, and does not take into account dissolution of any solute grains that may be present in the powder bed.

The above concentration dependent viscosity was best fit to an exponential curve such that viscosity (cP) $\eta(x)= 1.6742\exp(11.166x)$, where x is the wt. fraction of E100 in ethanol. The concentration during evaporation is time dependent, and x=C(t). The concentration over time can be given by considering evaporation out of a printed unit cell with dimensions Δw (line spacing), Δh (layer height) and an arbitrary length Δl, such that

$$C(t) = \frac{fV_i\rho_b}{RSt + V_i\rho_b} \qquad 3.7$$

where f is the solids loading fraction of solute in solution, $V_i = \Delta l \Delta w \Delta h$, S = surface area available for evaporation, R is the evaporation rate(negative), and ρ_b is the density of the binder solution. The viscosity (C(t)) for evaporation of 12wt% E100/ethanol from a printed feature of typical line spacing of 120μm, typical layer height of 200μm, and typical tablet length of 1cm, is shown in Figure 3.20 below.

Figure 3.21 shows that the viscosity increases sharply over times less than 30 seconds depending on the surface area available for evaporation. A

surface area of 100% represents evaporation from the top surface of the unit cell of 1 cm in length and 12μm in width and assumes no spreading. The viscosity at the solubility limit of E100 in ethanol (~17wt%) was estimated from the viscosity dependence on concentration shown in Figure 3.20 above. Evaporation happens within 20 seconds before this limit for the surface areas considered.

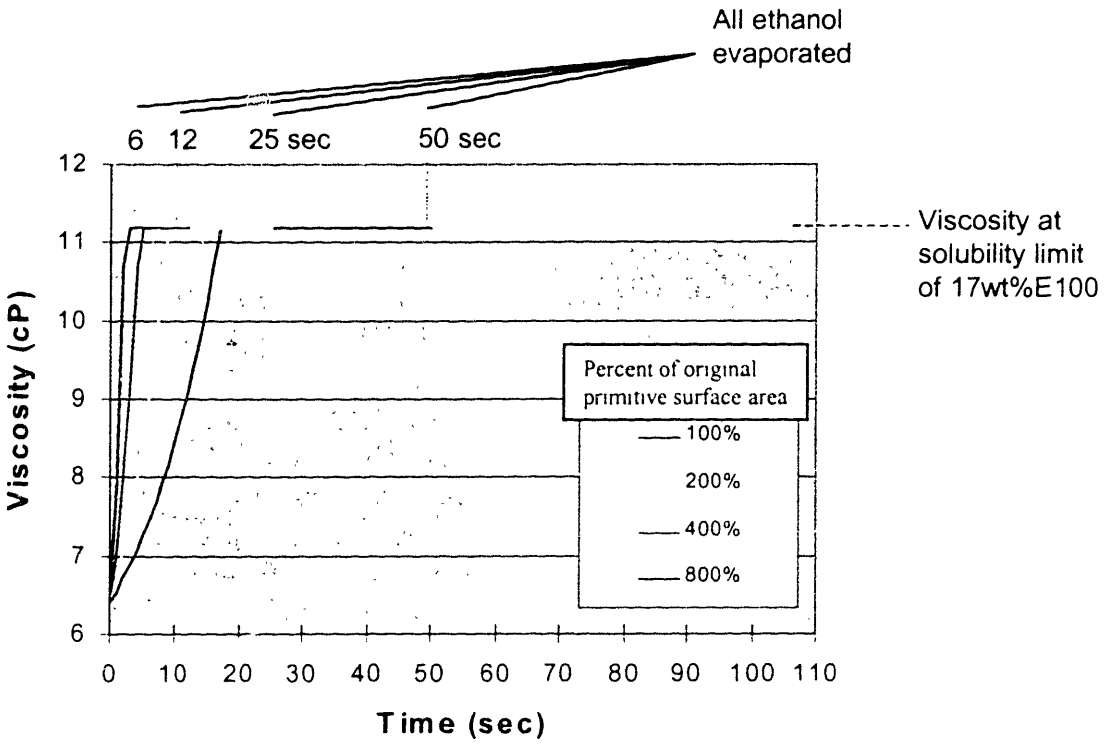

Figure 3.21 Viscosity over time during evaporation from a printed unit cell

3.2.2.3 Porosimetry and SEM of Lactose Samples with Varying L100 vol %

Powder samples of spray-dried lactose in the size range of 53-74μm were tested for intrusion volume available for infiltration or porosity using mercury porosimetry. Three samples were measured to determine the effect of saturating the powders with L100/ethanol solutions to achieve different polymer volume fractions. Two of the three powder samples of 1 cc tapped to tap density were saturated with L100/ethanol solutions to fill part of the void volume of the powder

such that sample 2 contained 3.2 vol% L100, and sample 3 contained 6.0vol% L100. Sample 1 was untreated lactose control powder. The powder samples were stirred well to achieve uniform saturation, and were allowed to dry at 30°C in a drying oven over night. The powder samples were then lightly ground with a mortar and pestle to break some of the necks formed in the process. Powder from the three samples was then both tested for infiltration volume by mercury porosimetry, and imaged using an SEM.

SEM: Samples containing 0 and 3.2vol% L100 polymer were observed using 5 KeV. The two images are shown in Figure 3.22.

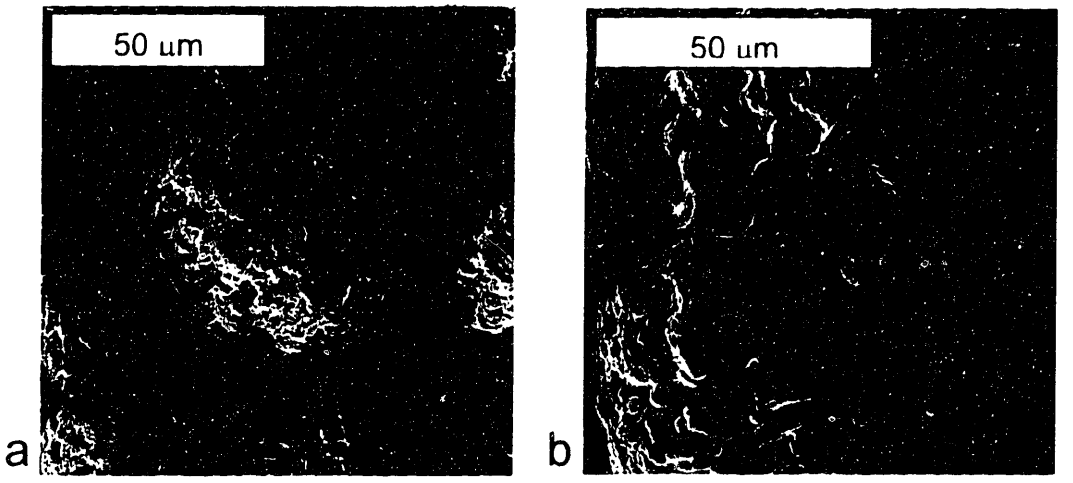

Figure 3.22 SEM micrographs of 0.0 Vol% and 3.2 Vol% L100 in Lactose powder 53-74µm

Mercury Porosimetry: Powder containing 0, 3.2, and 6.0vol% L100 were tested for infiltration volume using low pressure porosimetry. (Micromeritics Autopore 9220) Figure 3.23 shows the Incremental mercury intrusion volume vs. pore size.

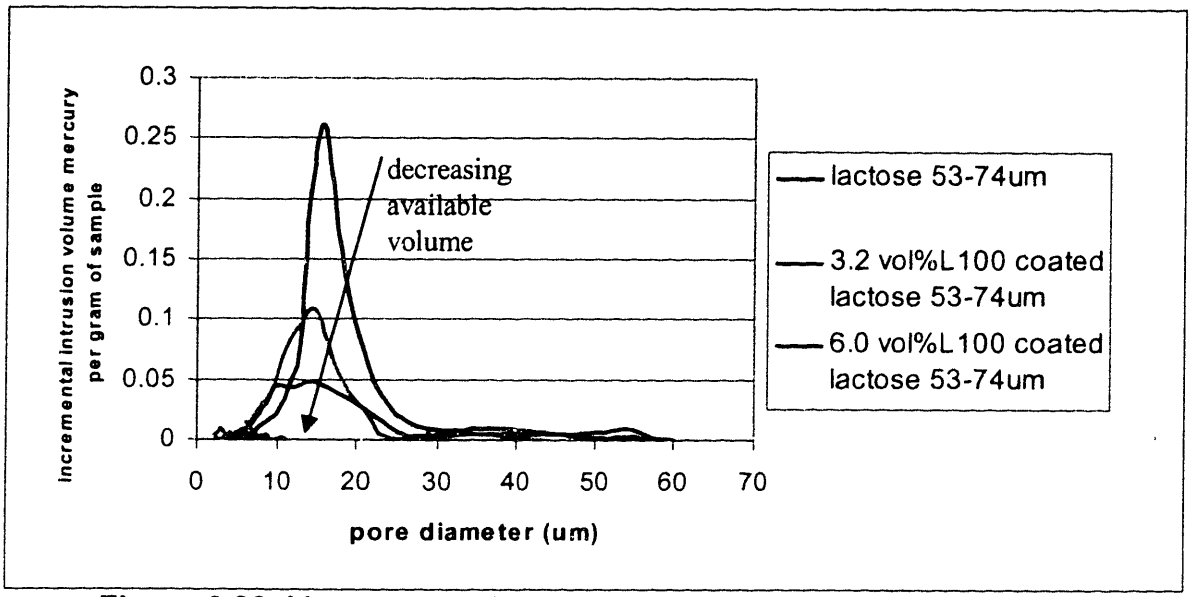

Figure 3.23 Mercury porosimetry low pressure incremental infiltration volume vs. pore diameter for 3 volume fractions of L100 polymer

The SEM images show that the L100 polymer tends to both close off pores within the lactose particles, and deposit at the necks between particles. The particle surface infiltrated with the 3.2 vol% L100 also appears smoother in some sections showing that some coating of the particle surface occurred. The Mercury porosimetry data also showed that the available volume for infiltration decreased as the polymer vol% increased. The pores within the lactose spray-dried granules become closed off or filled during the saturation and precipitation process.

3.2.2.4 Printed Sandwich Structures

Sandwich structures were fabricated by 3DP with the design shown in Figure 3.24 below.

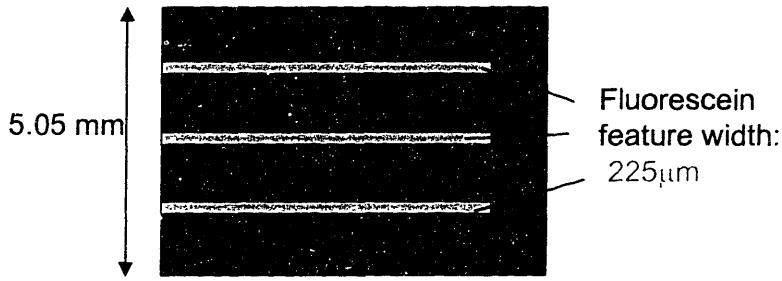

Figure 3.24 Design of sandwich structures

The sandwiches were designed such that layers 1-4, 6-10, and 18-22 were printed with only binder fluid, and layers 5, 11, and 17 contain binder solution with fluorescein tracing dye. The dye was used to visually map the migration of fluid out of the printed layer and into the surrounding layers.

Four sets of samples were fabricated. Two of the sets were printed with aqueous binder fluid, 40wt% sucrose in D.I. H_2O, and the other two were printed with ethanol based binder solution, 7wt%E100 in ethanol. The samples were all printed to 100% saturation. Each binder solution was then printed into two types of powder beds: lactose 74-106μm, or lactose 74-106μm + fine migration inhibitor particles. The fine particles (<38μm) mixed into the powder were cornstarch (see Appendix 1) for the aqueous binder solution, and E100 for the ethanol based solution. Furthermore, the four sets of samples were split into two groups: one group of samples was dried every printed layer for 15 seconds with a heating lamp (temperature at the powder bed was estimated to be 80°C after 15 seconds) and one group was not dried between layers. It took approximately 2 minutes to complete one print cycle before each subsequent layer was spread and printed during which some evaporation occurred in all samples. The 8 resulting samples are listed below in Table 3.4 below.

Table 3.4 Eight sandwich structures

Sample	Binder	Powder additive	Layer drying
1	40wt% sucrose / D.I. H_2O	-	No
2	40wt% sucrose / D.I. H_2O	-	Yes
3	40wt% sucrose / D.I. H_2O	10wt% cornstarch fines	No
4	40wt% sucrose / D.I. H_2O	10wt% cornstarch fines	Yes
5	12wt%E100 / ethanol	-	No
6	12wt%E100 / ethanol	-	Yes
7	12wt%E100 / ethanol	20wt% E100 fines	No
8	12wt%E100 / ethanol	20wt% E100 fines	Yes

The sandwich structures were allowed to dry for 2 days in a nitrogen filled glove box. They were then set in EpoThin™ (Buehler) epoxy and cross-sectioned perpendicular to the slow axis direction and parallel to the fast axis direction. Each of the samples were photographed under 37.5X magnification on a fluorescence microscope (*source*) using a UV light source and fluorescein compatible filter. The same settings were used to image all samples. The micrographs for the samples that were not dried each layer are shown below in Figure 3.25.

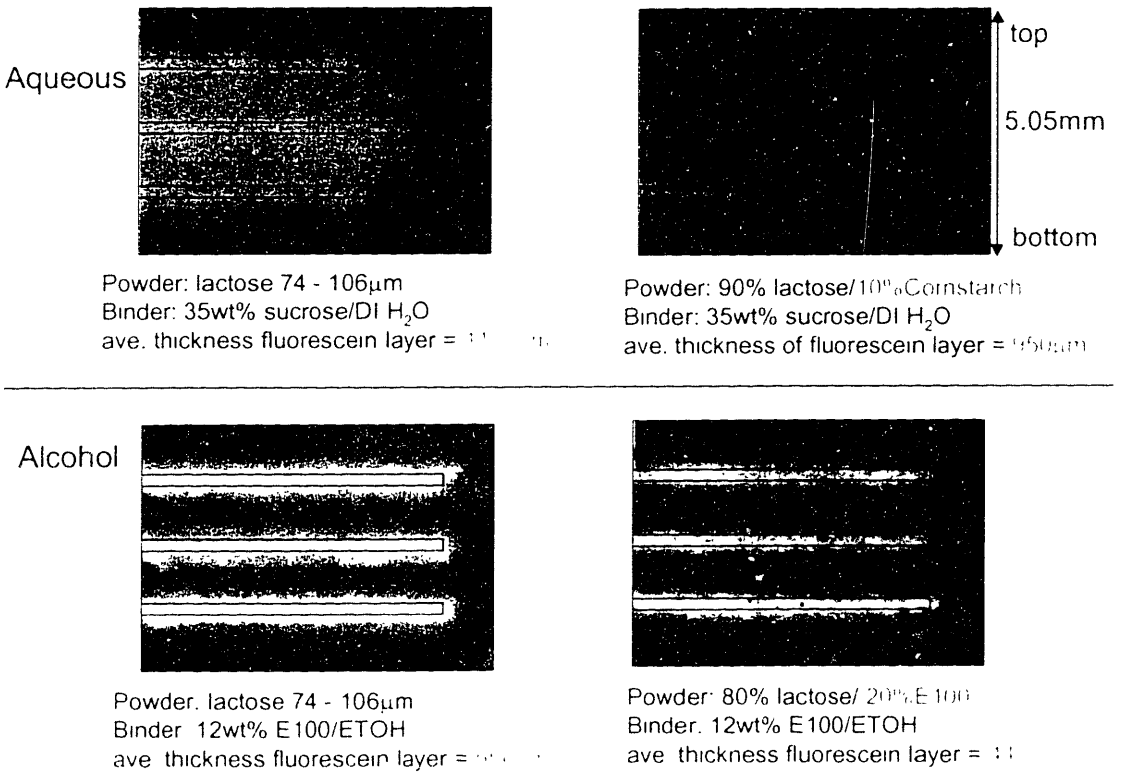

Figure 3.25 Micrographs of the 4 sandwich structures (without layer drying)

The dye position in the vertical (perpendicular to the fast axis) and lengthwise (parallel to the fast axis) was then compared to the intended design. This was done by analyzing the UV micrographs such as those shown in Figure 3.25 for green pixel intensity using a Lab View program[47]. The LabView program was written to across the scan the images, and average the number of green pixels over distance as shown below in Figure 3.26. The output is green pixel number vs. position. The technique was calibrated by scanning UV micrographs of known fluorescein concentrations (in lactose powder) taken with the same photographic parameters. The results of the calibration show that fluorescein concentration scales linearly with green pixel intensity for solutions of 0.05 to 0.15wt% fluorescein saturated to 100% in lactose powder.

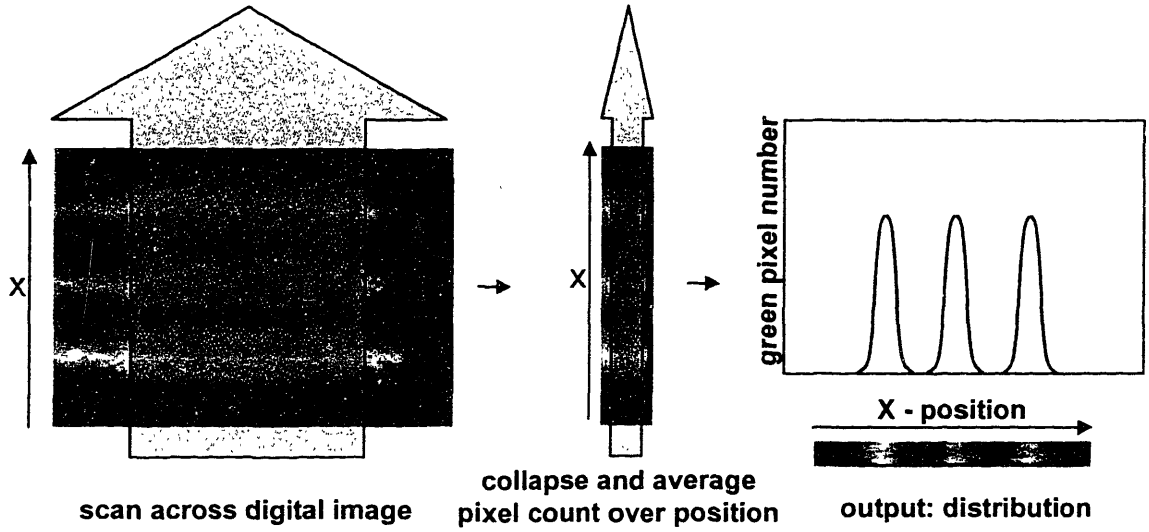

Figure 3.26 Scanning images for green pixel distribution

The fluorescent feature width was defined as the full width at half maximum of the green pixel number peaks. This procedure was done in the two image directions to capture fluorescein migration in the vertical direction and in the direction parallel to the fast axis. The fluorescent feature widths were then divided by the feature width of the printed design (shown in figure 3.23) to give a phenomenological migration ratio:

$$\text{Migration ratio} = MR = \text{fluorescent feature width} \div \text{intended design width} \quad 3.8$$

The intended design width is the layer thickness used into which the fluorescein binder was printed. A migration ratio equal to unity would imply that no stitching of layers would exist in the vertical direction, and no interaction would occur between regions of different composition in the other directions. A migration ratio greater than one is therefore expected to obtain structure cohesion, but large migration ratios would imply that resolution is poor.

The green pixel density for the ethanol binder with E100 fines added as a migration inhibitor is shown in Figure 3.27.

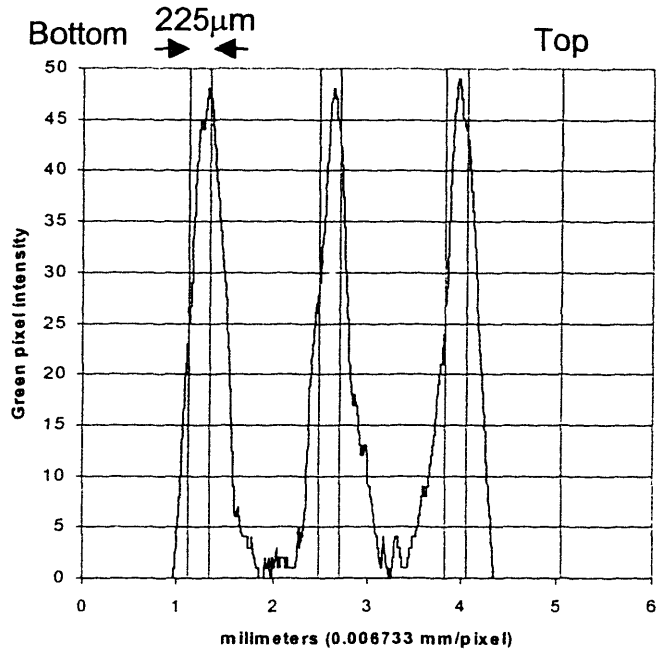

Figure 3.27 Green pixel intensity vs. intended placement for 2wt%E100/ethanol binder printed into 80wt% lactose / 20wt% E100 fines powder

The top of the structure is the right side of the figure, and the bottom of the sample is the left. The green pixel peaks are shown to be centered around the intended regions, with a slight shift to the right (or top) of the structure. Such upward migration of the fluorescein in the binder may result from wicking upward into freshly spread powder.

Table 3.5 below shows the results for migration ratio for the 8 sandwich structures in the vertical direction MR_z. Also given is the average horizontal migration out of the side of the intended regions.

Table 3.5 Migration ratios for the 8 sandwich structures

	Solvent	P_{vapor} [48] (KPa 25C)	Additive	drying	Vertical feature width	MR_z	Horizontal migration μm
1	water	3.17	-	No	1150	5.11	870
2	water	3.17	-	Yes	870	3.85	-
3	water	3.17	cornstarch	No	950	4.22	530
4	water	3.17	cornstarch	Yes	630	2.80	-
5	ethanol	7.9	-	No	550	2.44	310
6	ethanol	7.9	-	Yes	550	2.44	-
7	ethanol	7.9	E100	No	440	1.95	190
8	ethanol	7.9	E100	Yes	430	1.91	-

The best case of migration inhibition is the ethanol based binder solution with E100 grains added to the powder bed. This migration ratio is given in Table 3.5 as MR_z=1.91. Drying the powder bed between layers limited the migration of fluorescein in all cases. The ethanol-based solutions also showed much better feature control than the aqueous-based solutions. The addition of migration inhibitors to both systems also helped to arrest migration.

3.2.2.5 Pre-Printing Migration Barriers

Tablets were constructed with pre-printed walls to limit the migration of aqueous drug solutions from intended regions of drug loading at the center of the tablets. It has been shown[30, 39] that powder exhibits lower capillary suction when it has been saturated. Given the choice of paths for migration, a fluid front would first move towards an un-saturated region, with greater capillary pull, than to a section that has already been saturated. A simple example of this phenomena is shown in Figure 3.28 where a red droplet of sugar water has first been dropped

into lactose powder, and then an equal sized green drop of sugar water is dropped onto the same region.

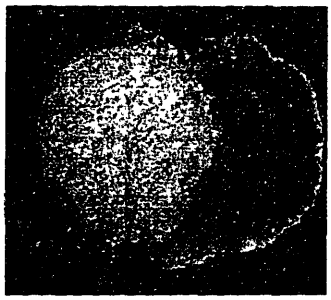

Figure 3.28 Red and green droplets show that saturation occurs preferentially in un-saturated powder of higher capillary suction

The red droplet saturates the powder first stopping upon equilibration. The green droplet does not saturate the same region, instead it saturates a region just outside of the red region.

Section 3.2.2.3 shows also that the available volume for capillary imbibition decreases upon saturation with polymer containing solutions. Furthermore it was shown in section 3.2.2.4 that the migration of ethanol based binder solutions was much lower than that of aqueous based binder solutions. Tablets were therefore designed with outer wall regions, printed first with L100/ethanol solution, and inner drug containing cores, printed second with a naproxen aqueous suspension.

The tablets were fabricated by CJ CD OSP 3DP as follows: 1) 50% Microcrystalline Cellulose (53-74μm) / 50wt% Lactose (53-74μm) was spread into the layer to be printed with thickness of 200μm. 2) Rings were printed into the powder of 11mm O.D. and 7mm I.D using 5wt%L100/ethanol binder solution, and allowed to dry for 2 minutes. The saturation during this first print pass was 1.0. 3) The rings were then re-printed at the same saturation to increase the volume L100 % to 4.8%. 4) Circles were then printed into the rings with 7mm diameters. The drug solution in this section was 22wt% naproxen suspension in D.I. water (Nanosystems, Inc.) + 0.05 wt% fluorescein dye printed with a

saturation of 1.0 for an overall Vol% Naproxen of 10.7%. This procedure is illustrated in Figure 3.29 below.

The tablets were allowed to dry for 72 hours in a nitrogen glove box. They were then set in EpoThin™ epoxy (Buehler) and cross-sectioned. Macrophotos were then taken under UV light. The macrophotos were then scanned for green pixel density using the LabView program described previously in section 3.2.2.4 across the radius of the circular cross-section. Figure 3.29 shows the cross-sectional area and the green pixel density over this area.

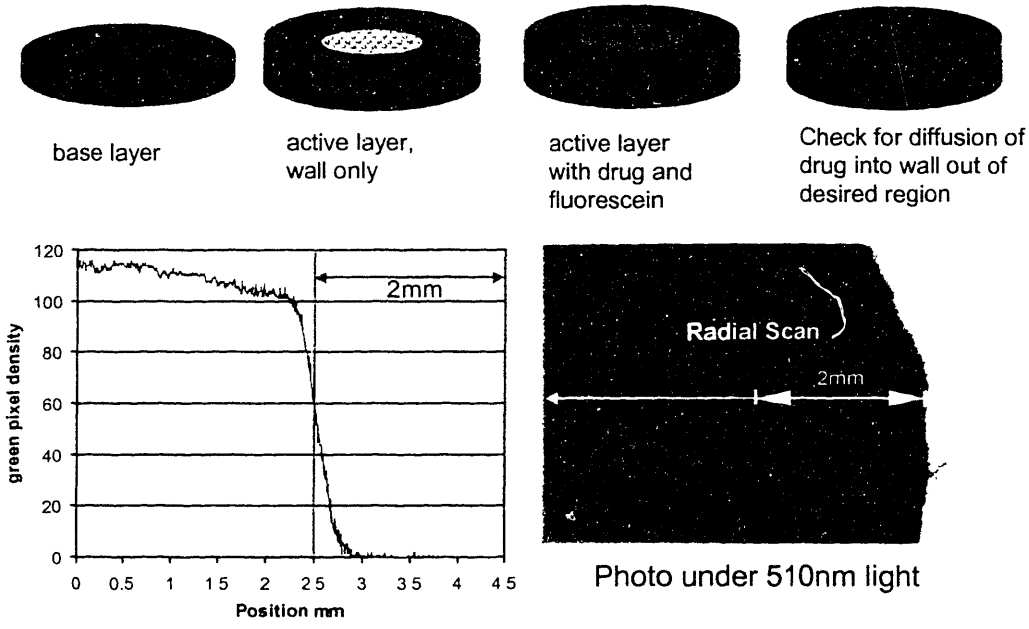

Figure 3.29 a) Procedure for printing pre-saturated walls
b) Radial green pixel density c) Cross-section

The green pixel density over the radius sharply falls off at a radius of 7mm indicating very little migration into the printed wall region. Migration occurs within a distance of ~300μm into the wall region. This can be compared to the migration in the lengthwise or horizontal direction of the aqueous binder solution

out of the intended region in section 3.2.2.4. The horizontal migration in that case was ~870μm.

3.2.3 Summary and Discussion

Migration inhibiting additives:

The addition of migration inhibitors has helped to arrest the migration of fluid in lactose powder beds. This is evident from considering the migration ratios obtained for cases with and without migration inhibiting additives. The cornstarch additive in the aqueous fluid system decreased the migration ratio of a printed feature by 17%. The addition of E100 fines to the ethanol fluid system decreased the migration ratio by 20%. The swelling of cornstarch grains <38μm in excess water to double in size was observed with microscopy on the scale of 10 seconds. The complete dissolution of E100 grains <38μm in size in excess ethanol was observed in ~3 seconds. Measurements also show that the viscosity of E100/ethanol solutions increase quickly with concentration.

The fluid volumetric flow rate through a cross sectional area of flow, U, in a porous media in a funicular state is given by the Hazen-Darcy equation:

$$U = \left(\frac{\kappa}{\eta}\right)\frac{\Delta P}{e} \qquad 3.9^{49}$$

where κ is the specific permeability or hydraulic parameter dependent on the matrix properties but independent of fluid properties, η is the dynamic fluid viscosity, ΔP is the difference in pressures, and e is the effective length of the pores. It can be shown with this equation that the fluid migration rate out of a saturated region is inversely proportional to viscosity, and proportional to the permeability characteristic of the porous media. The viscosity increase observed from the increase in E100 concentration would act to slow the migration rate.

Swelling cornstarch grains within the powder bed would act to close off void volume and block passages of flow, thereby decreasing the permeability of the powder. This decrease in permeability would also result in a decreased migration rate.

Evaporation:

Drying the powder bed between build layers was shown to decrease the migration ratio for the aqueous fluid system. The migration ratio decreased by 25% when drying was employed. Drying in the ethanol fluid system showed little to no improvement in migration ratio. The ethanol fluid systems furthermore showed much smaller migration ratios than the aqueous fluid systems in all cases.

These results show that evaporation plays a major role in the control of migration within these structures. Increasing the evaporation rate in each layer, either by using solvents with higher vapor pressures or by drying, brings the layer to the pendular state more quickly. The pendular state is that in which the fluid in the pores becomes disconnected and has no mobility, and the saturation is below a critical limit, S_{wo}.

Drying each layer in the aqueous fluid system helped to limit the migration due to diffusion within the pores between layers by lowering the saturation. It would take approximately 55 minutes to dry a fully saturated powder of p_f=0.5 and layer height of 200μm from a surface of 1cm^2 in area using an evaporation rate of 2.85 nL/sec-cm^2 [1] for water from an un-vented pool surface. The evaporation rate has been reported to be shorter for evaporation from powder surfaces due to an increased surface area available for evaporation, and evaporation of only ~70% of the fluid is needed before the fluid becomes immobile.[39] It would take ~20 minutes for the saturation to decrease to S_{wo} if the surface area for evaporation is doubled.[1] The approximate time for one print

cycle is 2 minutes, and thus the water in the layers still has enough mobility for inter-layer diffusion to occur within the connected pores.

Drying each layer did not significantly change the migration ratio for the ethanol fluid systems. The evaporation rate of ethanol (~10nL/sec-cm^{2} ^{1}) is significantly higher than that of water. It would take approximately 16 minutes to dry the same fully saturated region, and only ~5.6 minutes for the saturation to decrease to S_{wo} if the surface area for evaporation is doubled. Significant evaporation therefore occurs between layers and additional drying is not advantageous.

Pre-Saturating Regions of the Bed:

The use of pre-saturated migration barriers has been shown to reduce the migration out of designated regions of the powder bed. This has been accomplished by pre-printing walls of ethanol-based fluid to confine interior regions of aqueous-based fluids. The migration of an aqueous fluid out of a printed region using a migration barrier was shown to be less than 300μm. This can be compared to the migration when no barrier was used of ~870μm.

The results of mercury porosimetry on pre-saturated lactose powder show that the available volume for infiltration decreases in the intra-particle pores as the volume fraction of L100 polymer increases.

Fluids in these cases first saturate the smallest pores of highest capillary suction. The fluid first intrudes the intra-particle pores of lactose, and then deposits solute inside the pores and on the particle surfaces. The saturation and deposition in this manner decreases the volume available for later infiltration.

It was shown that fluid will migrate in the direction of highest capillary suction. The capillary pressure depends on the saturation of the powder and available volume for infiltration.[39] The capillary suction of these pores decreases significantly with saturation. This phenomena is shown in Figure 3.16. A

migrating fluid will therefore first migrate into an area of low saturation. This is depicted in Figure 3.28 in which a droplet of fluid avoids pre-saturated powder and migrates into un-saturated powder. This explains why there was less migration for the case where a pre-saturated wall acted to confine newly printed fluid.

The capillary pressure also depends on the contact angle. The contact angle of D.I. water on a smooth pressed lactose surface was measured to be 30°. The contact angle of D.I. water on a smooth pressed L100 surface was measured to be 50° . This means that the pre-printed wall region became less wetting to the water than the designated interior region.

Relative Timing:

Migration can occur either during the initial stages of droplet interaction when the droplet imbibes the powder, or later by diffusion through pores connected with a continuous fluid phase. It is important to consider the timing of these two events.

The initial imbibition stage occurs up until the point of capillary equilibration with surrounding dry powder. It has been previously reported that initial imbibition and drainage of droplets into powder beds during 3DP takes on the order of milliseconds.[30]

The dissolution of E100 grains and the swelling of cornstarch grains, in ethanol and aqueous fluids respectively, occur on the order of a few seconds in these studies. The evaporation of ethanol and aqueous solvents as also been shown to occur in tens of seconds. Viscosity increases due to both the dissolution of E100 grains and the precipitation from solution during evaporation during these time periods. The permeability of the powder in the aqueous case also decreases on the order of seconds as the cornstarch grains swell.

The time scales for dissolution and swelling are too long to affect the migration of material in the initial imbibition and drainage stage. They do,

however, directly compete with migration that occurs during the constant rate of drying, or the funicular state, when the fluid in the pores has finite mobility and the ability to diffuse between layers. It has been shown in Figure 3.21, for example, that it takes on the order of <~50 seconds for complete evaporation from a single printed line of a 12wt%E100 / ethanol solution, and only <~15 seconds for the printed solution to reach the solubility limit of E100. The constant rate period of drying for these features occurs up until the point where the saturation is approximately s_{wo}=~30%. The fine grains of E100 were shown to dissolve with an average time of 3 seconds in excess ethanol. These grains have enough time to dissolve before sufficient fluid has evaporated, and therefore the dissolution in is direct competition with diffusion occurring in connected pores. The increase in viscosity due to the dissolution of E100 grains therefore decreases the migration that occurs due to evaporative transport and due to fast diffusion within connected pores.

This is especially true for the case of aqueous fluids. Capillary equilibration occurs rapidly, but evaporation is sufficiently slow to limit diffusive transport through connected pores. Powder beds printed with water at saturations near unity take longer to reach a pendular state than those with printed with higher vapor pressures such as ethanol. The use of a high vapor pressure solvent, or the use of drying in each layer, was shown to greatly decrease the migration in the lactose powder beds. This is evidence that migration occurs by mixing and diffusion over time within connected pores. The migration ratio decreases when the time between initial fluid interaction and the attainment of a pendular state decreases.

3.3 Summary for Chapter 3

Electrostatic forces limit the size of powder that can be used in dry powder spreading. It has been found that ~40μm is the lower limit for polymeric powders such as those used in the fabrication of 3DP pharmaceuticals both by theoretical calculations of the Hamaker attractive force and by qualitative observation. The smallest layer height that can be achieved has been found to be ~125μm using these powders. Optimal layer heights have been found based on the particle size range used in spreading. These optimal layer heights are the smallest layer height that can be spread to tap density. Layer height determines the stepping phenomena along a curved surface, and the particle size determines the surface roughness along the steps.

Spray-coating was found to decrease the surface roughness of tablets printed by 3DP, but the technique did not eliminate stepping using a layer height of 200μm. Uniaxial pressing of 3DP tablets was shown to greatly enhance the external resolution while not degrading the resolution between two interior regions of different compositions. Material was found, however, to migrate from a region of low void volume and high density to a region of high void volume and low density during compression.

The use of migration inhibitors was found to decrease the migration in both aqueous and ethanol-based binder solutions. The use of these migration inhibitors, present as fine grains of soluble polymer and swellable material, was found to decrease the migration that occurs during evaporation and diffusion between connected pores in the funicular state. The increase in viscosity due to dissolution and the decrease in hydraulic permeability due to swelling did not occur fast enough to provide complete arrest of any initial migration that occurs during droplet interaction and drainage. Overall, the migration of fluorescein in printed features was less for higher vapor pressure solvents and for features that

were dried after printing, thus allowing saturation to be decreased below S_{wo} before the next layer was printed above.

Pre-printing migration barriers helped to confine printed fluid to designated regions of the powder bed. The pre-printed, pre-saturated regions were determined to have lower capillary suction, higher contact angle, and less available volume than the designated neighboring regions.

Controlling both the exterior resolution and interior resolution of tablets printed by 3DP is vitally important. Tablets need to be smooth for both good aesthetic and mechanical properties. It is also important to have good control over the placement of material within the printed device since migration can degrade the functionality of these tablets. These attributes can be achieved best by using migration inhibiting additives and barriers during the fabrication process, and by using post-processing techniques such as uniaxial pressing.

CHAPTER FOUR

Accuracy and Range of Dosage in 3DP™ Forms

3DP is able to deliver precise quantities of material into a three dimensional matrix with high placement accuracy. This attribute makes it ideal for fabricating pharmaceutical devices in which dosage control is required. This chapter explores the limits of dosage attainable by the technology.

It has been demonstrated by Yoo[52] on a pilot scale 3DP CJ Mask machine that 1 μg dosage forms of salicylic acid can be fabricated reproducibly with good dosage control. Fifty 1μg tablets were assayed for drug content by spectrofluorimetry for uniformity, linearity, and recovery. The tablets were shown to contain a mean dosage of 1.017μg with 2.0% relative standard deviation (RSD) as shown below in Figure 4.1. This lies well within the USP[52] limits of 15% of label claim with RSD < 6%.

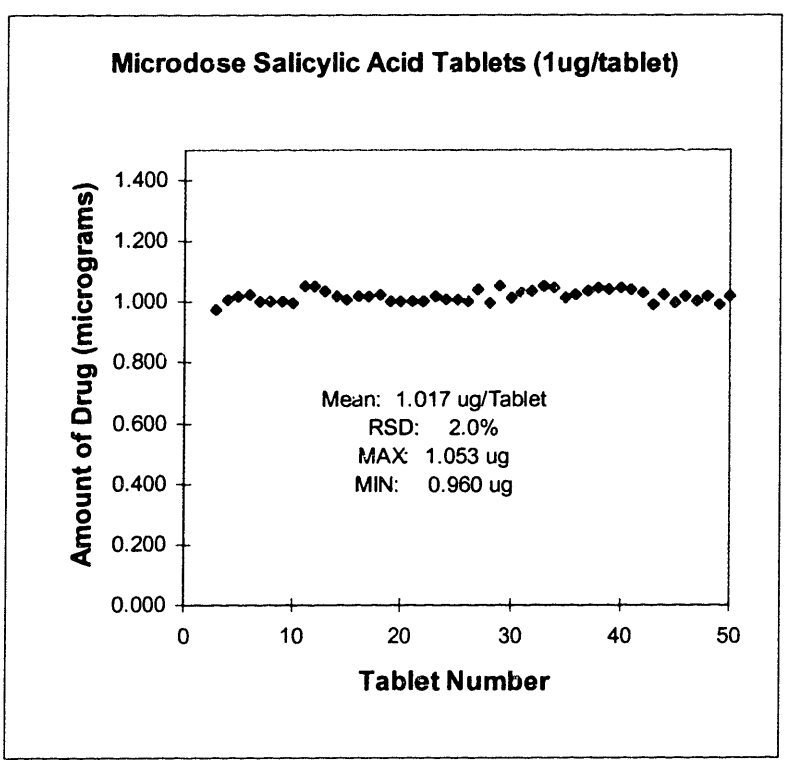

Figure 4.1 Microdose salicylic acid tablets[52]

High dosage forms, however, are more difficult to fabricate with the 3DP technology due to a few process limitations such as available volume for loading and solubility limits. Previous proof of concept drug devices fabricated by 3DP have had dosages in the milligrams. Dosage forms with ~4mg chlorpheniramine maleate have been fabricated using a solution-based drop-on-demand printing 3DP technique.[31] Other antihistamine forms have been fabricated by CJ Mask 3DP with 4.5 mg.[1] These dosages translate into approximately 14mg per unit device volume (cc).

This chapter introduces the experiments that have been conducted to test the precision and accuracy of the technology, and to probe the lower and upper limits of drug dosage per unit tablet volume fabricated by 3DP. Tablets have been fabricated by solution printing, suspension printing, and by both techniques followed by uniaxial compression. Section 4.1 discusses the 3DP fabrication and detection of low nanogram dosage tablets. Section 4.2 discusses techniques to overcome limitations in the fabrication of high dosage forms by 3DP.

4.1 Low Dosage Forms by 3DP

Solution printing of drug substances with 3DP is ideal for fabricating low dosage forms. Other fabrication technologies encounter problems such as the micronization of actives, electrostatic charging, uniform mixing and segregation. This leads to problems with content uniformity and validation. It was shown in section 2.2.2.3.2 that single 90μm droplets could deposit 15nL of fluid at a time. The ability to print such small dosages with accuracy makes the technology especially suitable for novel drug compounds that need to be delivered in microgram, nanogram, or even picogram quantities.

4.1.1 Fluorescein Tablets

Tablets were fabricated using low dosages of fluorescein disodium salt to determine the lower limit of dosage and to test the accuracy of 3DP in dosing tablets. Fluorescein was used in this study as a surrogate drug compound to detect 3DP dosing because of its strong fluorescence that persists even when diluted to extremely small concentrations.

An activated binder solution was prepared by adding 16mL of 0.001M fluorescein solution to 500mL of a standard 3DP binder solution. The standard solution used was 22w/w% PVP (polyvinyl pyrrolidone) / 0.1w/w% Tween 20 (polyoxyethylene 20 sorbitan monolaurate) / D.I. H_2O. The resulting "activated" binder contained 3.20×10^{-5} moles of fluorescein per liter of binder solution.

A solenoid valve jet technique was used to fabricated the tablets. The droplet frequency was 800Hz using a flow rate of 1.601 g/min. Nine columns and ten rows of 1x1 cm^2 samples were printed 16 layers high with the standard 22% PVP/0.1%Tween/H_2O binder, saturating a powder of ~100μm Lactose Monohydrate to 100%. This provided a base foundation. A final layer was

printed into the samples using the fluorescein activated binder by varying the number of drops per tablet deposited in each column as shown in Figure 4.2.

The amount of fluorescein contained in one single droplet was calculated to be 1.02×10^{-12} moles given a flow rate of 1.682 g/min, frequency of 800Hz, solution density of 1.10g/cc and 3.20×10^{-5} $moles_{fl}$/Liter. This translates into 3.84×10^{-10} grams or 384 picograms of fluorescein per droplet.

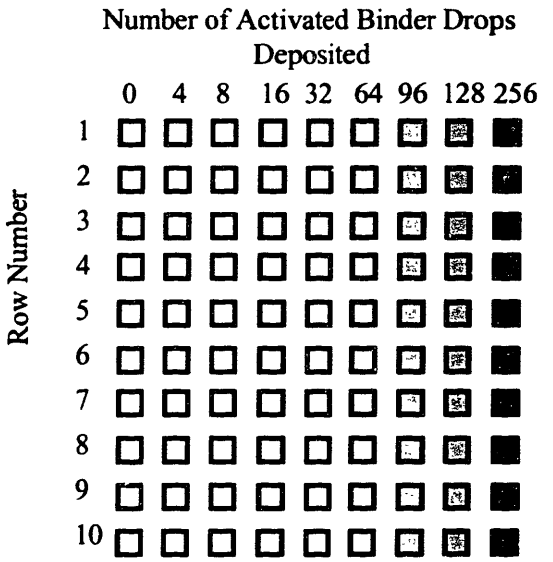

Figure 4.2 Fluorescence tablets – number of droplets deposited in each tablet

Fluorescein concentration in each of the lactose-PVP tablets was measured by dissolving the tablet in 20mL DI H_2O and then tested for fluorescence using a QM1 Luminescence Spectrophotometer. Maximum fluorescence emission is detected at 513nm using an excitation wavelength of 491nm. The detection limit of fluorescein in solution is about 0.1 nanomolarity. A calibration experiment was conducted and showed a linear correlation between the detected fluorescent counts per second and the actual concentration of fluorescein. This correlation was used to determine the fluorescein loading in the printed tablets.

The fluorescein detected per tablet was averaged over the 10 samples, and is shown along with the calculated fluorescein loading per tablet in Figure 4.3.

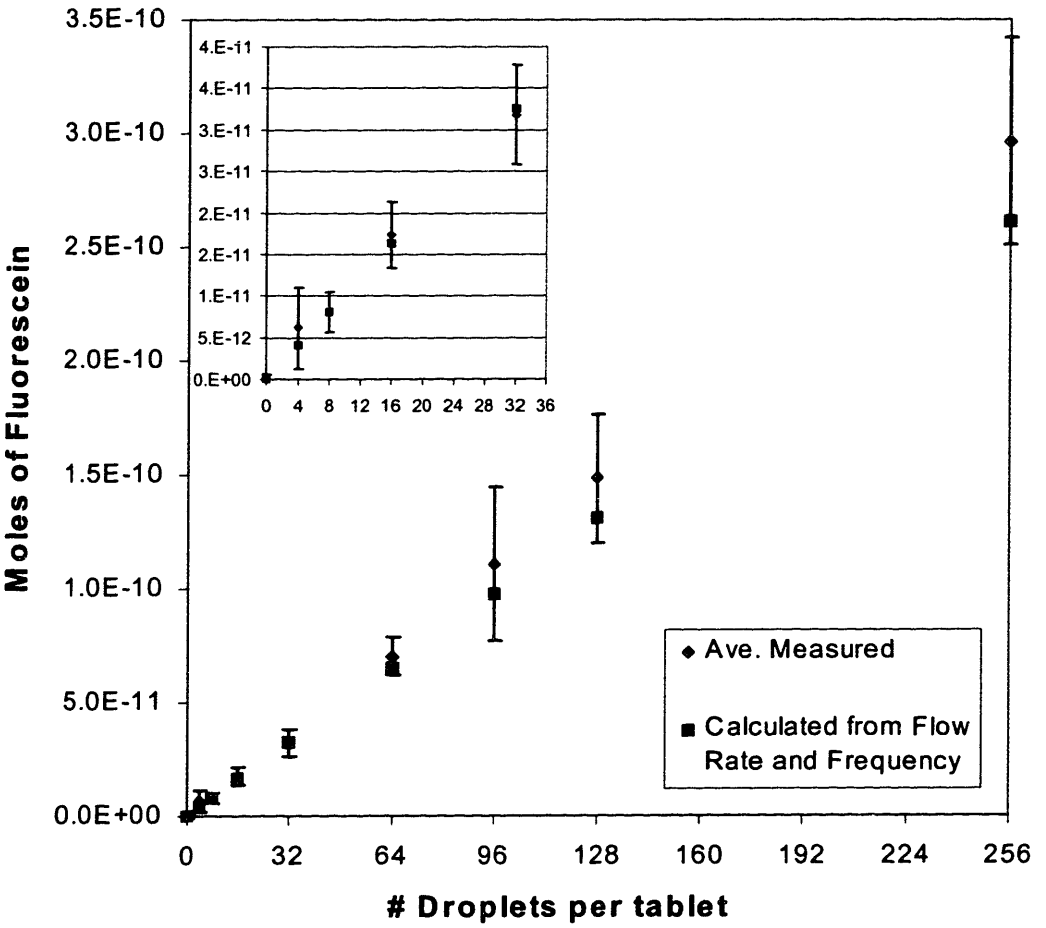

Figure 4.3 Detected fluorescein loading in the 9 samples of varying droplet number vs. the calculated loading based on printing parameters.

Figure 4.3 shows the correspondence between the actual amount of fluorescein printed and the predicted amount based on calculations from the printing parameters. The lowest dosage of fluorescein printed and detected in this study was 6.13×10^{-12} +/- 4.88×10^{-12} moles compared to the predicted 4.08×10^{-12} moles. This translates into 2.31 +/- 1.84 nanograms as compared to the predicted 1.54 nanograms.

4.1.2 Discussion

The calculations of fluorescein loading based on spherical droplet geometry, initial drug solution concentration, and flow rate correlate well with the detected fluorescein loading based on the fluorescence calibration. This correlation shows the ability of the printing method to both predict and dose these forms accurately. It also validates the volume of the droplets used in printing.

The lowest dosage detected in this study was 2.31 nanograms. It is expected that lower dosages may also be accurately printed using this technique by diluting the starting active solution. This expectation is based on the result that the volume per droplet has been validated, and therefore the dosage will scale with the concentration in that volume.

There is no true lower limit to dosage using this technique should dilution be employed. The only limitation would be in the detection of such small quantities of active in solution. This becomes a validation limit.

4.2 High Dosage Forms by 3DP

It has shown been that several 3DP printing techniques are able to print very small dosages on the order of nanograms. High dosage forms, however, are more difficult to fabricate with the 3DP technology. This is due to several process limitations. The main inherent limitation to consider when designing drug devices is the available void volume within the powder bed. Typical dry powder beds used in 3DP contain approximately 50% void volume at tap density. This means the maximum drug:excipient ratio possible becomes 50:50 should the drug substance completely fill the available void volume. The upper limit of dosage is found by assuming complete filling of the available volume with drug substance:

$$Dosage_{\max} = V_{device}(1 - p_f)_{powder}\,\rho_{drug} \qquad 4.1$$

where V_{device} is the volume of the tablet or device, p_f is the packing fraction of the powder, and ρ_{drug} is the bulk density of the drug substance. A tablet of 5mm in height and 5mm in radius could therefore contain a maximum of 196mg of a drug substance of bulk density 1g/cc.

The second limitation is the lack of efficient filling of the available volume with drug substance. A drug is printed within a fluid phase, either a solution or a suspension. The dosage acquired during one print pass is limited by the ability of the fluid to saturate up to 100% of the available void volume. The fluid then evaporates depositing the drug substance in the regions of greatest capillary influence, in small pores and in areas of high curvature. This process incompletely fills the void volume. Precipitation may close off porosity, and subsequent print passes into the same region will inefficiently fill the remaining void volume. Incomplete evaporation from one print pass may also lead to over-saturation, bleeding, and further inefficient filling. It is therefore desirable to saturate a powder bed once for these reasons. This leads to the last limitation.

The third limitation applies to solution printing. The solubility limit of the drug substance limits the dosage printed for a given saturation. A drug substance with a solubility limit of 20wt% in a solution of density 1g/cc printed into a tablet of 5mm in height and 5mm in radius assuming a void volume of 50% and a saturation of 100% will result in a dosage of 39mg. It becomes clear that in order to increase this dosage, more drug solution needs to be printed into the same space by increasing the number of print passes, or the concentration of the drug in the solution needs to increase. This dependency is shown in Figure 4.4 below.

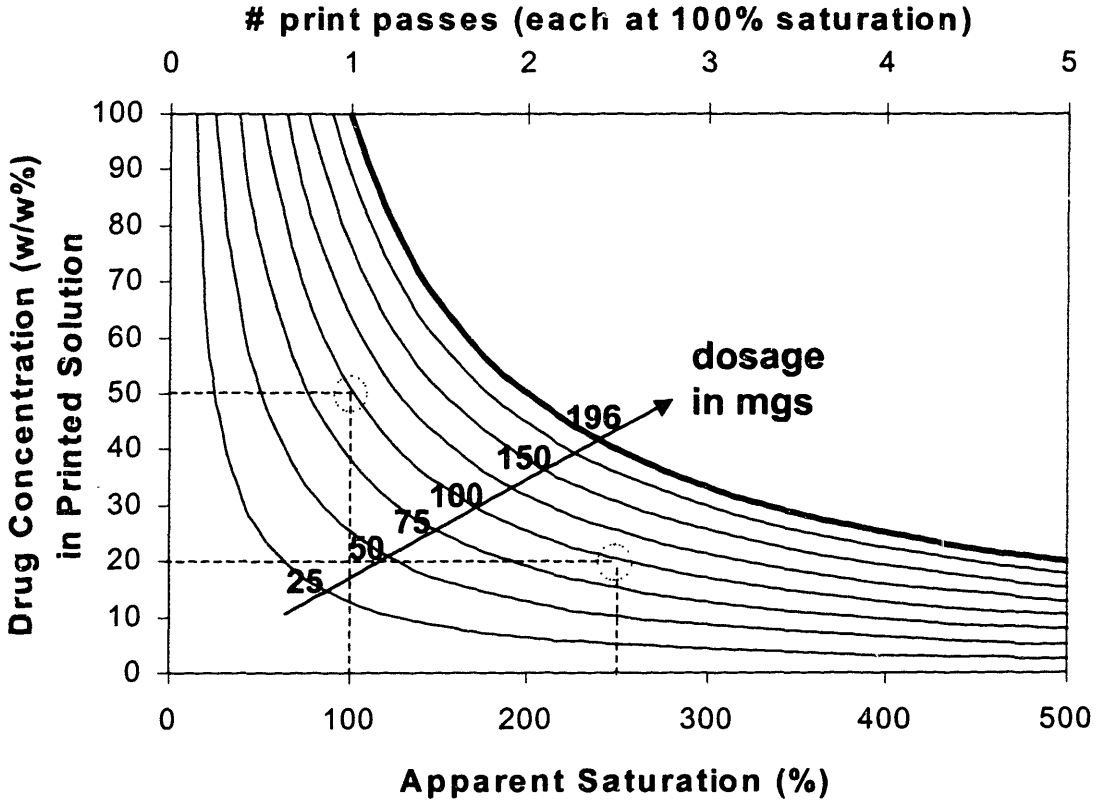

Figure 4.4 Iso-dosage lines in drug concentration vs. saturation
Assumptions: cylindrical shape device of radius 5mm and height 5mm, solution density = 1g/cc, packing fraction = 0.5

Figure 4.4 shows that in order to achieve a certain dosage, corresponding pairs of drug concentration and saturation are needed. A saturation of ~250% is needed to obtain 100mgs using a drug solution with 20w/w% drug concentration. This means the same area needs to be printed ~2.5 times using a saturation of 100%. As the saturation requirement increases, the number of print passes over the same region also increases. Repeated printing passes greatly increase the time required to fabricate one layer as the build time scales linearly with number of print passes. Subsequent print passes also have less and less chance of filling the remaining void volume efficiently. It is therefore desirable to keep the number of print passes low.

A drug concentration of ~50w/w% would be needed to obtain 100mgs if the powder bed was saturated once to 100%. This is an extremely high drug concentration for drug substances in solution. The only way to achieve a concentration close to this in a printable fluid phase is by the use of suspensions. Suspensions are not bound by solubility limits, instead they are limited by the highest solids loading that may be well dispersed throughout the fluid phase with good stability.

An important parameter when considering the dosage attainable by 3DP is the dosage per unit device volume, or δ, measured in mg/cc.

$$\text{Dosage per unit device volume } = \delta = S_{app}(1 - p_f)\rho_{sol}C_{drug} \qquad 4.2$$

where S_{app} is the apparent saturation, equal to the saturation fraction S per print pass x the number of print passes, p_f is the powder packing fraction, ρ_{sol} is the printed solution density, and C_{drug} is the w/w fraction of drug in the solution. The dual-dependency of δ on drug concentration in the printed solution and the apparent saturation is shown in Figure 4.5 for a typical packing fraction of 0.5.

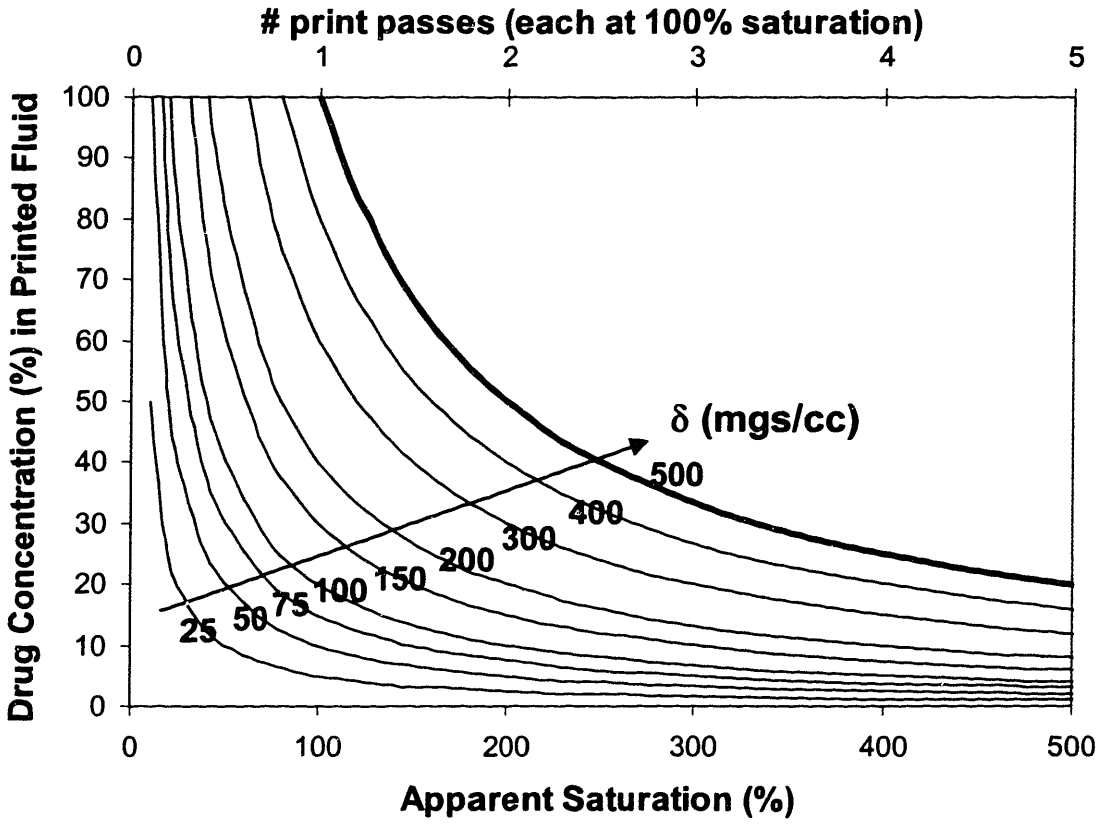

Figure 4.5 Iso-δ lines and their dependency on drug concentration and apparent saturation. Assumptions: p_f=0.5, ρ_{sol} =1g/cc.

4.2.1 Fabrication and Detection of High Dosage Forms

4.2.1.1 Diclofenac Solution-Printed Tablets

Fabrication

Four sets of tablets containing the drug substance diclofenac sodium (Sigma Chemical Co.) were fabricated using the CJ CD OSP printing technique. The powder bed consisted of 70wt% Lactose and 30wt% HPMC (Methocel K4M, Dow Chemical Co.) with a packing fraction of 0.412. The drug solution printed into these tablets was 18wt% diclofenac and 1wt% PVP dissolved in methanol.

set 1: Tablets were fabricated by printing diclofenac solution using a line spacing of 120μm, a layer height of 300μm, a flow rate of 0.97g/min, nozzle orifice diameter of 50.4μm, raster speed of 150cm/sec and a modulation frequency of 42.0KHz to achieve a saturation of 0.57. Each layer took approximately 2 minutes to build. The tablets were printed into a cylinder shape of diameter 10.42mm using 16 layers to give an overall height of 4.8mm. The dosage printed into each tablet was calculated to be 22.08 mg of diclofenac.

set 2: Two of the first set of tablets were then pressed under uniaxial compression of 15000 PSI in a cylindrical tablet die 11mm in diameter. The resulting pressed tablets were 11.17mm in diameter and 1.78 mm in height.

set 3: The same printing conditions were then used to fabricate a third set of tablets by printing drug solution 4 times into each layer. The tablets were each printed with one print pass, and allowed to dry for ~3 minutes between print passes. Each layer took approximately 15 minutes to build. This gave an apparent saturation of 4 x 0.566 or 2.26. The dosage printed into each tablet was calculated to be 88.16 mg of diclofenac.

set 4: Two of the third set of tablets were pressed under uniaxial compression of 15000 PSI in a cylindrical tablet die 11mm in diameter. The resulting tablets were 11.17 mm in diameter and 2.33 mm in height.

Dissolution and Detection

The tablets were allowed to completely dissolve in 900mL of phosphate buffer solution with pH 7.4 at 37°C. Absorbance was measured using a spectrophotometer (Beckman DU 640) with the peak absorbance wavelength for diclofenac sodium, 275nm. An absorbance/concentration calibration experiment was conducted for absorbance of diclofenac in phosphate buffer solution and showed a linear dependence on concentration for concentrations in the range of 0.5mg/L – 50mg/L.

The first two sets of tablets, printed with a saturation of 0.57, were shown to contain 21.98mg +/- 0.22mg as determined by comparison with the absorbance/concentration calibration curve for diclofenac. The un-pressed tablets contained δ =53.74 mg/cc, and the pressed tablets contained δ =115.08 mg/cc.

The second two sets of tablets, printed with an apparent saturation of 2.26, were shown to contain 87.98mg +/- 0.28mg as determined by comparison with the absorbance/ concentration calibration. The un-pressed tablets contained 215.11 mg/cc and the pressed tablets contained 350.52 mg/cc.

4.2.1.2 Naproxen Suspension-Printed Tablets

Fabrication

Four sets of naproxen tablets were fabricated using the CJ CD printing technique. The first two sets were printed with a 22wt% naproxen suspension (Nanosystems, Inc.), and the second two sets were printed with a 41.5wt% naproxen suspension (Nanosystems, Inc). The suspensions contain ~200-500nm naproxen particles and contains approximately 0.1w/w% PVP based on naproxen loading for steric dispersion in D.I. water. The suspensions were first filtered, and then measured for wt% solids loading. The suspensions were printed through a nozzle of 50μm orifice diameter, and droplets were charged and deflected to obtain the correct dosage in the tablets.

The fabrication of the first set of tablets printed with 22wt% naproxen suspension were described in section 3.1.1.5. 25 layers, 200μm in height, 7mm in diameter, were saturated to 1.0. The powder bed was comprised of 50wt% microcrystalline cellulose (Avicel PH301) and 50wt% Lactose (53-74μm) with a packing fraction of 0.428. The overall calculated dosage in these tablets was 26.2mg.

Two of the first set of naproxen tablets were then pressed under uniaxial compression of 15000 psi in a tablet die. The pressing procedure for these tablets is described in section 3.1.1.5. The pressed drug region diameter was 8.16mm and the drug region height was 2.47mm as determined by cross-sectioning the tablets.

The third set of naproxen tablets were fabricated using the 41.5wt% naproxen suspension. Ten layers were printed in to diameters of 10.42 mm with a layer height of 200μm, line-spacing of 120μm, and saturation of 1.0. The powder bed was composed of 50wt% microcrystalline cellulose (Avicel PH301) and 50wt% lactose (53-74μm) with a packing fraction of 0.428. The overall dosage per tablet was calculated to be 50.14 mg based on the printing parameters.

Two of the third set of naproxen tablets was then also pressed with 15000 psi in the same manner as above. The diameter of the pressed tablets was 11.15mm and the height was 1.18mm.

Dissolution and Detection.

The tablets were allowed to completely dissolve in 900mL of phosphate buffer solution with pH 7.4 at 37°C. Absorbance was then measured using a spectrophotometer (Beckman DU 640) with the maximum absorbance wavelength for naproxen, 332nm. An absorbance/concentration calibration experiment was conducted for absorbance of naproxen in phosphate buffer

solution and showed a linear dependence on concentration for concentrations in the range of 1mg/L – 50mg/L.

The first two sets of tablets, printed with the 22 wt% naproxen suspension, were shown to contain 26.7 +/- 0.7mg as determined by comparison with the absorbance/concentration calibration. The un-pressed tablets contained δ =139.1 mg/cc in the drug region, and the pressed tablets contained δ =207.0 mg/cc.

The second two sets of tablets, printed with 41.5wt% naproxen suspension were shown to contain 50.0 +/- 0.8 mg as determined by comparison with the absorbance/concentration calibration. The un-pressed tablets contained δ =293.2 mg/cc in the drug region, and the pressed tablets contained δ =426.7 mg/cc.

Table 4.1 summarizes the results from the fabrication of high dosage forms.

Table 4.1 δ Values for high dosage forms (mg/cc)

	Solution (18wt% diclofenac)		Suspension	
	1 Print Pass S=0.566	4 Print Passes S_{app}=2.26	22wt% naproxen	41.5wt% naproxen
Un-Pressed	53.74	215.11	139.1	293.2
Pressed	115.08	350.52	207.0	426.7

Figure 4.6 shows the results for detected dosage per unit volume, δ, for each of the above un-pressed tablets, as compared to the calculated δ contours for a powder with packing fraction of 0.42.

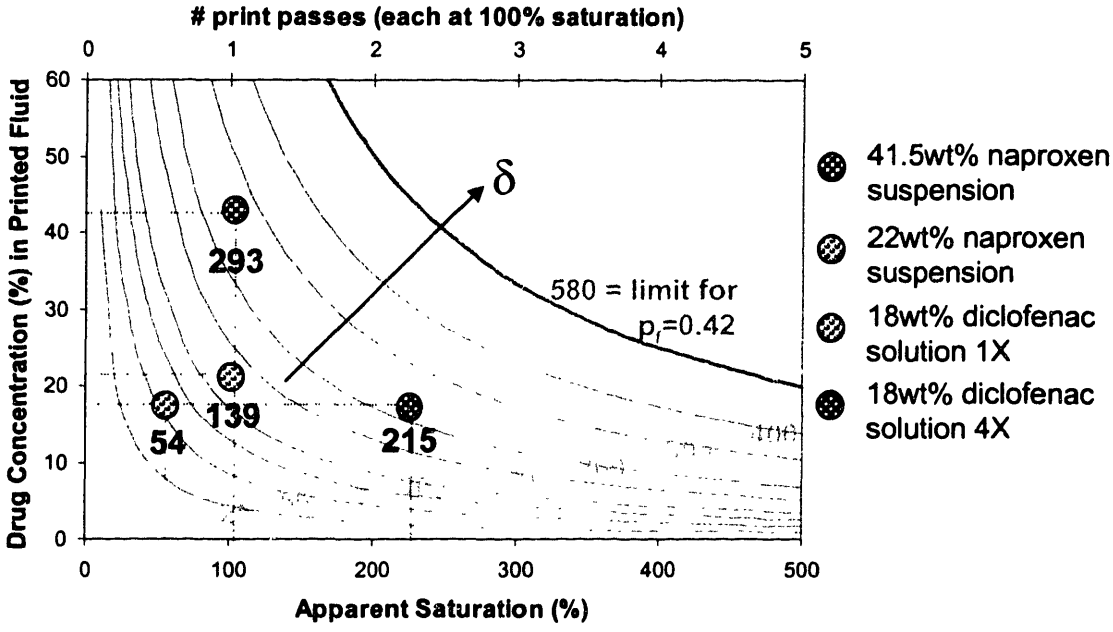

Figure 4.6 δ (mg/cc) measured vs. predicted for un-pressed samples

Figure 4.7 shows all of the δ values achieved in this study. Pressing enhances the drug concentration by decreasing the volume for the same dosage. The 41.5wt% naproxen suspension printed at 100% saturation, for example, was measured to have a dosage of 45.6 mg and volume of 0.196cc before compression, and a volume of 0.126cc after compression. This gives a δ before of 293.2mg/cc and a δ after compression of 426.7mg/cc. The black arrows indicate how the δ changes when the tablets are pressed.

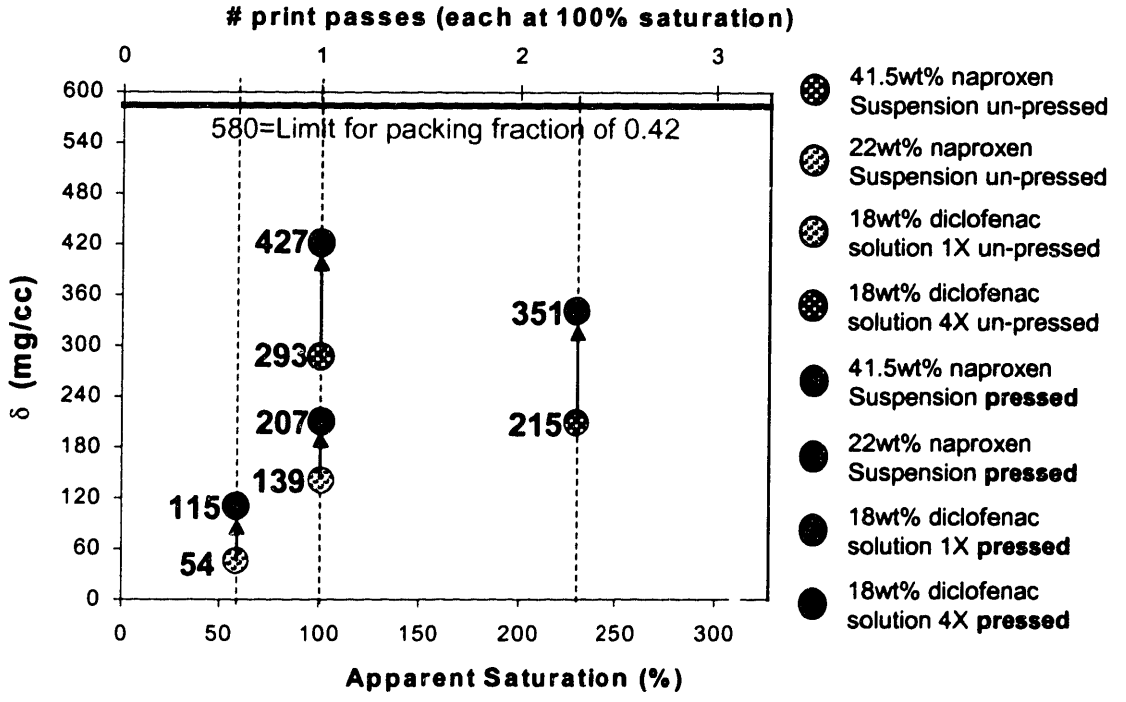

Figure 4.7 δ Values achieved in this study

4.2.2 Discussion

High δ values ($mg_{drug}/cc_{drugregion}$) are desired for printing high dosage forms. Tablets with high δ concentrations can be printed smaller while maintaining the same tablet dosage as those with low δ concentrations. High δ values also allow the design of more complex internal geometries for tablets of the same size and loading.

Solution printing is limited by the solubility of the drug substance in the printed solution. In these studies, 18wt% diclofenac in methanol was found to be the highest concentration drug solution printed without jetting problems. (See section 2.4.2.2) The solubility limit of diclofenac in methanol is ~30wt%, but due

to the high vapor pressure of methanol, much lower concentrations are used to avoid crystallization at the nozzle surface. Solutions printed with lower drug concentrations would result in lower δ values.

Re-printing a region with several passes has been shown to effectively increase the drug loadings per unit volume. This technique, however, has the disadvantage of taking more time when comparing two equivalent size tablets. The same area needs to be re-printed several times, and this additional print time may be expensive. Filling also occurs inefficiently upon subsequent print passes as there is less available volume for infiltration, and some porosity becomes closed during precipitation and coating (see also section 3.2.2.3). It is therefore desirable to keep the number of print passes low, and the drug concentration in the printed fluid high.

Post processing the tablets using uniaxial compression was shown to increase the δ values by decreasing the volume while maintaining dosage. Tablets can be fabricated tall and then pressed to conventional dimensions. This post processing technique is proposed to be eventually added in-line after printed tablets have been dried. Pressed tablets have been shown in section 3.1.1.5 to maintain internal geometry.

The highest δ values were obtained by printing with suspensions of drug crystals dispersed in water. The suspensions are not limited by solubility limit, and therefore can be printed with concentrations up to the viscosity limit or up to the dispersion limit. Highly concentrated drug suspensions were printed using one print pass to achieve δ = 293.2 mg naproxen per unit tablet volume and pressed tablets of naproxen were fabricated with δ = 426.7 mg/cc. This represents filling ~74% of the total available volume based on a powder packing fraction of 0.42.

4.3 Conclusions for Chapter 4

It has been shown that it is possible to accurately print dosages down to at least 2.3 nanograms using the 3DP solenoid printing technology. There is no true lower limit for the dosage, as the printed drug solution can be diluted to obtain lower concentrations.

The upper limit for drug dosage depends on the available void volume in the powder bed, and the ability to fill this void volume efficiently. Multiple print passes were able to achieve higher dosages at the expense of fabrication time. The use of high solids loading suspensions increased the dosage per unit tablet volume considerately. Further enhancement of dosage per unit volume was achieved with uniaxial pressing of the 3DP tablets.

Specific Complex Dosage Forms Printed with 3DP™

The current study examines the fabrication of proof-of-concept oral drug delivery devices using 3DP™ and standard pharmaceutical materials and actives. One objective was to confirm the ability to modulate release properties of devices by changing the printing parameters. Another objective was to fabricate complex drug delivery devices based on these properties. Six devices have been constructed and tested for release characteristics. The first two devices, erosion and diffusion release tablets, have been fabricated with varying volume fractions of rate-controlling polymers to show the ability for 3DP to print functionality into oral dosage forms. The last three devices are more complicated dosage forms that release by the coupling of mechanisms or by complicated internal geometries. These tablets are listed in Table 5.1.

Table 5.1 Oral dosage forms fabricated by 3DP

Device:	**Attributes**
Erosion Release Tablets[21]	Tablets have been designed to erode at different rates and lag times based on printing parameters
Diffusion Extended Release Tablets	Tablets have been designed with varying diffusion coefficients based on printing parameters for extended release.
Break-away Tablets	Tablets are composed of a continuous soluble phase surrounding insoluble extended release sub-units. These drug-containing sub-units break away from the original device to release via diffusion.
Enteric Dual Pulsatory	The continuous polymer phase is enteric in nature and dissolves only in intestinal conditions. Drug is printed into two sections for erosional release twice in the intestines.
Two Phase Dual Pulsatory	Two sections of opposite pH solubility nature contain drug. One section erodes in the stomach to release one pulse and the other enteric section releases a pulse in the intestines

5.1 Materials and Methods

5.1.1 Materials and Fabrication

Eudragit™ E100 erosion type dosage forms[21]

Erosion-type tablets were constructed using microcrystalline cellulose powder (Avicel PH301, FMC Corp.) with a particle size range of 74-106μm, and packing fraction of 0.40. [21] The binder solution printed into the powder bed was 20wt% E100 (Rohm Pharma) in ethanol. E100, described in Appendix 1, is a cationic methacrylic ester copolymer that is soluble below pH 5 and permeable above pH 5. Tablets were fabricated using the CJ mask 3DP technique using parameters of 200μm powder layer height, a mass flow rate of 1.4 g/min., a printhead velocity of 150cm/sec, and varying line spacings to achieve polymer volume percentages of θ_{E100}=8.9, 10.7, 13.4, and 17.9%. The circular tablets had an outer diameter of 10mm. A 20wt% chlorpheniramine maleate/water solution was then printed into a concentric circular region with diameter of 7mm. The tablets were printed with six placebo layers forming the bottom of the tablet printed with polymeric binder only. Next, eight active containing layers were printed, followed by another six placebo layers to form the top cap of the dosage form. Each sample contained 3.4 mg of active, present only in the center of the form. Placebo samples were also manufactured with the active replaced by an aqueous solution of red dye.

Eudragit™ RLPO diffusion type dosage forms

Diffusion-type tablets were constructed using microcrystalline cellulose powder (Avicel PH301, FMC Corp.) with a particle size range of 74-106mm, and packing fraction of 0.40. The binder solution was 20wt% Eudragit® RLPO (see Appendix 1) in acetone. RLPO is expandable and permeable and its properties are independent of pH. Tablets were fabricated using the CJ mask 3DP to

produce 10mm O.D. samples. The 20w/w% RLPO/acetone solution was printed through a 45μm nozzle with a flow rate of 0.85 g/min. A total of 20 layers of 200 μm each were used in tablet construction. The print head velocity was 140 cm/s. Three rows of devices were printed with line spacings of 70, 100, and 130 μm to produce devices with volume % of θ_{RLPO} = 14.0%, 9.8%, and 7.5% by volume, respectively. The overall surface area of the tablet shape was 2.8cm^2. A 20wt% diclofenac sodium solution was then printed through concentric circular masked regions with diameter of 7mm at a flow rate of 0.9g/min with line spacing of 120μm. The tablets were printed with six placebo layers forming the bottom of the tablet printed with polymeric binder only. Next, eight active containing layers were printed, followed by another six placebo layers to form the top cap of the dosage form. Each sample contained 5.50 mg of diclofenac, present only in the center of the form.

Break-Away Tablets

Breakaway tablets were constructed with drug containing units separated by a Quick dissolving matrix. Figure 5.1 shows a schematic of a prototype fabricated with 3DP™.

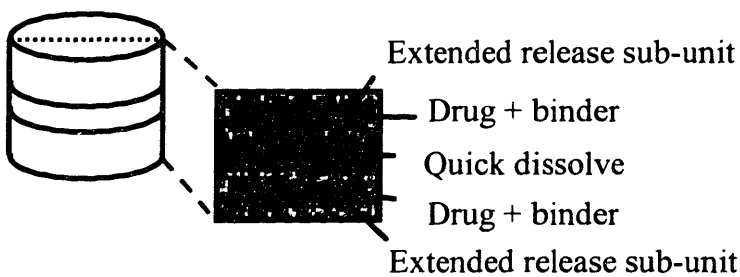

Figure 5.1 Break-away tablet design

The powder used for construction of the breakaway tablets was 30 wt.% Avicel PH301, 30 wt.% Pharmatose DCL 11 Spray Dried Lactose, and 40 wt.% Eudgragit® L100. The drug containing units were fabricated by printing placebo layers of 15% (w/w) Eudragit® RLPO solution in acetone. Layer thickness was

250 μm, line spacing was 200 μm, printhead velocity was 150 cm/sec, and the flow rate was 1.15 g/min. The placebo layers were followed by layers printed with the same binder solution followed by a solution of 30% (w/w) diclofenac, 2.5% (w/w) Kollidon K-25 in methanol. This solution was printed with line spacing 100 μm, printhead velocity 105 cm/sec, and a flow rate of 0.9 g/min. The active containing region was then capped off with additional placebo layers.

The quick dissolve section was then printed using a solution of 22% (w/w) Kollidon K-25 in water. Layer thickness was 300 μm, line spacing was 80 μm, printhead velocity was 150 cm/sec, and the flow rate was 0.96 g/min. A second drug unit was fabricated on top of the quick dissolve section in the same manner as the first drug unit.

Enteric Dual Pulsatory Tablets

The Enteric Dual Pulse dosage form was constructed from Eudgragit® L-100, an anionic methacrylic ester copolymer which is soluble only above pH 6. Using this enteric polymer as a binder makes it possible for the tablets to pass through the stomach without degrading. Drug was printed into the tablet in two different compartments as shown in Figure 5.2. The release mechanism is erosion, and therefore drug is exposed as the tablets dimensions decrease.

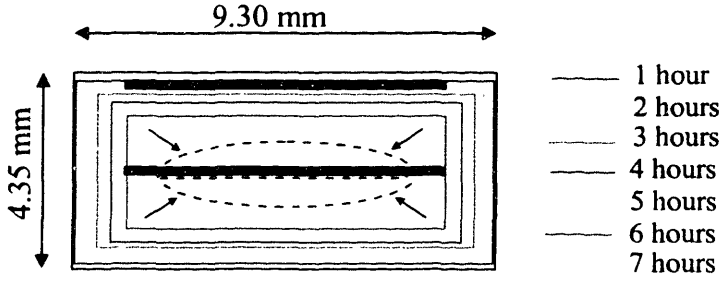

Figure 5.2 Enteric Dual Pulsatory Tablet design

The powder used in the manufacture of these devices was 30 wt.% Avicel PH301, 30 wt.% Pharmatose DCL 11 Spray Dried Lactose, and 40 wt.% Eudgragit® L100. The binder solution was 5% (w/w) Eudragit® L100 in ethanol. The printing parameters were 200 μm layer thickness, 100 μm line spacing, 105 cm/sec printhead velocity, and 1.1 g/min flow rate. Six placebo layers were printed, followed by a layer of binder and diclofenac solution, printed as above. Six additional placebo layers were then printed, followed by an additional active containing layer. A final two placebo layers were printed to cap off the active regions. Total active content of these devices was 3.4 mg diclofenac.

Two Phase Dual Pulsatory Tablets

The Two Phase Dual Pulsatory devices were designed to release once in the stomach at low pH and once in the intestine at high pH. This was accomplished by printing drug compartments inside different polymer environments. One drug compartment was printed into a section of cationic nature (Eudragit® E-100) and another drug compartment into a section of anionic nature (Eudragit® L-100). These dosage forms were manufactured with a dose of 25 mg diclofenac. A schematic of the device is shown in Figure 5.3.

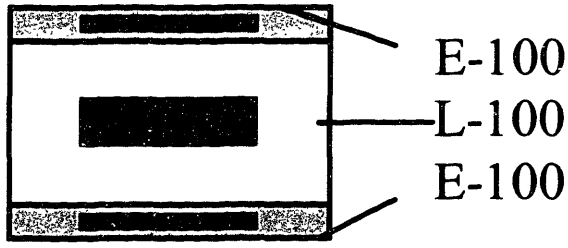

Figure 5.3 Two Phase Dual Pulsatory Tablet design

The powder used for these devices was the same 30/30/40 mixture as the Enteric Dual Pulse devices. The L-100 binder was also the same and was printed with the same parameters. The E-100 sections of the device were

printed with a solution of 13.5% (w/w) Eudragit® E-100 in acetone. The printing parameters were 200 μm layer thickness, 100 μm line spacing, 105 cm/sec printhead velocity, and 1.28 g/min flow rate.

Two E-100 placebo layers were printed, followed by 3 drug containing layers and two additional E-100 placebo layers to complete the first compartment. The second compartment was 6 placebo L-100 layers, 6 active containing layers, and 6 placebo L-100 layers. The top compartment was identical to the first compartment.

5.1.2 Drying and Dissolution

Drying

Printed oral dosage forms were allowed to dry for two days in a nitrogen glove box and then placed into a vacuum oven for 48 hours. Excess unbound powder was then removed, and the devices were carefully removed from the build plate.

Dissolution Testing

The Eudragit® E-100 tablets and break-away tablets were subjected to dissolution conditions in aqueous simulated gastric acidic media of pH 2 at room temperature. Tablets were individually placed into scintillation vials containing 10 cc of solution. The vials were placed onto a RotoMix® shaker, and sink conditions and constant pH were assumed. 5 cc aliquots were taken at appropriate intervals and replaced with fresh pH 2 solution for the duration of the experiment. The aliquots were centrifuged to remove powder sediment and analyzed with UV-vis spectrophotometry. Absorbance was measured in silica cuvettes at 261 nm and compared to an absorbance/concentration linear curve for chlorpheniramine maleate in the simulated gastric fluid.[21]

USP Dissolution

The RLPO extended release tablets, enteric dual pulsatory tablets, and the two phase dual pulsatory tablets were subjected to dissolution conditions according to the U.S. Pharmacopeia specifications. A Logan Instruments Corp. D-800 dissolution testing apparatus was used to perform the assay. A paddle stirrer was rotated at 50 rpm for the duration of the test. 900 mL of solution at 37°C was used as the dissolution medium. Six vessels were run simultaneously with one vessel containing the appropriate calculated diclofenac concentration as a standard. A peristaltic pump (Gilson Medical Electronics) continuously pumped the dissolution medium through flow cells within a UV-Vis spectrophotometer (Beckman Instruments). The tablets were enclosed in wire cages to reduce buoyancy and were subjected to two stages of dissolution as described in the protocol. The first stage included a 0.1 N hydrochloric acid solution for one hour to simulate gastric conditions. The tablets were transferred to the second stage solution, pH 7.5 NaOH monobasic potassium phosphate buffered solution, for six hours to simulate intestinal conditions. Absorbance readings were taken at 275 nm using an eight-cell translating sample holder.

5.2 Results and Discussion

Eudragit® E-100 Tablets

Tablets manufactured with Eudragit® E-100 binder diminished in size through erosion during dissolution testing as shown in Figure 5.4. Figure 5.5 shows the change in diameter of these tablets with dissolution time. Dissolution testing showed release profiles that vary with polymer content as shown in Figure 5.6.

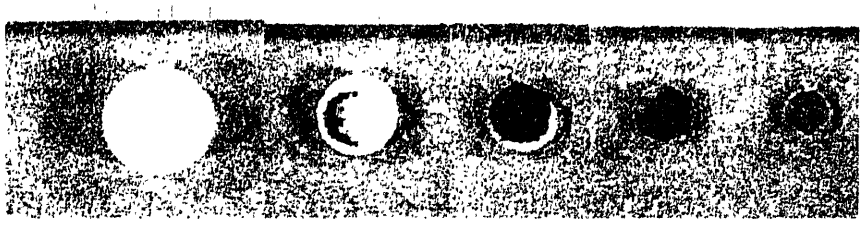

Figure 5.4 E100 placebo tablet during dissolution testing[21]

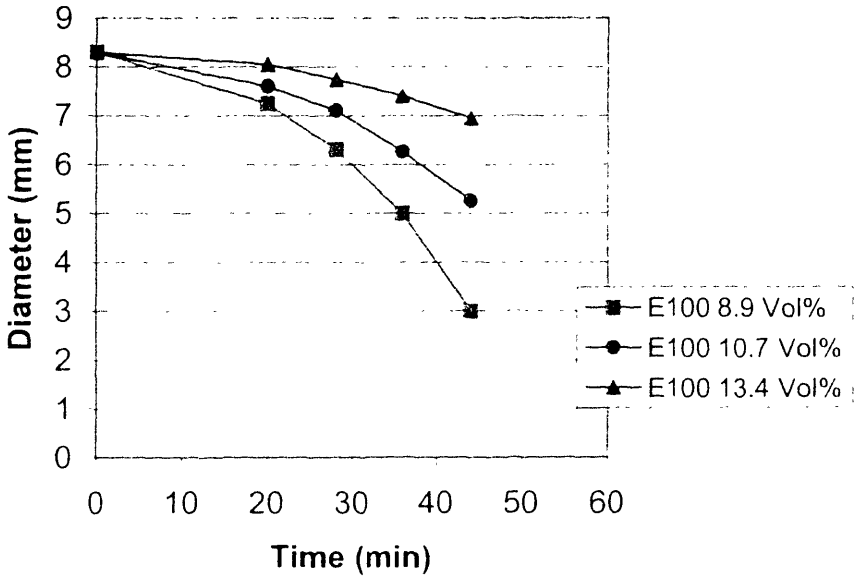

Figure 5.5 Change in diameter of E100 placebo tablets

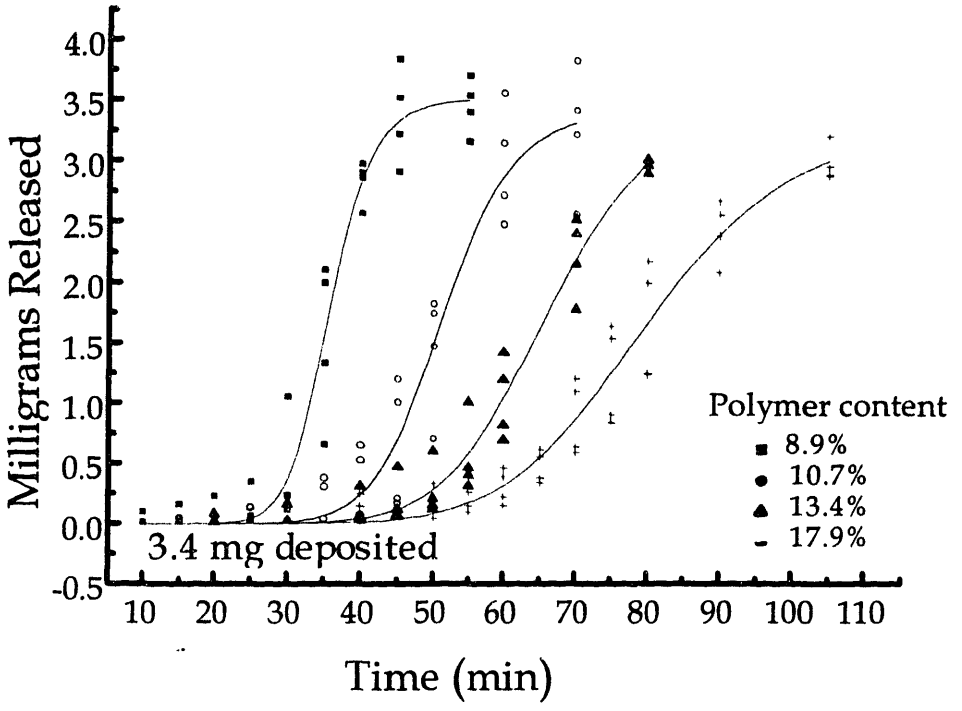

Figure 5.6 Dissolution profiles for varying Vol% E100[21]

Tablets printed with Eudragit® E-100 binder exhibited delayed release as the polymer shell around the active core eroded. The lag time increases, the peak-release-rate decreases, and the overall drug release interval becomes longer as the polymer content goes up. Increased lag time can be explained by a decreased erosion rate.

The active is printed into this dosage form in regions that already contain polymer binder. As the E100 dissolves, the tablet erodes and the active is exposed. This would explain the decreased release rate and increased duration interval with increasing polymer content. Sharper "pulses" of release can be realized if a compartment within the tablet was printed solely with active solution into the loose powder. Lag time would then come from the thickness and polymer content of an exterior "shell" or barrier around this area.

RLPO Extended Release Tablets

Tablets fabricated with RLPO polymer swelled in the dissolution medium as shown in Figure 5.7. Drug was released through these matrices by diffusion as shown in Figure 5.8.

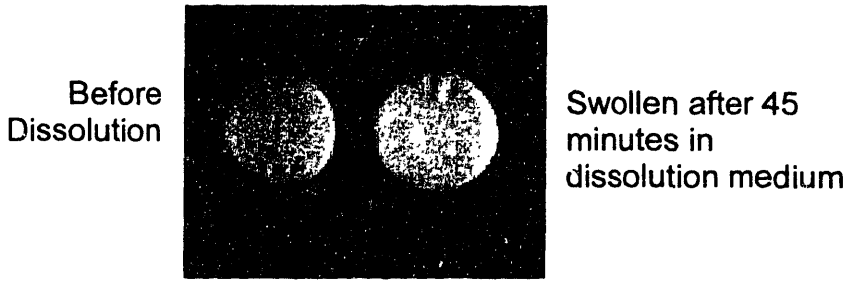

Figure 5.7 Swollen 3DP matrix of RLPO and cellulose

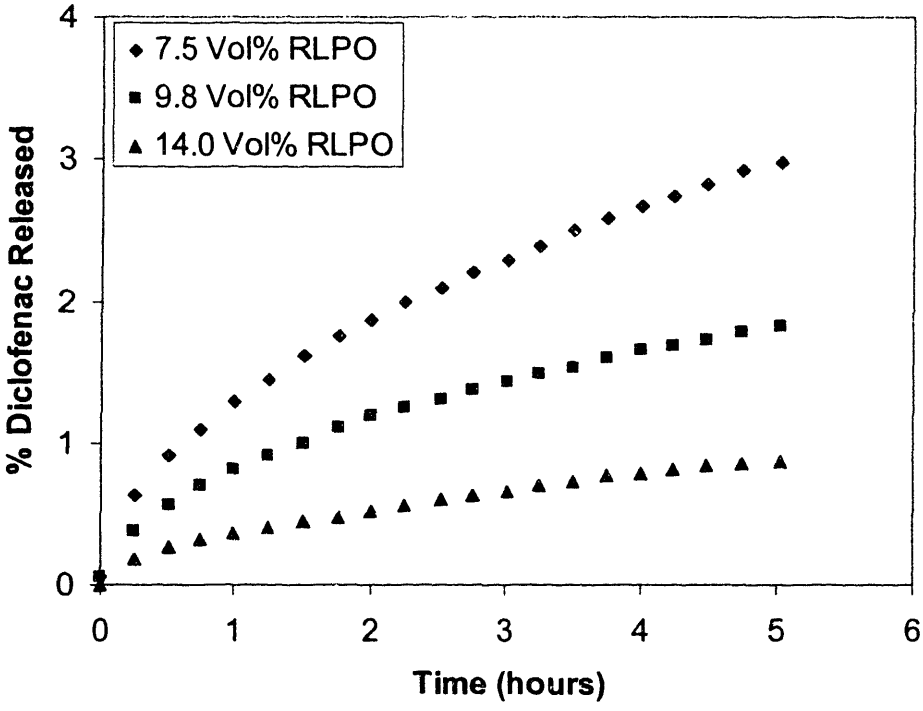

Figure 5.8 Dissolution of RLPO Extended Release Tablets with varying Vol% of RLPO

The permeable matrices of RLPO released diclofenac over time with decreasing release rate as is characteristic for a diffusional mechanism of release. The highest polymer volume fraction tablet shows the slowest release of diclofenac over time. As RLPO Vol% is decreased, the release proceeds more quickly.

The above results were plotted on a Higuchi[53] plot for release vs. the square root of time. This is shown in Figure 5.9.

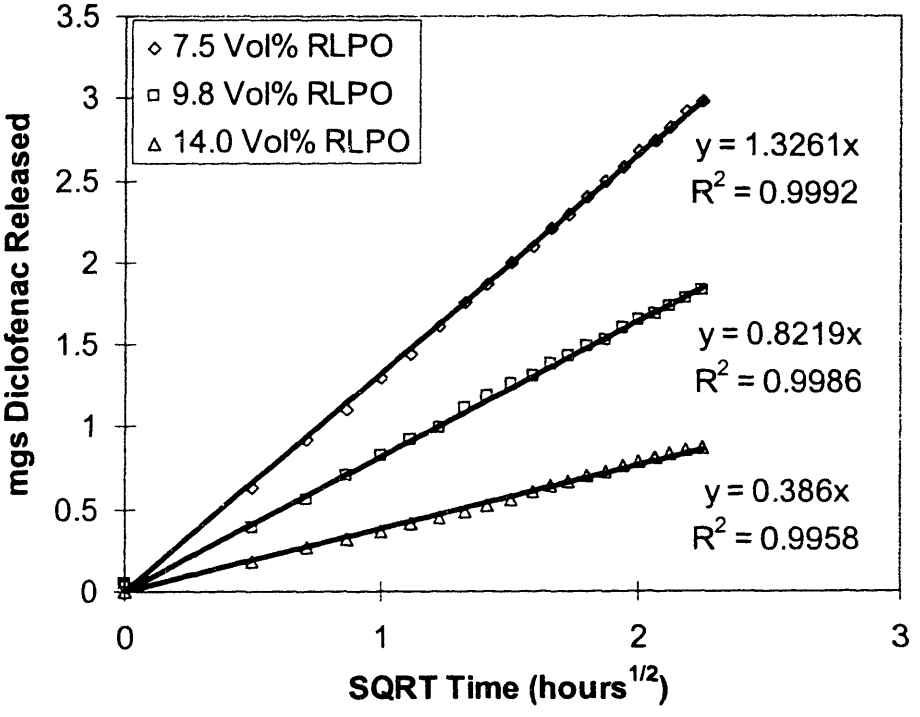

Figure 5.9 Higuchi plot of release vs. $t^{1/2}$

True diffusional release follows a linear curve when plotted against $t^{1/2}$. Diffusional release according to this model has the following dependence:

$$Q = (D_m c_d (2A - c_d)t)^{1/2} \qquad 5.1$$

where Q is the amount of drug released per unit area of matrix, D_m is the diffusion coefficient of the drug in the matrix, c_d is the solubility of the drug, A is

the total initial amount of drug in the matrix, and t is time. The solubility of diclofenac, the initial dosage, and the area for release are the same for the three 3DP extended release tablets of varying RLPO matrix polymer. The only difference between the samples is the diffusion coefficient, D_m, which is therefore dependent on the printing parameters used to form the three matrices.

$$Q \propto D_m^{1/2} t^{1/2} \qquad 5.2$$

The slopes of the lines in Figure 5.9 are proportional to $D_m^{1/2}$. The volume fraction of RLPO is inversely related to the diffusivity of the drug through the matrix. The time to exhaustion increased with increased volume fraction RLPO, but the lag time was not affected.

Break-Away Tablets

The break-away tablets were designed to split into several coherent releasing sub-units. Figure 5.10 shows this break-away mechanism. Samples were fabricated to break apart 15-45 minutes into dissolution. The sub-units were not tested for drug release profile.

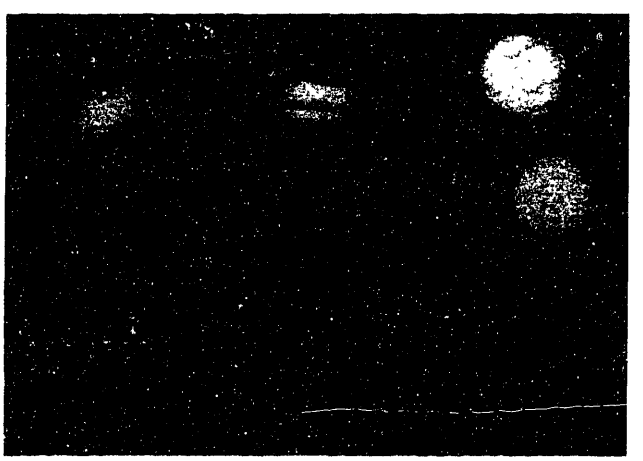

Figure 5.10 Break-away Tablets

The break-away tablets demonstrate the ability to confine erosion within sections of a tablet. This type of tablet might prove to be important for certain types of drug compounds that need to be distributed along the gastro-intestinal tract.

Enteric Dual Release Tablets

Figure 5.11 shows the USP dissolution profile for the Enteric Dual Pulse device. During the first acid stage (pH 1.2) of dissolution, the tablets remained coherent. The first drug compartment nearest to the tablets face released in the beginning of the second phase of dissolution with pH=7.5. The second release from the central compartment started 4 hours later.

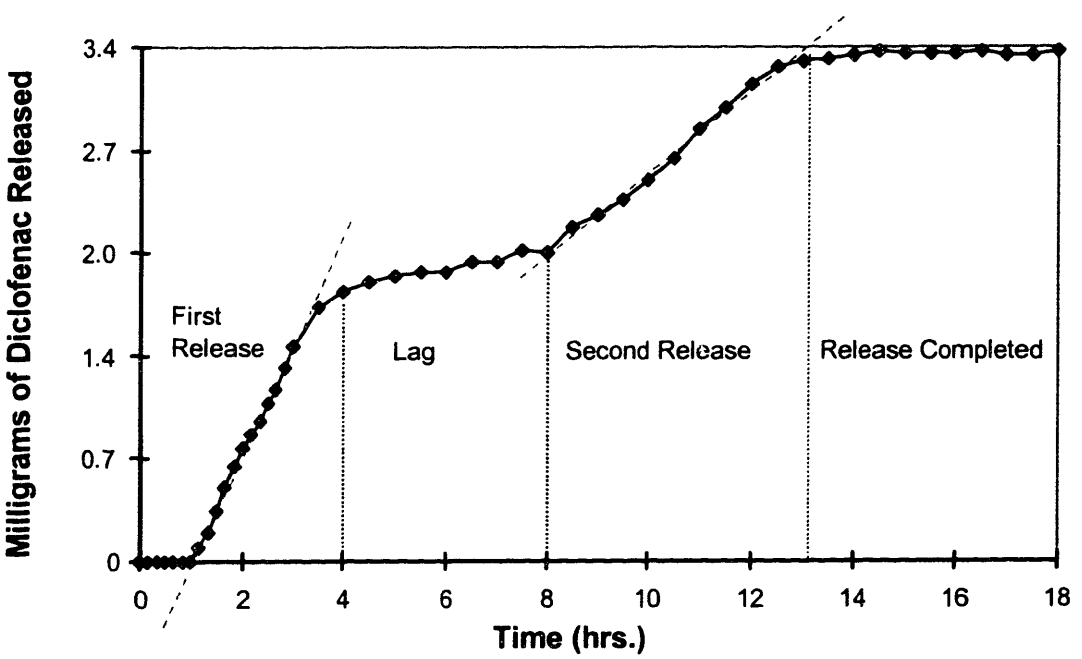

Figure 5.11 Dissolution profile for the Enteric Dual Release Tablet[54]

The enteric dual pulse device showed two pulses of drug released, one immediately after the tablet was immersed in simulated intestinal fluid (t=1.0 hr). The second pulse began after a lag time of 4 hours. The lag time was created by the erosion of the placebo shell surrounding the active. The difference in the relative release rates can be explained by the difference in the surface area of the drug compartment that was exposed with time. Figure 5.2 also shows this erosion front with time.

Figure 5.12 shows the dissolution profile for the two-phase dual pulsatory device. During the first stage of dissolution at pH 1.2, the section composed of E-100 binder eroded rapidly within one hour. This was followed by approximately 4 hours of lag time in pH 7.5 intestinal fluid. Then the drug was released from within the section of L-100 enteric section.

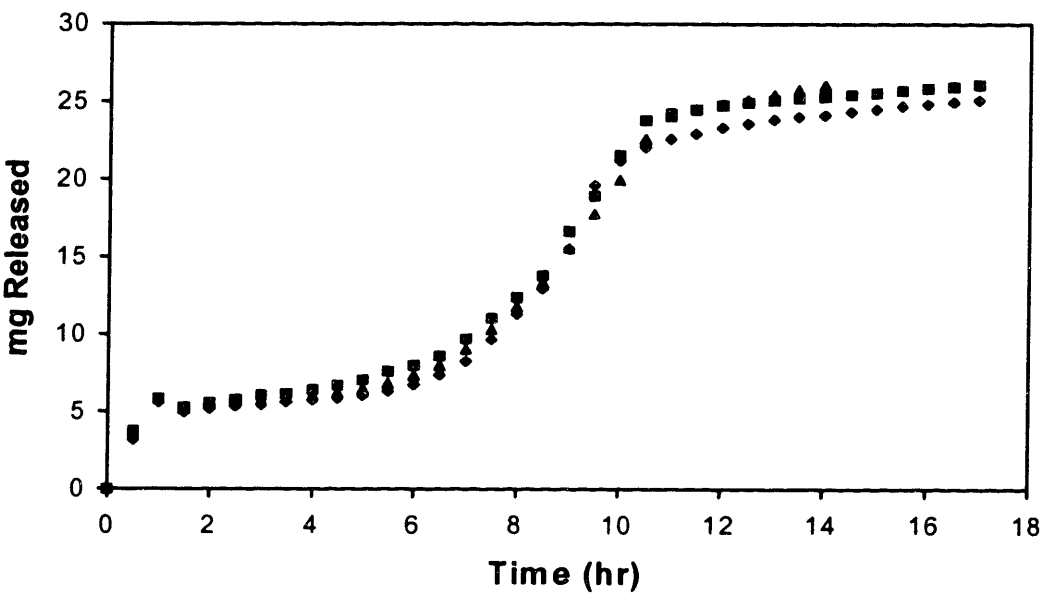

Figure 5.12 Dissolution profile for the Two-Phase Dual Release Tablets[54]

The dual release dosage forms depicted in Figure 5.12 show an immediate release in the stomach as the outer E-100 section erodes. The second release of diclofenac is released from the L-100 section at t=7 hr. The lag time of the second release is controlled by the erosion of the L-100, and the geometry of the device can be altered to produce lag times of 1-16 hours. Additional compartments of active can also be incorporated, producing more than two releases.

The dual release devices were constructed to have two equal 12.5 mg pulses. The release data indicates that the first pulse released only ~6 mg. This shows that the first release was not completed during the first hour of dissolution (acid medium stage pH=1) before the dissolution fluid was changed over to phosphate buffer of pH 7.4. The E100 polymer surrounding the first drug region is not soluble in this pH. It is instead swellable and permeable above pH 5. The remaining ~6 mgs were then released gradually by diffusion through the E100 matrix. The body's pH gradient is not as abrupt, and therefore the E100 is expected to remain soluble for a longer time in-vivo. This would allow a complete first release by an erosion process. The total amount of active released of 25 mg was equal to the desired dose.

5.3 Summary

Oral dosage forms can be manufactured by Three Dimensional Printing to exhibit erosion or diffusion release mechanisms. Both types of tablets exhibited varying lag times and release rates based on the quantity of polymer printed into the tablet during manufacturing. Timing of the release from 3DP tablets can be designed into the manufacturing process by controlling the printing parameters to deliver a specified quantity of polymer into each tablet. Dosage forms have also been fabricated that exhibit complex functionality. Tablets were constructed that contained a quick dissolve region to break the tablet into controlled release

subunits. Devices were fabricated to release two pulses in the intestine, or one pulse in the stomach and a second in the intestine. Lag time between the pulses is controlled by the geometry of the device.

It is important to note that the release mechanism demonstrated by any of these devices is independent of the active printed into the core of the device. 3DP™ allows great flexibility in the formulation of dosage forms by separating the portions of the tablet that contain the active and the sections of the tablet that control the release. This allows rapid formulation of new products by simply changing the solution carrying the active in the printing process.

Modeling, Designing, Printing, and Characterization of Complex HPMC Based Tablets:

Dual Release and Zero Order Formulations

The first step in the fabrication of oral dosage forms by Three Dimensional Printing is modeling and predicting a drug delivery system based on initial empirical inputs about a materials system and other constraints imposed by printing parameters. The complete process of inventing a drug delivery device using 3DP involves many steps, the first of which involves design and prediction based on materials selection, geometry and modeling. Tablets are then fabricated and characterized.

The previous chapters describe the development of this fabrication technique as a tool used for fabricating devices with attributes similar to other pharmaceutical forms (i.e. surface finish, loading), and release profiles unlike other pharmaceutical forms (i.e. lag times, complex release, dual release).

This chapter serves to illustrate how this tool may be used in its fullest extent. Two types of release systems have been invented using information about a specific materials system, modeling techniques, and 3DP to fabricate the dosage form. The first of these tablets is a dual release tablet. The second type is zero order release tablets. Both types of these dosage forms are based on a materials system comprising hydroxypropyl methylcellulose, lactose monohydrate, and Eudragit® L100 copolymer, and release via a surface degradation/erosion mechanism.

Erosion rates were obtained for both chlorpheniramine maleate and diclofenac sodium drugs within matrices of HPMC and varying percentages of lactose adjuvant. These results were then modeled with a surface degradation/erosion model. The information obtained was used to design the two types of complex delivery forms based on non-uniform drug distribution within the 3DP printed matrix.

6.1 Materials Selection for Surface Degradation

The materials system chosen to fabricate zero order and dual release dosage forms was based on the hydrophilic matrix component hydroxypropyl methylcellulose, or Methocel® HPMC (Dow Chemical Company). HPMC powder mixed with adjuvant lactose monohydrate (Pharmatose DCL11) composed the powder bed into which the above drug gradient was printed.

HPMC, a hydrophilic polymer, is a well characterized pharmaceutical excipient.[55, 56, 57, 58] As a matrix material, HPMC quickly hydrates to form a protective gel barrier layer. As water diffuses into the matrix, the HPMC concentration in the hydrated gel layer decreases. The outermost layer of the matrix becomes dilute enough for individual chains to disentangle from the surface by reptation and go into bulk solution. This occurs when the polymer concentration is diluted below a critical polymer concentration, resulting in surface erosion from the matrix.[55] Release kinetics are described as a coupling of drug diffusion and polymer dissolution, i.e. surface erosion. This surface reaction allows dosage forms to be designed and constructed using geometrical considerations.[58, 59]

The release of highly water soluble drugs from such a system has been shown to depend on movement of the diffusion front in the gel layer.[56] It is this relaxation front moving into the center of the dosage form that dictates the kinetics of release from the inner gel boundary.

For release of water insoluble drugs and/or the use of lower viscosity grades of HPMC, the bulk dissolution of the HPMC, or the erosion of the gel itself from the outer regions of gel, may contribute significantly to the overall release kinetics.[58]

Either case suggests that HPMC based formulations have the ability to maintain drug release at the surface of the device.

6.2 Modeling Release Kinetics from Erodible Cylindrical Devices

Analytical relationships describing the kinetics of drug release from erodible polymeric infinite cylinders have been derived by Hopfenberg.[60]. The overall kinetic process in this analysis is characterized using one rate constant, k_o, which does not specify the exact mechanism controlling the erosion process. Instead, it is assumed the erosion process could include dissolution, swelling, chemical reaction of a host polymer, etc. This phenomenological rate constant, k_o, could also describe a combination of the individual relaxations ultimately leading to the surface degradation of the matrix.[60]

Considering the cross-section of a cylinder perpendicular to the cylinder axis and undergoing surface erosion or relaxation, the fractional amount of additive released is

$$\frac{Q}{Q_T} = 1 - \left(1 - \frac{k_o t}{C_o a}\right)^2 \qquad (6.1)^{60}$$

where k_o is the rate constant in mg/hr-cm^2, C_o is the initial concentration, and *a* is the radius.[60] The concentration here is the same as the δ used in Chapter 4. This model is useful in describing the kinetics of any erosion process regardless of the fundamental nature of the mechanism, and assuming there are no other time dependent diffusional resistances.

This model, however, does not consider the release of drug from the top and bottom surfaces of a cylindrical tablet shape. It only describes radial release. Katzhendler et. al. have developed a model to describe drug release from erodible tablets (circular cylinders) undergoing surface erosion.[59] The model, based on the Hopfenberg equation (6.1), takes into account the 3 dimensions of cylindrical release. Katzhendler was able to successfully predict the release of amoxicilin from tablets consisting of two viscosity grades of HPMC.

The kinetics of drug release from erodible cylindrical tablets is analyzed using two coordinates: r, radial, and h, vertical. It is assumed that the erosion front, positioned by coordinate r, moves towards the center of the tablet during dissolution with a constant velocity. This velocity is equal to an erosion constant, k_r, divided by a tablet's uniform and constant concentration, C_o measured in mg/hr-cm^2 and mg/cc respectively.

$$\frac{dr}{dt} = -\frac{k_r}{C_o} \qquad (6.2)^{59}$$

A similar equation is established for the vertical coordinate, h, and because the erosion occurs from two surfaces,

$$\frac{dh}{dt} = -2\frac{k_h}{C_o} \qquad (6.3)^{59}$$

and further integration yields relationships for r and h with respect to time and initial conditions:

$$r(t) = r_o - \frac{k_r t}{C_o} \qquad (6.4)^{59}$$

$$h(t) = h_o - \frac{k_h t}{C_o} \qquad (6.5)^{59}$$

The fractional amount of drug released from the tablet over time, Q/Q_T, is given by:

$$\frac{Q}{Q_T} = 1 - \frac{\pi r^2 h}{\pi r_o^{\,2} h_o} \qquad (6.6)^{59}$$

By substituting equations (6.4) and (6.5) into the above expression (6.6), a new expression, similar to Hopfenberg's equation (6.1) is found:

$$\frac{Q}{Q_T} = 1 - \left(1 - \frac{k_r t}{C_o r_o}\right)^2 \left(1 - \frac{2k_h t}{C_o h_o}\right) \qquad (6.7)^{59}$$

Equation 6.7 describes the drug release from a surface eroding cylindrical device. If it is further assumed that the erosion rate constants in the radial and

vertical directions are the similar, i.e. $k_r \approx k_h \approx k_o$, then equation 6.7 can be further simplified:

$$\frac{Q}{Q_T} = 1 - \left(1 - \frac{k_o t}{C_o r_o}\right)^2 \left(1 - \frac{2k_o t}{C_o h_o}\right) \qquad (6.8)^{59}$$

6.3 Surface Degradation Characteristics of Hydrophilic HPMC Matrices

Equations 6.7 and 6.8 above describe the release of drug from eroding cylindrical geometries assuming that degradation occurs at the surface with constant rates in the radial and vertical dimensions. It is therefore important to determine if the degradation in the materials system selected, HPMC/Lactose, is occurring at the surface and with constant rate.

Tablets were fabricated by 3DP and tested for this purpose. The powder was 70% lactose 53-74μm and 30% HPMC K4M 53-74μm, and the drug solution was 18wt% diclofenac sodium + 0.05wt% fluorescein sodium in methanol. Tablets were printed 32 layers high, and pressed under uniaxial compression to yield tablets 11 mm in diameter and 4.8mm in height. The overall drug loading was 101.8 mg. The printing parameters are detailed in Appendix 3a.

One tablet was pressed between two glass microscope slides, and the assembly was clipped together using standard 1.9cm binder clips as shown below in Figure 6.1. The assembly was then placed in the standard USP dissolution cell using the USP paddle technique with speed of 100RPM in 900mL of phosphate buffer of pH 7.4 at 37°C. The assembly was then removed at various time points and photographed under UV light and white light to show front movement over time.

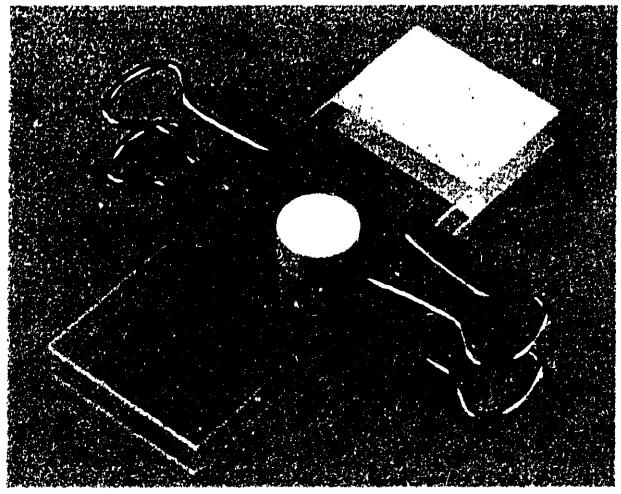

Figure 6.1 Glass slide assembly

Figure 6.2 shows a photograph of the assembly at t=0.5 hr. Degradation was observed to occur at the surface of the tablet as a gel layer was almost immediately formed around the edge preventing the diffusion of water into the interior. The gel layer is very complex. It begins at the hydration front where the HPMC chains begin to disentangle, and continues outward where the gel is increasingly weaker and easy to shear. [57] A clear distinction can be made at the solid/hydrated polymer front. This is represented by the boundary between regions **a** and **b**. The HPMC begins to hydrate and reptation begins at this point, as has also been shown in the literature.[57] The complex gel region is represented by **b**, and the weak diffuse gel/water solution is represented by **c**. The outermost visible circle is the water meniscus.

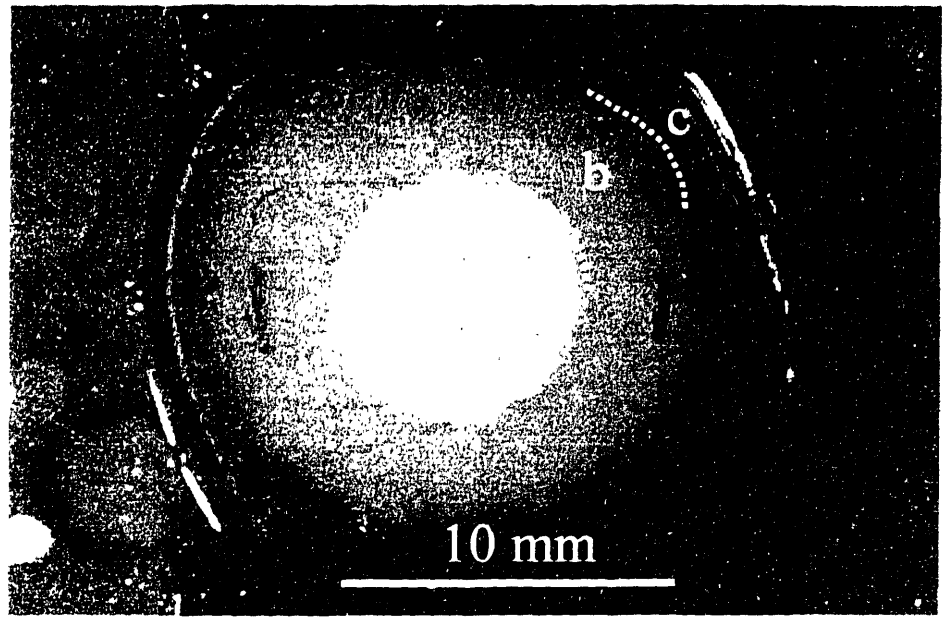

Figure 6.2 Tablet at 30 minutes with gel barrier

It has been shown that polymer relaxation stress at the solid/hydration front contributes to drug transport for both high and low solubility drug compounds and varying drug loadings.[56] Under UV light, very little fluorescein was observed beyond the solid/hydration front. Fluorescein is a highly water soluble compound with strong fluorescence down to very dilute concentrations. The fluorescent yellow coloration disappeared quickly, within 1 mm of the hydration front in all cases. This suggests that the release occurs as a function of the solid/hydration front position. The diameter and radius of the solid region was measured in four radial directions and averaged to give the solid/hydration front position over time shown in Figure 6.3.

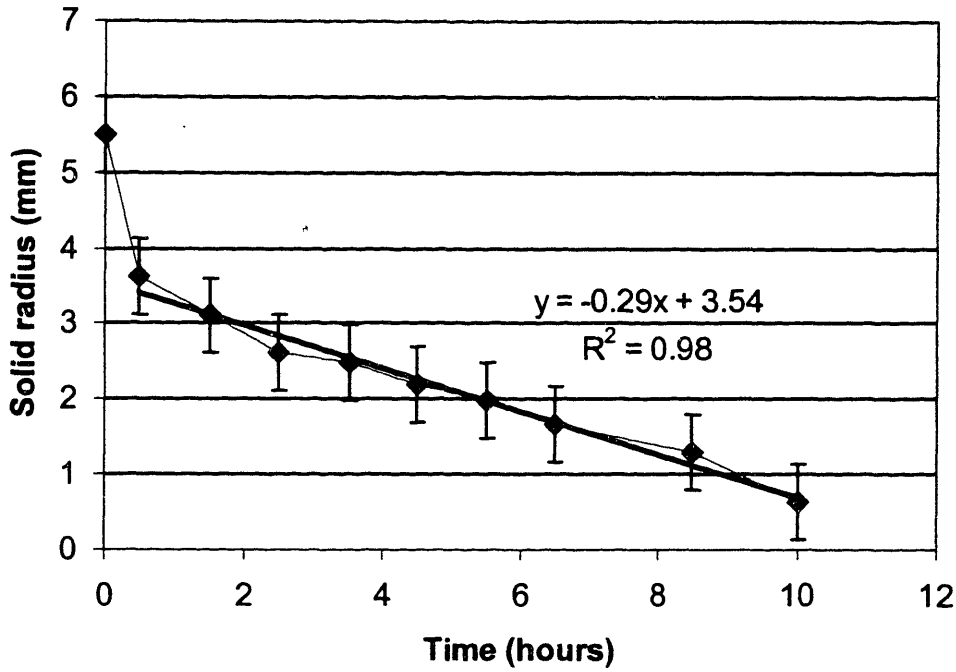

Figure 6.3 Solid/hydration front movement as measured by the solid radius

This solid/hydration front moves with constant rate after an initial stage. During this initial stage, the gel is established as water diffuses rapidly into the surface of the device. This initial effect is also known as the burst effect, and has been shown to cause immediate drug release before the gel layer is established in similar hydrophilic matrices[57] A linear regression through the curve after this initial induction time gives a rate of ~0.29 +/- 0.9 mm/hr. This rate, which follows the solid/hydration or polymer relaxation front, has been shown to be a good estimate of the actual drug release rates for diclofenac and chlorpheniramine maleate, as shown in section 6.4.

6.4 Determination of Erosion Rate Constants of HPMC Matrices

Conventional tablets containing varying proportions of lactose and HPMC K4M were fabricated, each with either 100mg of diclofenac sodium (solubility

limit, c_s= 50mg/ml) (Sigma Chemical Co.) or 100 mg of chlorpheniramine maleate (c_s= 100mg/mL) (Sigma Chemical Co.) to illustrate the dependence of wt% lactose on release kinetics in the HPMC matrices. Combinations of powders of Lactose, HPMC K4M, and drug, given in Table 6.1, were ground together with a mortar and pestle, and then pressed using a tablet die of 11mm in diameter and a pressure of 15000 psi. 5 tablets of each were fabricated. Each was 11.16 mm in diameter and 3.65mm tall as measured by digital calipers after compression. These tablets were then dissolved using the USP dissolution basket method in simulated intestinal fluid of pH 7.4 at 37°C with a speed of 100RPM for 12 hours. The dissolution profiles for the diclofenac tablets are shown in Figure 6.4

Table 6.1 Composition of conventional tablets

Drug	mg drug	mg Lactose	mg HPMC	Lactose:HPMC	C_o (δ) mg_{drug}/cc
diclofenac	100	279	31	90:10	280
diclofenac	100	248	62	80:20	280
diclofenac	100	217	93	70:30	280
diclofenac	100	186	124	60:40	280
diclofenac	100	155	155	50:50	280
chlorpheniramine	100	248	62	80:20	280
chlorpheniramine	100	217	93	70:30	280
chlorpheniramine	100	186	124	60:40	280

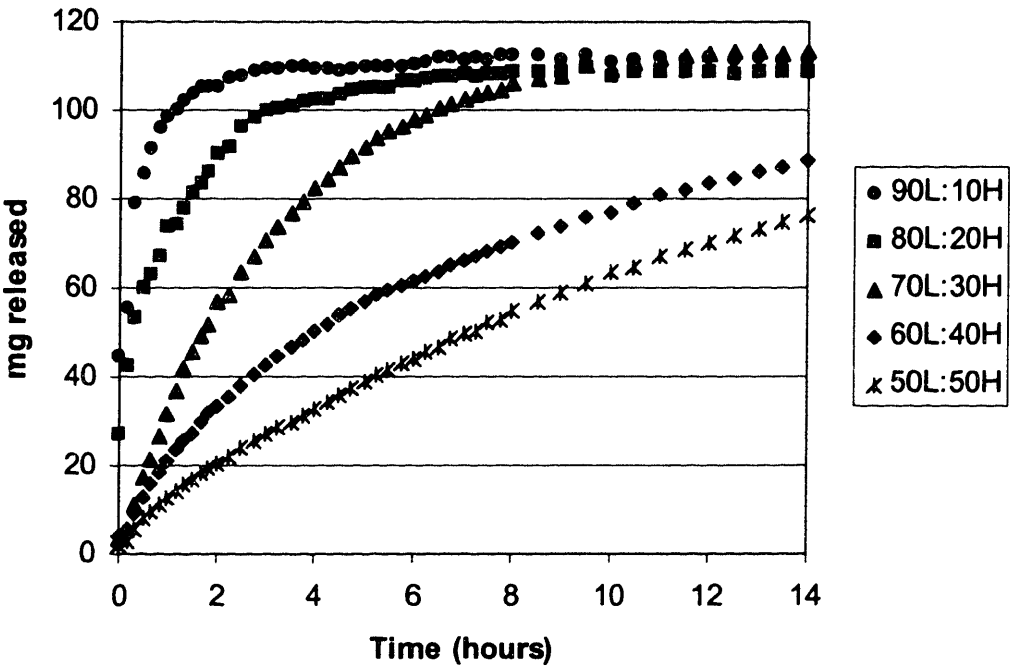

Figure 6.4 Dissolution profiles of diclofenac tablets with varying ratios of Lactose:HPMC

Each of the dissolution curves were fit to equations 6.7 and 6.8 by minimizing the squared difference between the empirical data and model. This was done to determine the relevance of the model, and to determine erosion rate constants for the powder/drug systems. Figure 6.5 shows the excellent fit between empirical results and the model given by equation 6.7 obtained for tablets with 100mg diclofenac and a powder system of 70% lactose and 30% HPMC using erosion rates k_r = 13.902 and k_h = 5.227 mg/hr·cm^2.

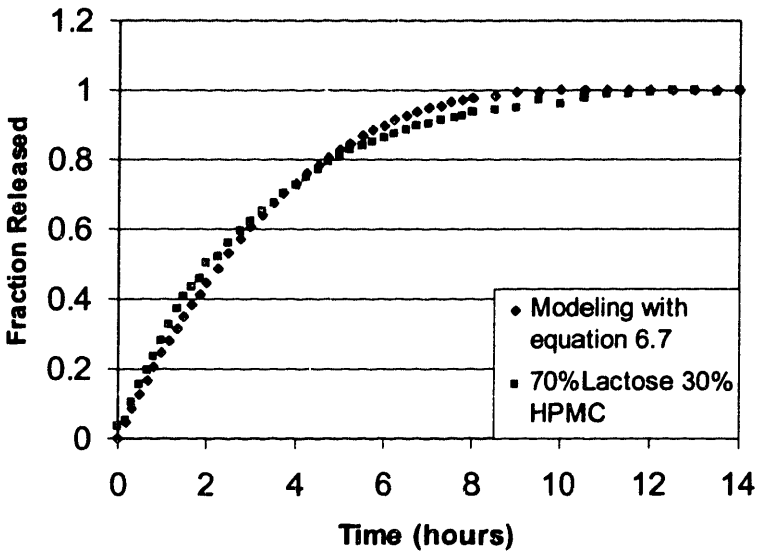

Figure 6.5 Dissolution profile for 70:30 Lactose:HPMC with diclofenac sodium fit to equation 6.7 using erosion rate constants of k_r = 13.902 and k_h = 5.227 mg/hr·cm^2

Table 6.2 summarizes the results of the dissolution tests and gives the best-fit parameters for equations 6.7 and 6.8 with respect to all of the tablets tested. The erosion rate constants are given in units of mg/hr·cm^2.

Table 6.2 Best fit parameters for equations 6.7 and 6.8

Drug	Lactose:HPMC	K_r	K_h	R^2 *(6.7)*	k_o	R^2 *(6.8)*
Diclofenac	60:40	9.097	3.421	0.9970	6.092	0.9886
Diclofenac	70:30	13.902	5.227	0.9979	9.540	0.9919
Diclofenac	80:20	37.884	9.693	0.9818	22.238	0.9871
Chlorpheniramine	60:40	10.136	3.771	0.9972	6.921	0.9901
Chlorpheniramine	70:30	14.823	5.541	0.9980	10.021	0.9876
Chlorpheniramine	80:20	39.214	10.142	0.9872	23.971	0.9872

6.4.1 Observations on the Addition of Lactose to HPMC Matrices

Table 6.2 shows that equations 6.7 (using independent k_r and k_h parameters) and 6.8 (using one k_o parameter) correlate well with the data obtained from the dissolution of these conventional tablets. The correlations between equation 6.7 (independent k_r and k_h parameters) and actual dissolution data are better than those obtained between equation 6.8 (one erosion rate constant, k_o). This is believed to be due to the additional degree of freedom granted by equation 6.7 in letting the two erosion rates in the radial and vertical directions differ. There is, however, no reason to suspect that the two rates would differ for tablets of uniform density and composition.

The addition of lactose to the matrix of tablet greatly accelerates the release rates for both the diclofenac and chlorpheniramine tablets. In both cases the addition of 33% more lactose (60g/100g to 80g/100g) resulted in a factor of ~3X the release rate.

The release rates of chlorpheniramine maleate are approximately 10% higher than the respective release rates of diclofenac sodium. This is due to the chlorpheniramine maleate's higher solubility constant in water. The release of drug from HPMC matrices has been shown to occur within the outer gel layer by a complicated mechanism involving drug diffusion and polymer relaxation of the gel. [58] The polymer relaxation of the matrices of equal fractions of HPMC and lactose may be similar, but the drug diffusion near the outermost portion of the gel layer promotes faster release of chlorpheniramine maleate due to its higher solubility in water.

The linear erosion rate constants for 70%Lactose: 30% HPMC were $\Delta r/\Delta t$= 0.341 mm/hr for diclofenac, and $\Delta r/\Delta t$ = 0.358 mm/hr for chlorpheniramine. These erosion rates are similar to the solid/hydration degradation fronts as measured by the visual experiment in section 6.3 of 0.29 +/- 0.09mm/hr, where the sample was bound between two glass slides and the convection around the sample may have been lower given the shielding.

6.5 Using Rate Constants and Surface Degradation Mechanism to Design Dual Release Tablets Fabricated by 3DP

The above information about the surface degradation mechanism and rate constants of the tablet compositions was used to design dual release tablets to be fabricated by 3DP. The ability of these matrices to degrade at the surface allows for the design of tablets that will release from the exterior of the device inward according to the drug distribution profile. 3DP has the ability to fabricate tablets with non-uniform drug distribution, and therefore the design of tablets for complex release is possible.

6.5.1 Design of Dual Release Tablets

Two tablets were designed to be dual release tablets for fabrication by 3DP. The cross-sectional design of these two tablets are shown in Figure 6.6 The first is a diclofenac sodium dual release tablet, and the second is a chlorpheniramine dual release tablet.

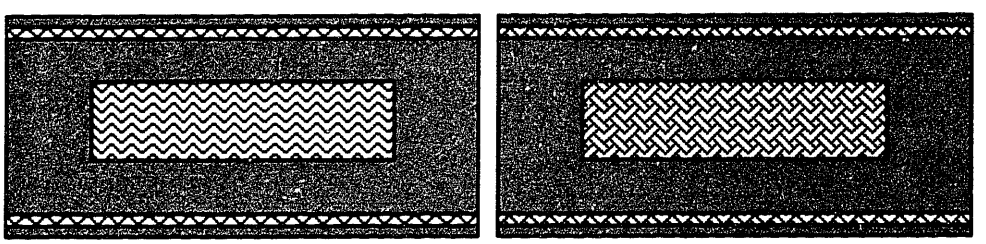

Figure 6.6 Schematic of Dual Release Design: a) Diclofenac sodium tablet b) Chlorpheniramine maleate tablet

These tablets were designed with 3 drug sections. The thin top and bottom sections were one layer tall, and extended the entire diameter of the tablet, 11mm. These two sections were designed to release quickly upon initial imbibition and outer surface deterioration. The center concentric section is 14 layers tall, 7mm in diameter and it is designed for a secondary delayed and

controlled release. The tablet was designed to be 36 layers overall, with a non-uniform drug distribution described in Table 6.3.

Table 6.3 Drug distribution along vertical axis in Dual Release Designs

N	Dosage	Diclofenac Tablets (mgs)	Chlorpheniramine Tablets (mgs)
2 layers	-	-	-
1 layer	$N \varepsilon \Delta z \, \delta \pi (0.55cm)^2$	3.26	2.90
10 layers	-	-	-
14 layers	$N \varepsilon \Delta z \, \delta \pi (0.35cm)^2$	19.30	17.18
10 layers	-	-	-
1 layer	$N \varepsilon \Delta z \, \delta \pi (0.55cm)^2$	3.26	2.90
2 layers	-	-	-

ε represents the compression factor, Δz is the layer height, and C_p is the printed concentration in that layer. Table 6.3 also shows actual tablets fabricated with this design, as discussed below (see section 6.5.2) for two samples, diclofenac sodium dual release tablets and chlorpheniramine maleate dual release tablets. For these tablets, the compression factor was 0.55, the layer thickness was 200μm, and δ(diclofenac) was 312mg/cc and δ (chlorpheniramine) was 277mg/cc.

Numerical methods were used to construct theoretical release profiles based on the above design and the erosion rate constants for matrices of 70% lactose 30% HPMC for both compounds, and an initial layer thickness of 200μm. The numerical methods used a spreadsheet to iteratively integrate a cylinder of reducing volume using time steps of 0.1 hour. It was assumed that the erosion rates were constant and therefore the degradation front movement into the sample was constant in both the radial and vertical directions. The resulting theoretical release plots, both incremental release vs. time and cumulative release vs. time, for chlorpheniramine maleate dual release tablets are shown in

Figure 6.7. Note that because equal time divisions were used, the incremental release also represents the release rate over time.

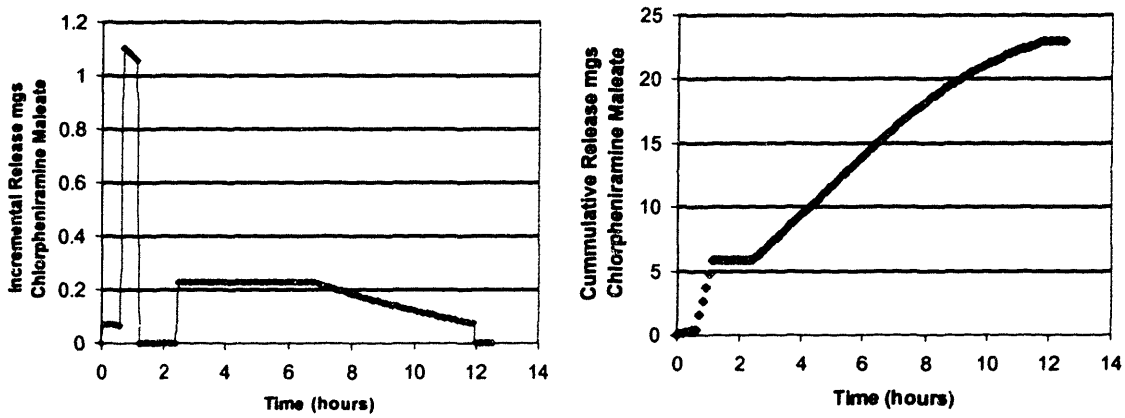

Figure 6.7 Theoretical release plots for Chlorpheniramine Maleate Dual Release Tablets

6.5.2 Fabrication of Dual Release Tablets by 3DP

Both diclofenac and chlorpheniramine tablets were fabricated by 3DP (CJ CD OSP) using 36 layers of 200μm layer thickness. The powder was 70wt% 53-74μm lactose and 30wt% 53-74μm HPMC K4M. The binder solution used for both was 5wt% L100 in ethanol and the drug solutions were respectively 18wt% diclofenac sodium in methanol and 20wt% chlorpheniramine maleate in 80:20 ethanol:D.I. H_2O. Post printed samples were allowed to dry for 2 days in a nitrogen glove box and then pressed in a tablet die of 11mm in diameter to final heights of 3.25 (+/- 0.04) mm as determined by digital calipers. Table 6.3 above shows the overall drug distribution printed into these tablets. Appendix 3b and 3c summarizes the printing parameters for these samples.

6.5.3 Dissolution of Dual Release Tablets

Two each of the diclofenac and chlorpheniramine dual release tablets were characterized by USP dissolution basket method in simulated intestinal fluid of pH 7.4 at a temperature of 37°C and basket rotation speed of 100RPM. The two dissolution profiles for each drug were averaged together, compared with the respective theoretical release profile, and are shown in Figures 6.8 through 6.11.

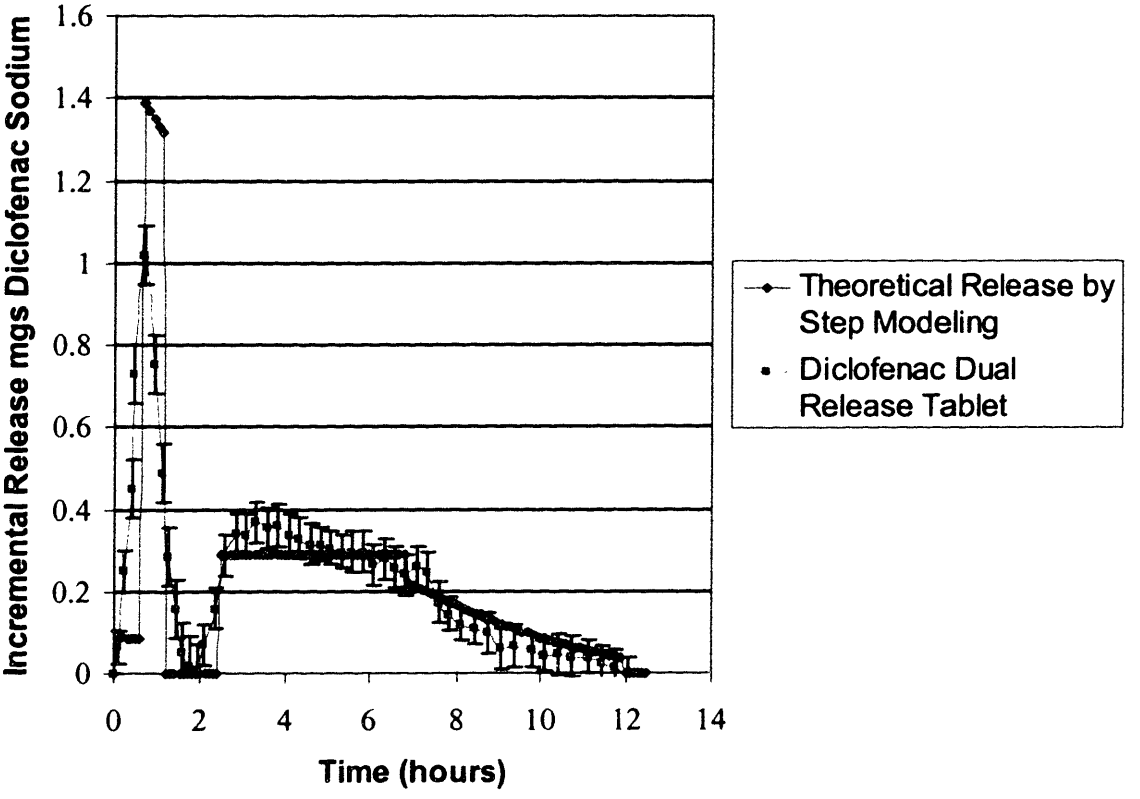

Figure 6.8 Incremental release over time of the Diclofenac Sodium Dual Release Tablets

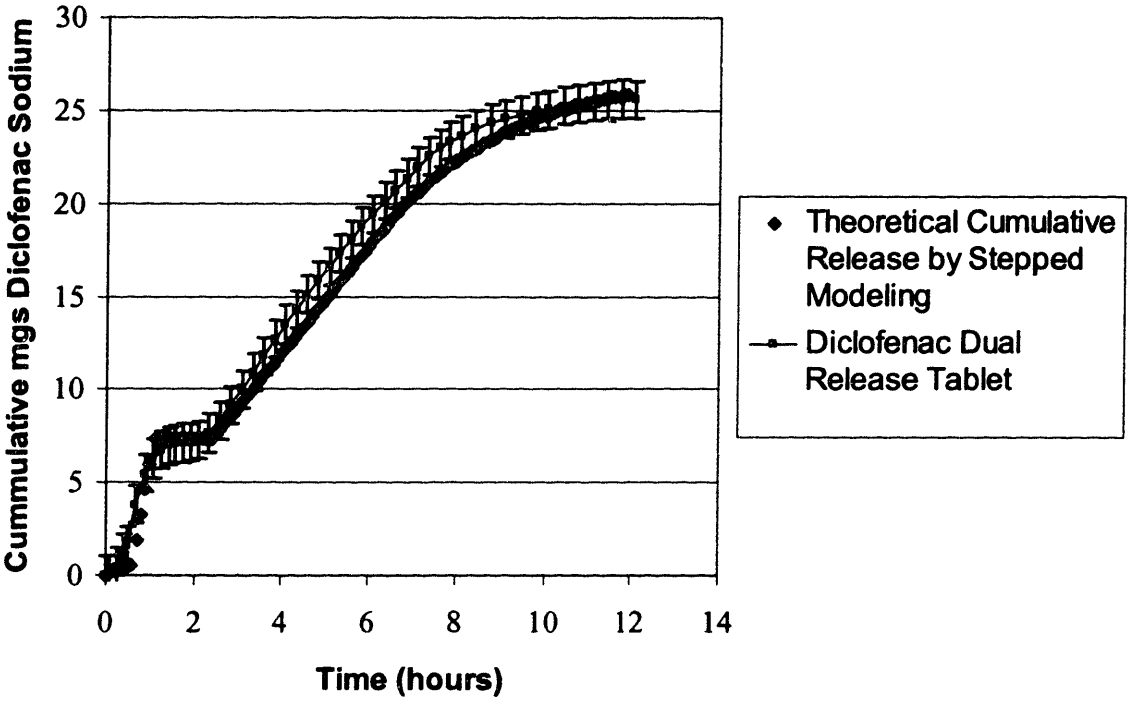

Figure 6.9 Cumulative release profile of the Diclofenac Sodium Dual Release Tablets

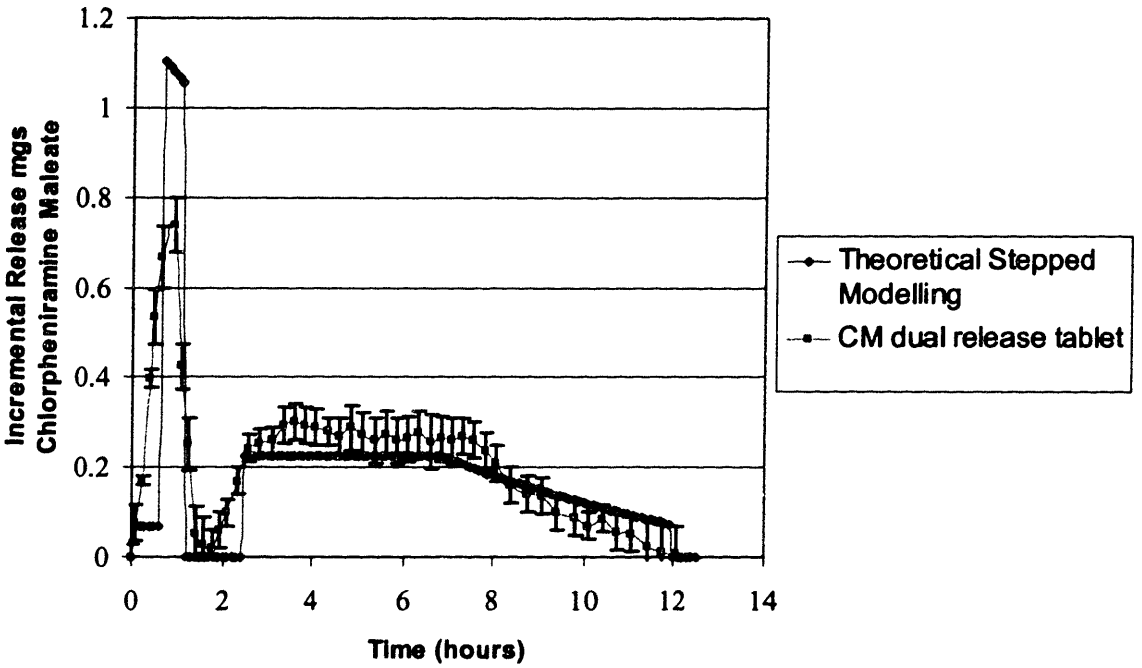

Figure 6.10 Incremental release over time of the Chlorpheniramine Maleate Dual Release Tablets

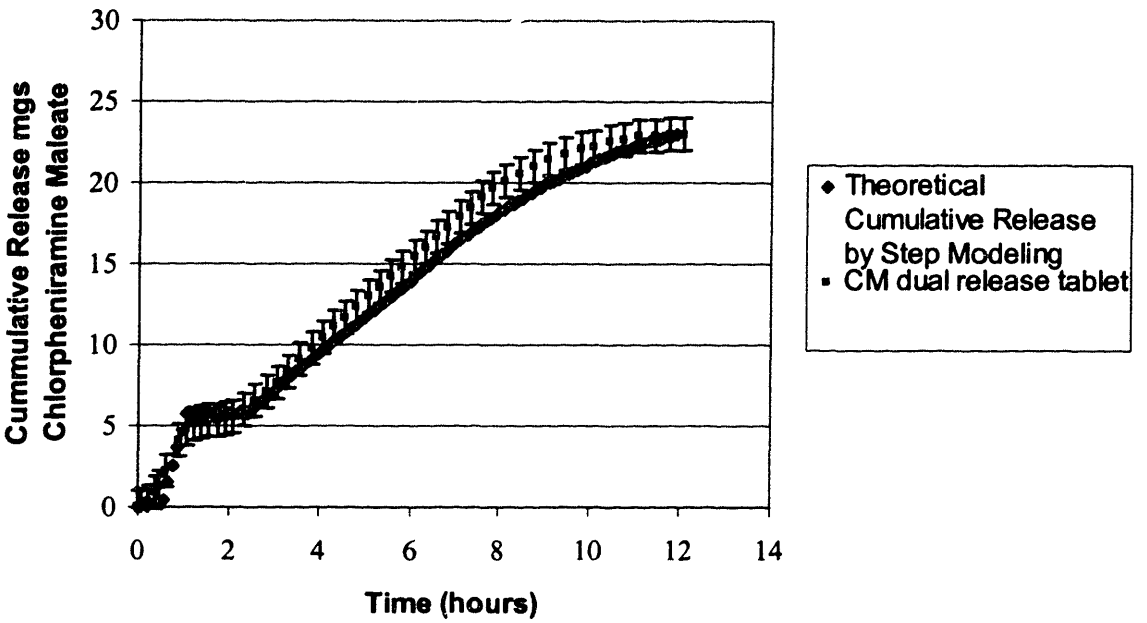

Figure 6.11 Cumulative dissolution profile for the Chlorpheniramine maleate Dual Release Tablets

6.5.4 Observations

Each of the release profiles for the diclofenac sodium tablets and the chlorpheniramine maleate samples do follow the theoretical release profiles as calculated from each system's respective erosion rate constants found in section 6.4. There are three small differences, however, between the empirical and predicted curves in these figures.

The first effect that can be seen especially in the incremental release plots, Figures 6.8 and 6.10, is a burst effect. Drug was released from the outermost drug regions prematurely as the initial gel layer was still being formed. This effect was illustrated in Figure 6.3, where the erosion rate was not constant during the first ~30 min. of dissolution. The theoretical model assumes constant erosion rate throughout the tablet, which explains why the theoretical plot shows lower release during the first 30 minutes. The entire first peak is shifted to the

left as the drug from the top and bottom sections is released sooner than predicted.

The second effect is a broadening of the release peaks. The actual release profiles above do not follow the strict, sharp release profile of the model tablet. The release peaks are wider, release begins sooner than predicted, and the release tends to end later. This can be partly attributed to drug migration in the powder bed during printing. It was previously shown in chapter section 3.2 that part resolution is limited by capillary effects in the powder bed. Such effects are needed to knit together the finite layers of the printed structure. The theoretical "model" tablet has been modeled neglecting such effects. It was modeled with a sharp stepped drug distribution profile.

The third difference can be best observed from Figures 6.9 and 6.11, the cumulative release profiles. The actual release seems to expire before that of the model tablets. The actual release curves are shifted somewhat to the left as compared to the model. This may be due to differences in the release rates between conventional tablets and 3DP tablets. The parameters used to establish the model system came from section 6.4, Table 6.2, for conventional tablets. These conventional tablets were pressed together from mixed powder mixtures, and were not printed. The conventional tablets were constructed with approximately the same drug concentration as the drug sections of the printed samples, they were approximately the same size, and they were tested under the same conditions. The only difference is the fabrication technique. It should be noted, however, that the information acquired from the conventional tablets is a good approximation, and provides a fast and easy alternative to data collection from 3DP tablets.

6.6 Zero Order Release Tablets Fabricated by Three Dimensional Printing

True zero order release is difficult to obtain with traditional tablet geometries.[59, 61] The surface area of an erosion-based tablet becomes smaller over time, and thus there is less drug released over time. This is apparent in figure 6.4 in which the release rates of the HPMC/Lactose tablets with uniform drug concentration decrease over time. The surface area is essentially constant for diffusion type matrices, but drug inside the matrix is not available in infinite supply, and therefore the driving force for diffusion out of the matrix decreases as the concentration within the matrix decreases.

Researchers have recently claimed zero order release from other geometries and devices. Zero order release has been achieved by Langer in surface-erodible thin slabs of uniform drug distribution.[62] Kerč[5] has approximated zero order release using a three phase pharmaceutical form in which the different phases degrade at different rates. A device has recently been invented by Odidi[61] which features a osmotic "push-pull" mechanism as a means to achieve zero order.

Three Dimensional Printing has the advantage of distributing drug non-uniformly throughout a matrix. This feature of the technology is used here to fabricate zero order tablets that undergo constant surface degradation, but have an increasing drug concentration to complement the volumetric non-uniformity of the eroding layers. Any decrease in volume released over time can be compensated with a corresponding increase in drug concentration.

6.6.1 Model of Drug Distribution in Erodible Tablets to Achieve Zero Order Release

Two geometries have been considered. The first is that of an infinite cylinder, or a tablet that is allowed to release from the lateral surface in the radial

direction only. The second is that of a true tablet shape in which release occurs from all three surfaces of a circular cylinder.

6.6.1.1 Model of Drug Distribution in Radial-Release Zero-order Tablets

It is assumed that the radial surface erosion rate, σ (in units of length/time), of an infinite cylinder is constant. For the case of erosion from the lateral side of a circular cylinder only,

$$\sigma = -\frac{\rho \cdot 2\pi r h \cdot \partial r}{\rho \cdot \pi r^2 h \cdot \partial t} = -\frac{2\partial r}{r\partial t} \tag{6.9}$$

where ρ represents the density of the erodible cylinder, and h is the constant height.

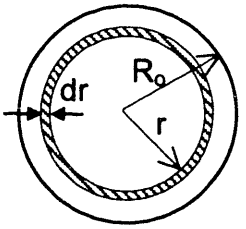

The release profile is defined as the fraction of material, Q, released divided by the total amount of material to be released, Q_T, or:

$$\frac{Q}{Q_T} = \frac{1}{Q_T}\int_r^{R_o} C(r) \cdot 2\pi r h \partial r \tag{6.10}$$

where C(r) is the drug distribution throughout the cylinder as a function of the radius.

The drug release rate in such a delivery form would decrease as the radius r decreases if the drug distribution is constant and uniform. A zero order release system, or a system with constant drug delivery rate, is obtained when the drug distribution complements the volumetric non-uniformity of the eroding layers.

The drug release rate will be a constant, q,

$$\frac{\partial}{\partial t}(\frac{Q}{Q_T}) = \frac{1}{Q_T}[-C(r)\cdot 2\pi rh]\frac{\partial r}{\partial t} = q \qquad (6.11)$$

if and only if the initial drug distribution, C(r), has the following form:

$$C(r) = \frac{Q_T q}{\pi\sigma h r^2} \qquad (6.12)$$

This analysis shows that in order to fabricate a cylindrical dosage form with radial drug release, the drug must be distributed in the dosage form in such a way that the concentration be inversely proportional to the radius squared.

$$C(r) \propto \frac{1}{r^2} \qquad (6.13)$$

6.6.1.2 Model of Drug Distribution in 3D-Release Zero-order Tablets

It is assumed that the surface erosion rates in the radial and vertical directions are constant and equal. The erosion front moves a fixed distance into the device, Δl, at every time interval, Δt, during surface erosion. The surface area, A, of this erosion front decreases as erosion continues, and the volume elements, $A\Delta l$, also decrease over time. The incremental drug release from each element is $CA\Delta l$ where C is the drug concentration in that element. The amount of drug released in one element must equal the amount of drug released from all subsequent elements in order to achieve a constant release rate, or

$$C_o A_o = C_1 A_1 = C_2 A_2 = C_3 A_3 ..... = C_n A_n \qquad (6.14)$$

6.6.2 Design of Zero Order Tablets for 3DP Fabrication

The above models for zero-order release from infinite cylinders and tablet shaped cylinders were used to design tablets for fabrication with 3DP. Section 6.6.2.1 below describes the design of Radial-Release Zero-order tablets that have been capped to allow release in the radial direction only. Section 6.6.2.2 describes the design of 3D-Release Zero-order tablets which release from all 3 surfaces of the tablet.

6.6.2.1 Radial-Release Zero Order Tablet Design

The concentration dependence on the radius of an infinite cylinder given in equation 6.12 was used to design a drug gradient in printed tablets. A drug concentration that decreases with r^2 was approximated by defining 5 concentric circles with corresponding radii to establish 5 concentration zones as shown in Figure 6.12. These 5 circles constitute printed areas within one printed layer; the first print pass deposits drug solution into the largest circle, the second print pass deposits drug solution into the second largest concentric area, etc. The result of this printing operation is a single layer in which the centermost and smallest circular region is saturated 5 times, and has a concentration that is 5 times greater than the outermost and largest circular region. This two dimensional pattern is illustrated in Figure 6.13.

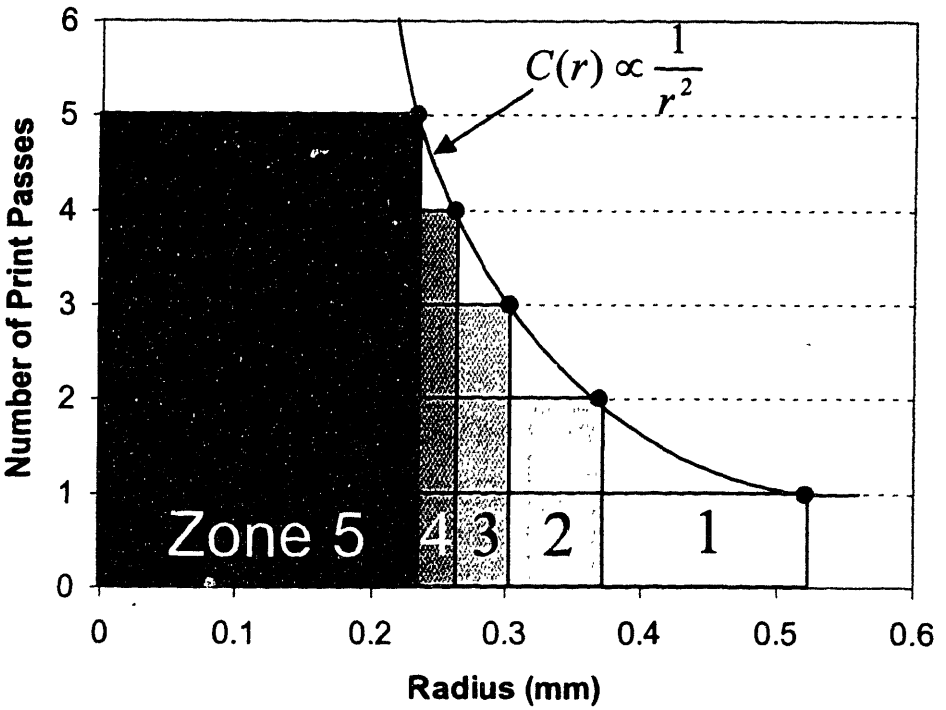

Figure 6.12 Drug concentration as a function of distance and 5 concentration zones

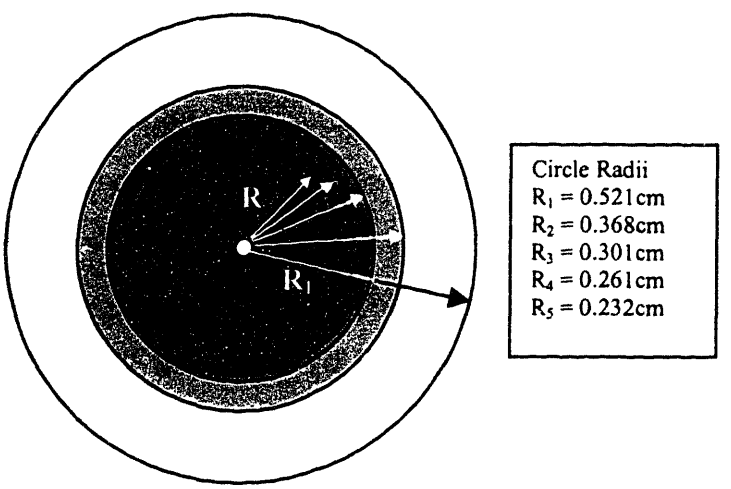

Figure 6.13 Concentric circle zones, approximation of gradient $C(r) \sim 1/r^2$

Three sections were then further established. These sections are shown in Figure 6.14. Sections 1 and 3 are low permeability, slow erosion end caps that prevent drug release in the vertical dimension. Section 2 has the above described concentration zones to allow radial release from the lateral surface. This multi-section tablet was designed to release drug radially from section 2, but not through the end caps, thus allowing it to be modeled by equation 6.1 for an infinite cylinder.

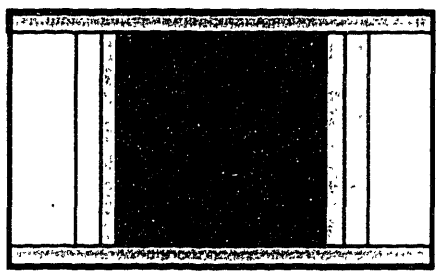

Figure 6.14 Radial-Release Zero-order Tablet Design

6.6.2.2 3D-Release Zero-order Tablet Design

Five concentration sections, C_1, $C_2=2C_1$, $C_3=3C_1$, $C_4=4C_1$, and $C_5=5C_1$, were used to define the printed drug distribution for 3D-Release Zero-order tablets. The multiplicity of these concentrations represent the number of print passes over one region in one layer. The concentration sections were found by starting with a tablet's outer dimensions and surface area, A_1, and the concentration obtained from one print pass, C_1, and solving for A_2 through A_5 with equation 6.14: $C_1A_1 = C_2A_2 = C_3A_3 = C_4A_4 = C_5A_5$. The radii and heights of the concentration sections are found by assuming that the surface erosion rates are equal in the radial and vertical directions. The ideal heights were then modified slightly to take into account the discrete layer thicknesses of the printing process, and the radii were also modified to take into account the discrete line

spacing of the printing process. Table 6.4 gives the radii, heights, and concentrations of each of the sections used for 3DP fabrication with line spacing of 120μm and layer height of 305μm. Figure 6.15 shows the schematic of the vertical cross section of a 3D-Release Zero-order tablet.

Table 6.4 Concentration, radii, and heights of concentration sections in 3D-Release Zero-order Tablets

Section	Concentration	Outer radius (mm)	Outer height (mm)
1	C_1	5.28	4.73
2	$2C_1$	3.72	3.20
3	$3C_1$	3.00	2.59
4	$4C_1$	2.64	2.28
5	$5C_1$	2.4	1.98

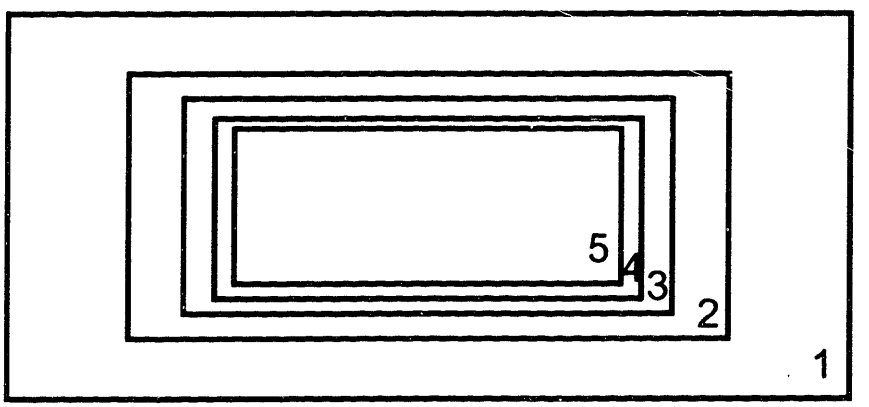

Figure 6.15 3D-Release Zero-order Tablet Schematic

6.6.3 Fabrication by 3DP

6.6.3.1 Fabrication of Radial-Release Zero-order Tablets

Two sets of 5 of the Radial-Release Zero-order tablets were fabricated as described in 6.6.2.1. One set of similar tablets was printed with a uniform drug

distribution in the center section for comparison. Each set of tablets were constructed with the same end caps, sections 1 and 3, but differ in the powder system used to construct section 2.

The mutual end cap sections 1 and 3 were printed using a 3wt% L100 in ethanol solution and 100% high viscosity blend HPMC K4M powder, in the size range 74-106μm. The saturation in these sections was 1.2. These cap sections are essentially impermeable in water. Similar discs pressed from 100% HPMC took weeks to swell and/or erode in independent tests. Each of the end cap sections were 8 layers tall with a layer thickness of 300μm.

The first set of tablets was fabricated with a center section composed of powder of 70% Lactose (53-74μm) : 30wt% HPMC K4M (53-74μm) and had a constant *uniform* diclofenac distribution and overall loading of 44.1mg of diclofenac.

The second and third sets of tablets were fabricated with the radial distribution from Figure 6.13. The second set was fabricated with a center section composed of powder of 80% Lactose (53-74μm) : 20wt% HPMC K4M (53-74μm) and an overall diclofenac loading of 101.8mg distributed radially in the 5 concentration zones. The third set of tablets was fabricated with a center section composed of powder of 70% Lactose (53-74μm) : 30wt% HPMC K4M (53-74μm) and an overall diclofenac loading of 100.7mg distributed radially in the 5 concentration zones.

The distribution of diclofenac in these devices is given in Table 6.5 through Table 6.7 below. All of the tablets were allowed to dry for a minimum of 48 hours in a nitrogen glove box and then pressed in a 11mm die to a pressure of 15000 psi. The resulting tablets had diameters of 11mm and cap thicknesses of 1.21mm and center sections of 4.82mm in height. The printing parameters for section 2 of the above devices are listed in Appendices 3d-3f.

Table 6.5 Constant uniform drug distribution for tablet set 1: 70:30 tablets

Zone	Radius (mm)	Volume (mm^3)	# Times saturated	Concentration (mg/mm^3)	Loading (mg)
1	0.521	411.03	1X	0.099	44.1
Total					**44.1**

Table 6.6 Radial drug distribution for tablet set 2: 80:20 tablets

Zone	Outer radius (mm)	Inner radius (mm)	Volume (mm^3)	# Times saturated	Concentration (mg/mm^3)	Loading (mg)
1	5.21	3.68	205.96	1X	0.108	22.34
2	3.68	3.01	67.87	2X	0.217	14.72
3	3.01	2.61	34.04	3X	0.325	11.08
4	2.61	2.33	20.95	4X	0.434	9.09
5	2.33	-	82.21	5X	0.542	44.58
Total						**101.8 mg**

Table 6.7 Radial drug distribution for tablet set 3: 70:30 tablets

Zone	Outer radius (mm)	Inner radius (mm)	Volume (mm^3)	# Times saturated	Concentration (mg/mm^3)	Loading (mg)
1	5.21	3.68	205.96	1X	0.107	22.1
2	3.68	3.01	67.87	2X	0.215	14.56
3	3.01	2.61	34.04	3X	0.322	10.96
4	2.61	2.33	20.95	4X	0.429	8.99
5	2.33	-	82 21	5X	0.536	44.10
Total						**100.7 mg**

6.6.3.2 Fabrication of 3D-Release Zero-order Tablets

3D-Release Zero-order Tablets were fabricated by 3DP with the geometry given in Figure 6.15. The printed drug solution was 18.0wt% diclofenac sodium/ 1wt% PVP, and 81wt% methanol. The powder consisted of 70wt% lactose and 30wt% HPMC K4M. A total of 30 layers were printed with layer thickness of 305μm for an overall tablet height of ~9.2mm. The printing parameters used during the fabrication are given in Appendix 3g. Tablets were allowed to dry for 36hours in a nitrogen glove box, and were then pressed at 15000psi in a 11mm diameter tablet die to an average of 4.37 +/- 0.03mm in height. Table 6.8 gives the concentrations and dosages printed into each of the 5 sections. The overall loading printed into each tablet was 71.65 milligrams.

Table 6.8 3D-Release Zero-order Tablets: Printed Drug Distribution

Section	Volume (mm^3)	Concentration (mg/mm^3)	Loading (mg)
1	256.23	0.110	28.19
2	60.63	0.220	13.34
3	21.21	0.330	6.99
4	13.07	0.440	5.75
5	31.59	0.550	17.38
Total			**71.65 mg**

6.6.4 Determination of Rate Constants for Concentration Zones in the Radial-Release Zero-order Tablets

Conventional diclofenac tablets were pressed containing varying concentrations of diclofenac sodium in the powder systems of 70:30 and 80:20 (Lactose:HPMC). Ten tablets, all approximately 3 mm tall and 11.15mm in diameter, were pressed using 15000 psi. Caps were then fabricated by pressing 100mg of HPMC powder. The caps were then slightly wetted on one side with water and adhered to the top and bottom of the tablets. The ensembles were then allowed to dry for 30 minutes at 35°C in a drying oven. (VWR) The tablets were then dissolved using the USP dissolution basket method in simulated intestinal fluid of pH 7.4 at 37°C with a speed of 100 RPM for 6 hours. During the dissolution, the caps were observed to stay in place and erosion occurred from the radius of the samples. The fraction of drug released over time was then modeled with the Hopfenberg equation (6.1) for infinite cylinders to obtain radial erosion rate constants, k_r. The best-fit erosion rate constants have been plotted below in Figure 6.16 versus the concentration of diclofenac per tablet volume for both powder systems.

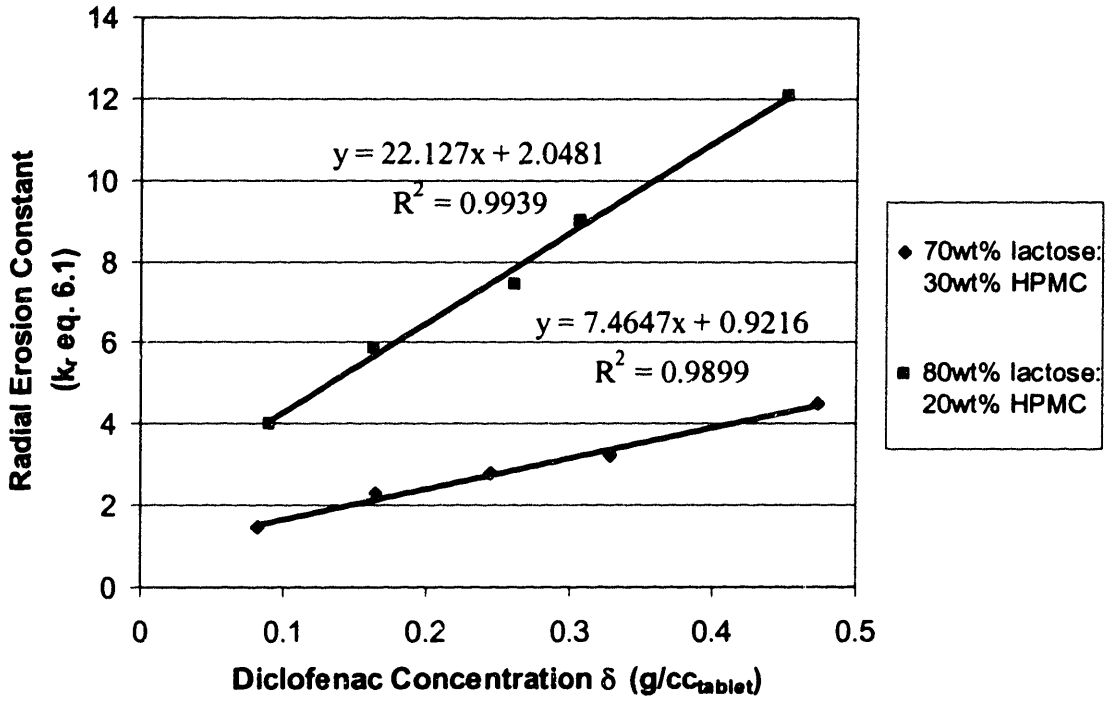

Figure 6.16 Radial erosion rate constants vs. diclofenac concentration

The erosion constants obtained from the Hopfenberg equation (6.1) seem to scale linearly with the diclofenac dosage for equal tablet volumes:

80%Lactose : 20% HPMC Powder: $k_r = 22.127(C_{diclo}) + 2.0481$ 6.15

70%Lactose : 30% HPMC Powder: $k_r = 7.4647(C_{diclo}) + 0.9216$ 6.16

This linear dependence on diclofenac concentration was then used to approximate erosion rate constants for the 5 concentration zones of the radial distribution tablets. The erosion rate constants for the 5 zones are given below in Table 6.9 (80:20) and Table 6.10 (70:30).

Table 6.9 Erosion rate constants for the 5 concentration zones in the 80:20 Radial-Release Zero-order tablets

Zone	C_{diclo} (δ) (mg/mm^3)	k_r (from eq. 6.15)
1	0.108	4.26
2	0.217	6.47
3	0.325	8.68
4	0.434	10.90
5	0.542	13.11

Table 6.10 Erosion rate constants for the 5 concentration zones in the 70:30 Radial-Release Zero-order tablets

Zone	C_{diclo} (δ) (mg/mm^3)	k_r (from eq.6.16)
1	0.107	1.67
2	0.215	2.41
3	0.322	3.16
4	0.429	3.91
5	0.536	4.65

6.6.5 Characterization of Radial-Release Tablets

The three types of printed tablets, represented in Tables 6.5-6.7, were dissolved in 1000mL of phosphate buffer solution, pH 7.4, at 37°C in a USP dissolution apparatus (Logan, Instruments D400) using the USP I basket method at 100RPM. UV absorbance was measured at 275nm, the peak absorbance wavelength for diclofenac sodium. The samples were referenced to the

absorbance of 100mg of diclofenac sodium dissolved in 1000mL of the buffer solution.

Figure 6.17 shows the dissolution results for the first set of tablets in which drug distribution was constant and uniform through the center section. The data is compared to the model for release from an infinite cylinder of constant uniform starting drug distribution (equation 6.1)

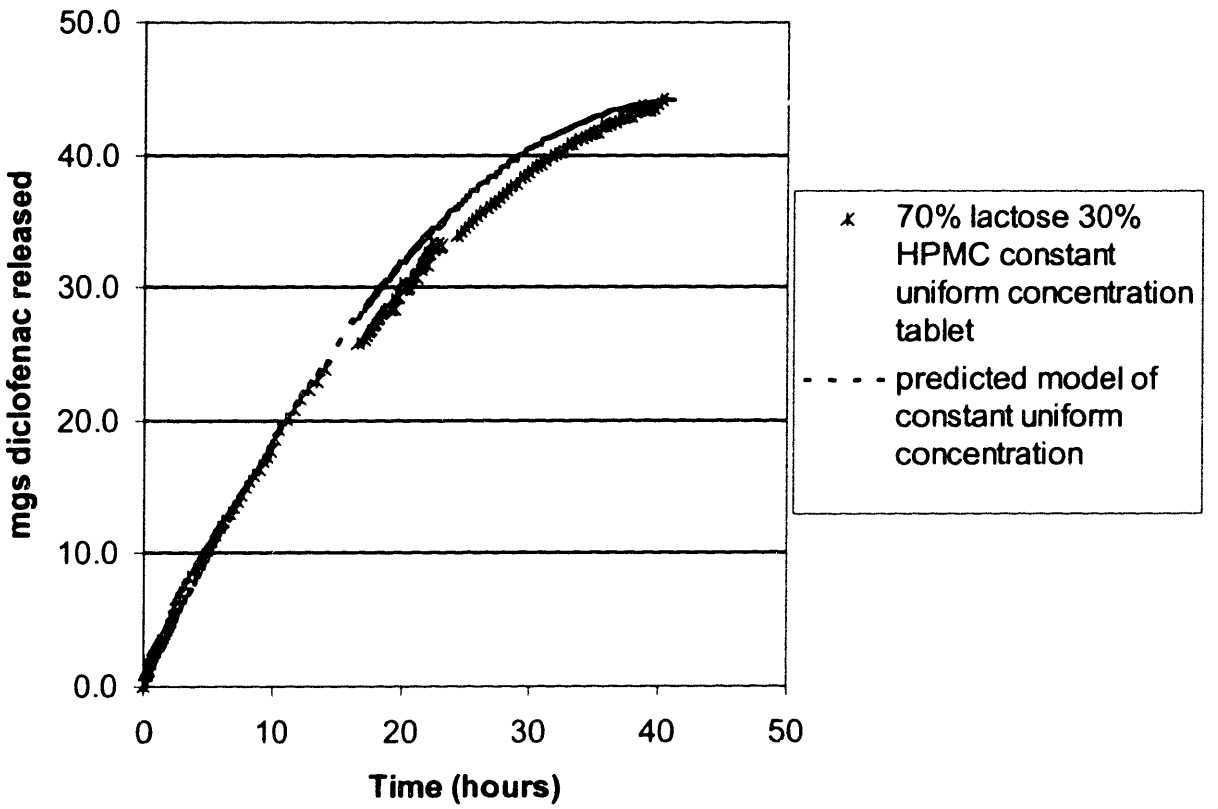

Figure 6.17 Release vs. model for constant concentration of uniform distribution

Figure 6.18 shows the dissolution results for the second and third set of tablets in which diclofenac was radially distributed throughout the center section. The data is compared to a model for release such that:

$$\frac{Q}{Q_{TOTAL}} = 1 - \left(1 - \frac{k_{r,zone1}t}{C_{zone1}r_1}\right)^2 \Bigg]_{r_1}^{r_2} + 1 - \left(1 - \frac{k_{r,zone2}t}{C_{zone2}r_2}\right)^2 \Bigg]_{r_2}^{r_3} + 1 - \left(1 - \frac{k_{r,zone3}t}{C_{zone3}r_3}\right)^2 \Bigg]_{r_3}^{r_4}$$

$$+ 1 - \left(1 - \frac{k_{r,zone4}t}{C_{zone4}r_4}\right)^2 \Bigg]_{r_4}^{r_5} + 1 - \left(1 - \frac{k_{r,zone5}t}{C_{zone5}r_5}\right)^2$$

6.17

This predicted release is a composite of several release curves, each describing the release from an infinite cylinder for 5 concentration zones. The release curves are added together such that each concentration and erosion rate begin at the appropriate radius. The diclofenac concentrations and erosion rate constants for each zone are given above in Table 6.9 and Table 6.10.

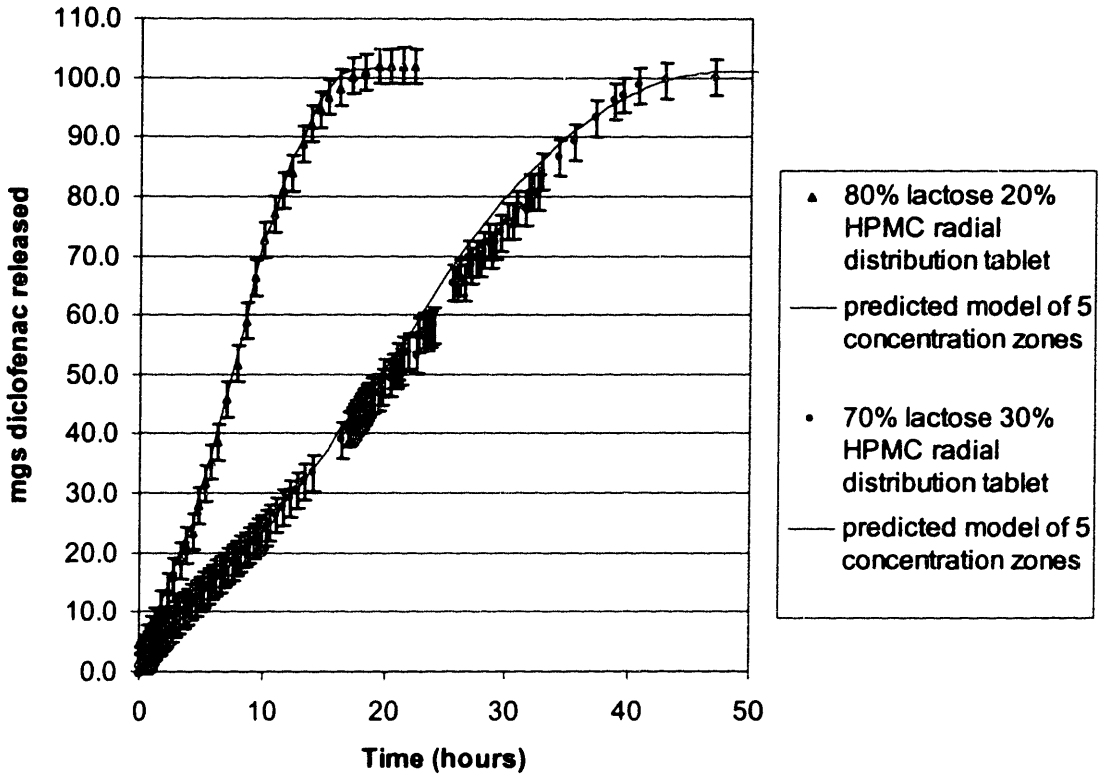

Figure 6.18 Diclofenac release vs. model for Radial-Release Zero-order Tablets

Figure 6.19 shows the actual dissolution data for the two radial distribution tablets as compared to linear regression lines. Such linearity would result from a printing a continuous gradient of drug concentration, such as given in equation 6.12, rather than the discontinuous 5 concentration zones.

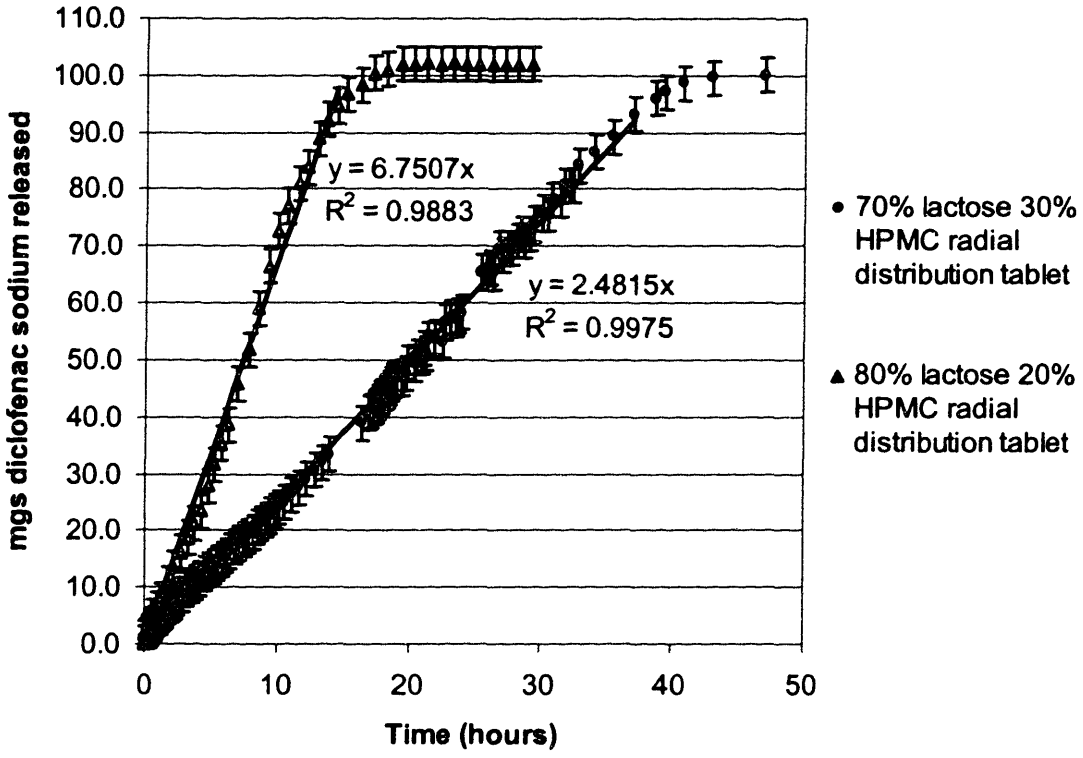

Figure 6.19 Diclofenac release from Radial-Release Zero-order Tablets vs. linear regression curves

6.6.6 Characterization of 3D-Release Zero-order Tablets

Two 3D-Release Zero-order tablets, represented in Table 6.8, were dissolved in 1000mL of phosphate buffer solution, pH 7.4, at 37°C in a USP dissolution apparatus (Logan, Instruments D400) using the USP I basket method at 100RPM. UV absorbance measurements were taken over time at 275nm, the peak absorbance wavelength for diclofenac sodium.

Figure 6.20 shows the cumulative release of diclofenac sodium from the 3D-Release Zero-order tablets over time. The results of the dissolution show that the tablets release over a 10-hour period. The cumulative release of 68.7mg is 2.6% lower than the predicted overall dosage of 71.56mg determined by printing parameters. Figure 6.20 also shows the predicted release profile for

perfect erosion of the tablet design from all three surfaces with a surface erosion rate of 0.32 mm/hr.

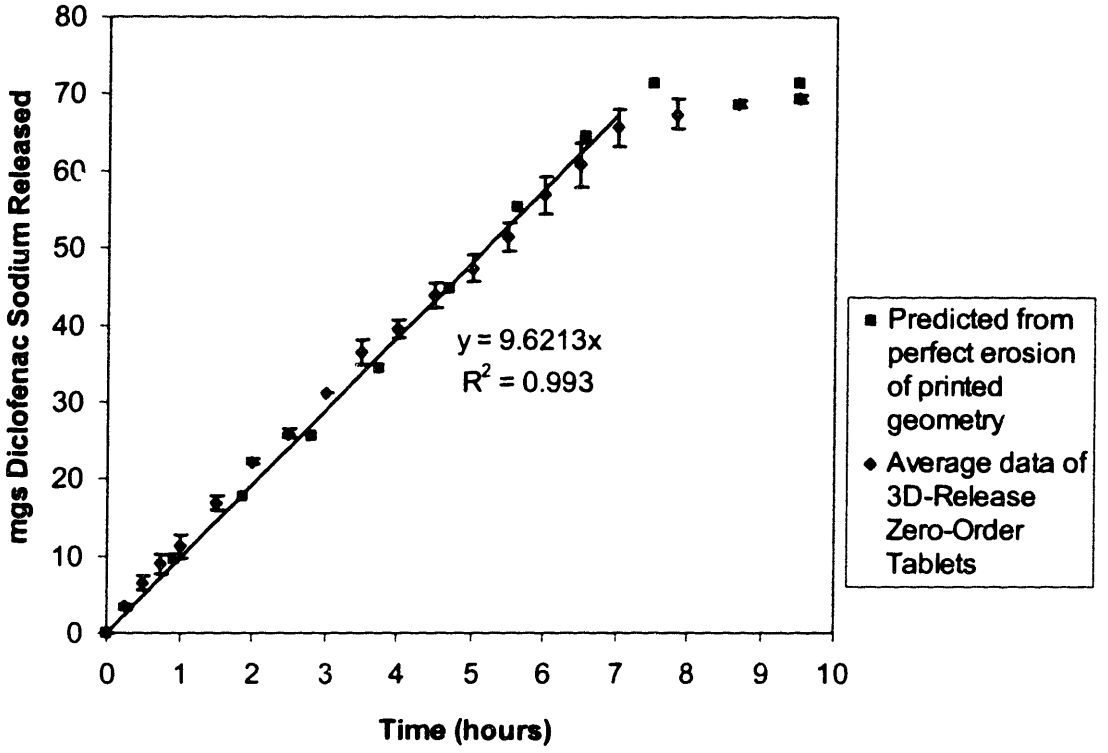

Figure 6.20 Diclofenac release from 3D-Release Zero-order Tablets vs. predicted release

6.6.7 Observations and Discussion

Radial-Release Tablets: Uniform distribution tablets and Zero-order Tablets

The data for the first set of Radial-Release tablets, those in which a constant uniform concentration of drug was printed into the center section, shows the typical curved release in Figure 6.17. The release rate decreases over time due to the decrease in volume released over time as the erosion front enters the tablet.

This can be compared to the release curves in Figure 6.18 for the Radial-Release Zero-order tablets fabricated with radial distributions of diclofenac. The erosion front enters these samples and encounters higher concentration of

diclofenac as the radius decreases in size. The competition between decreasing volume released and increasing concentration in those elements has been balanced in the tablet design and has resulted in near linear cumulative release.

The modeled curves in Figure 6.18 (from equation 6.17) make the assumption that the concentration zones are discretely defined. Any migration effects during the printing or pressing of the tablets have been ignored in the model. It is plausible that some migration would occur, especially between concentration zones. This would result in more diffuse concentration steps, and a more continuous gradient. A continuous gradient would be an enhancement of the device in this case, since that is what was originally conceived in the $C(r) \propto 1/r^2$ model.

Figure 6.19 shows the data for the Radial-Release Zero-order tablets and linear regression curves. The 80:20 tablet shows a fit of R^2 = .9883 for the portion of the curve 1-15 hours with a release rate of ~6.8mg/hr. The data tails of after 15 hours due to the constant concentration of the center zone 5. At this point in the curve the tablet acts like the constant concentration tablet, and releases with a polynomial order of 2. The 70:30 tablet shows a fit of R^2= 0.9975 for the portion of the curve 1-36 hours with a release rate of ~2.5mg/hr. The data also tails off for this tablet after 36 hours due to the constant center concentration. Typically the mouth-to-exit transit time in an adult is 35 hours for approximately 50% of the population, and about 10% have transit times shorter than 20 hours[R6.4]. The pH-independent zero-order releases obtained in these two samples are of the correct time scales for these examples. The release rate has also been shown to depend on the lactose adjuvant present in the powder, and can be tailored to achieve faster or slower release rates.

3D-Release Zero-order Tablets

Figure 6.20 shows the diclofenac release from the 3D-Release Zero-order tablets. These tablets were able to achieve zero-order release over a period of

~8 hours without the use of end-caps or membranes. A constant release rate of 9.62 mg/hour was achieved from the release of diclofenac from all 3 surfaces of the tablet geometry. The release data correlates well with the predicted release from a tablet undergoing perfect erosion at 0.32mm/hr. with the calculated geometric concentration profile given in Table 6.4.

Radial-Release vs. 3D-Release Zero-order Tablets

Both the Radial-Release and the 3D-Release tablets showed near zero-order release kinetics although the designs are different. The HPMC caps of the Radial-Release do not contain drug, and this lowers the effective δ or loading per unit tablet volume. Thinner caps that still act to prohibit erosion in the vertical direction are therefore desirable. The current design of the Radial-Release tablets still have ~7% more drug loading than the 3D-Release tablets of the same tablet volume and concentration zones, and this percentage would be even higher if thinner caps were used. This is because the 3D-Release tablets have an added drug gradient in the vertical direction leading to less available volume for the innermost and highest concentration drug regions.

The 3D-Release tablets erode much more quickly than the Radial-Release tablets. Radial-Release tablets fabricated from 70:30 Lactose:HPMC showed a constant release rate of only 2.5mg/hr, while the 3D-Release tablets showed a release rate of 9.6 mg/hr. This is attributed to the difference in available surface area for erosion. The Radial-Release tablets only erode from the radial surface while the 3D-Release tablets erode from the radial, top, and bottom surfaces.
The period of zero-order release also decreases as both of these dosage forms decrease in size. A higher fraction of HPMC could be used in the powder, or other excipients could be incorporated to compensate for this and decrease release rate.

6.7 Summary and Conclusions for Chapter 6

Mixtures of Hydropropyl Methylcellulose and Lactose were used to fabricate tablets capable of release by surface degradation.

The hydration/relaxation front between the dissolution and un-dissolved matrix moves with constant radial rate into the tablet after an initial induction period or burst effect. This front was shown to control the drug release. Fluorescein present in the matrix disappeared quickly past the hydration front in observation under UV light. The hydration/relaxation front position over time was also shown to agree with the radial erosion rates obtained with drug release modeling.

Erosion rate constants were determined for HPMC tablets with varying concentrations of lactose adjuvant. Lactose was shown to increase erosion rate constants for tablets of equal size, shape, and drug dosage. It was also shown that the release rates of chlorpheniramine maleate were ~10% higher than those obtained for diclofenac sodium. The difference is attributed to the difference in solubilities and solubility rates of the two drug substances.

Dual Release tablets were designed and fabricated by 3DP based on the surface degradation mechanism of these tablets. Tablets contained three drug regions, two for immediate release, and one for extended release. Predicted release curves were generated based on surface erosion from the designed geometry using the appropriate erosion rate constants. The dissolution data for two tablet types, one printed with chlorpheniramine maleate and one printed with diclofenac sodium, follow the predicted release curves closely. The burst effect was present in the data, but was not taken into account in the predicted curve, which assumed constant radial erosion rate. The release peaks are also somewhat broader in the data as compared to the predicted release peaks.

Radial-Release Zero-order Tablets were also designed and fabricated by 3DP based on the surface degradation mechanism. The tablets were designed

for release in the radial direction only. The drug was distributed in 5 zones such that the concentration complemented the volumetric non-uniformity of a radial erosion process. Predicted release curves were generated based on surface erosion from the 5 concentration zones using appropriate erosion rate constants. The dissolution data for two tablet types, one fabricated from 70wt% lactose : 30wt% HPMC and one fabricated from 80wt% lactose : 20wt% HPMC, follow the predicted release curves. Zero-order release occurred over a period from 1-15 hours for the 80:20 tablets, and over a period of 1-36 hours for the 70:30 tablets. The data tails off after the zero order release portion due to the constant concentration of the center zone, as it would with conventional tablets of uniform drug distribution.

A second type of zero-order release tablet was also designed and fabricated by 3DP. These 3D-Release Zero-order tablets were designed to release in all three dimensions from the tablet's surface without the use of membranes or cap layers. The drug was distributed in 5 sections to approximate a three-dimensional concentration gradient. This concentration gradient was designed so that the drug loading in each of the eroding shells was equal and therefore would lead to a constant release rate. A predicted release curve was generated based on the assumption that the surface erosion rate is constant and equal in the radial and vertical directions and that erosion occurs perfectly and the core remains cylindrical. The dissolution data for the 3D-Release Zero-order tablets correlate well with the predicted release curve with a surface erosion rate of 0.32 mm/hr. The portion of the release profile between 0 and 8 hours is linear with an R^2 of 0.993 and release rate of 9.6mg/hr. The data for these tablets again tails off at the very end of the release as the center core of the tablet releases like a conventional erosion-type tablet since the concentration is uniform.

Conclusions

Viscosity, conductivity, and other fluid characteristics such as viscoelasticity and dispersion limit have been used to determine printing spaces for common 3DP pharmaceutical fluids on the CJ CD OSP. These printing spaces can be easily generalized for the cases of aqueous Newtonian fluids, organic solvent Newtonian fluids, viscoelastic fluids, and aqueous suspensions.

Electrostatic forces limit the particle size of powder that can be used in dry powder spreading. The limit for polymeric materials used in this study was found to be ~40μm from theoretical calculations and 38-53μm from empirical observations.

The particle size limits the size of the layer height that can be used. It was found that a layer height of greater than 2 times the maximum particle size is needed to obtain a powder spread density that is equal to the tap density of the powder. Powders that are spread with densities below tap density are not stable, whereas those at tap density are stable and will result in uniform density matrices. The minimum layer height was found to be ~125μm for powder of the size range 38-53μm.

The post-processing techniques of spray-coating and uniaxial pressing were employed to enhance exterior surface characteristics. Spray coating was shown to decrease surface roughness, but did not eliminate stepping along a curved surface. Uniaxial pressing greatly enhances the all aspects of the exterior surface. The resolution of interior boundaries was not altered. Material was shown to move, however, in the direction of lower density and higher void volume during compression.

The use of migration inhibitors, such as fine polymer grains for dissolution or swelling, was shown to decrease the migration of printed fluids out of features within the powder bed. Using higher vapor pressure solvents such as ethanol, or drying aqueous systems every layer, was shown to also decrease the migration effects. The time scales for dissolution and swelling of additives were found to be on the order of seconds. These periods are too long for the migration enhancement to happen during the initial imbibition or drainage of fluid during capillary equilibration. Instead, the time scales for dissolution and swelling directly compete with the drying process. They have therefore been found to limit migration during times before sufficient evaporation has occurred when fluid is still continuous throughout the porous network, and is free to diffuse between pores or layers.

Pre-printing or pre-saturation regions of the powder bed has been employed to create migration barriers and confine drug regions. This has been found to help direct fluid into designated regions of the powder bed during initial imbibition and drainage. The pre-printed regions have been shown to have lower capillary suction, higher contact angle to the drug fluid, and less available volume for infiltration than the neighboring designated un-printed regions.

It has been shown that it is possible to accurately print dosages down to at least 2.3 nanograms. There is no true lower limit to dosage, however, since printed fluids can be diluted with no limit. The only limit would be the detection limit for these drugs for validation purposes.

The upper limit for dosage in 3DP matrices depends on the void fraction of the powder and the ability to efficiently fill this volume. Multiple print passes are required for high dosage tablets using printed solutions constrained by solubility limits. This can be done at the expense of print time and filling efficiency. Drug

suspensions have been used in this study to overcome the solubility limits present for solutions. Suspensions of naproxen have been printed with the CJ CD technique using solids loadings up to 41.5 wt%. Printing once to 100% saturation with this suspension has resulted in tablets with higher δ values (mg/cc) than those obtained by printing 4 times to 226% saturation with highly concentrated solution. Uniaxial pressing of 3DP tablets has also greatly increased δ values by decreasing the tablet volume for a fixed dosage. The highest δ value obtained in this study was 426.7 mg/cc for pressed suspension-printed tablets. This represents filing ~74% of the total available volume.

Oral dosage forms have been fabricated with 3DP to exhibit erosion and diffusion release mechanisms. The properties of these tablets have been modulated by adjusting matrix properties by changing the printing parameters. Dosage forms have also been fabricated to exhibit complex functionality. Prototype devices have been fabricated to give pH-dependent dual release in the stomach and intestines and dual release in the intestines. The lag times between pulses are controlled by the geometry of the devices.

Mixtures of Hydropropyl Methylcellulose (HPMC), lactose, and L100 were used to fabricate tablets capable of surface degradation. Drug release from these tablets was determined to occur at the water hydration / polymer relaxation front. Erosion rate constants were determined for matrices containing varying concentrations of lactose adjuvant. The addition of lactose was shown to increase erosion rates in these systems. Erosion rate constants were also determined for tablets containing either diclofenac sodium or chlorpheniramine maleate. The drug release rate for chlorpheniramine maleate was ~10% higher than that of diclofenac sodium. This is attributed to the difference in solubility limits and solubility rates of the two drug substances.

Two types of complex 3DP tablets were designed and fabricated using this materials system: dual release tablets and zero order release tablets. Models to predict release from these tablets were developed based on empirical erosion rate constants, drug loading, and geometry.

Dual release tablets were fabricated containing three drug regions, two for immediate release and one for extended release. The dissolution data for the two drugs from these tablets followed the predicted model for release. A small burst effect was present in the data, which was not taken into account in the model, and the release peaks of the data are broader compared to the sharp predicted peaks. The broadening of the release peaks is attributed to small migration effects at the drug region boundaries and the non-exact nature of fluid imbibition and dissolution testing.

Two types of zero-order tablets were modeled, designed, and fabricated. The first type is the Radial-Release Zero-order tablet for erosion-type release in the radial direction only. The second type is the 3D-Release Zero-order tablet for erosion-type release from all three dimensions of a cylindrical tablet shape.

Zero order release from an infinite cylindrical geometry was modeled for use in designing the Radial-Release tablets. This model shows that drug concentration should be inversely proportional to the radius squared so that the drug distribution complements the volumetric non-uniformity of eroding layers during dissolution. 3DP tablets were designed and fabricated with 3DP to approximate this concentration dependence by establishing 5 concentric concentration zones. The dissolution data for diclofenac tablets designed with this geometry from two HPMC-based matrices followed the predicted model for release closely. Zero order release of diclofenac sodium was obtained over a period of 1-15 hours from tablets based on a powder system of 80wt% lactose

and 20wt% HPMC (K4M), and over a period of 1-36 hours for 70wt% lactose and 30wt% HPMC (K4M).

Another model was established for use in designing the 3D-Release Zero-order tablet. This model shows that the product of the drug concentration and the surface area of eroding shells must be equal in order to achieve a constant delivery rate. Tablets with 5 drug concentration sections were designed and printed with diclofenac sodium to approximate the three-dimensional gradient required by the model. The dissolution data for a tablet fabricated with a powder of 70wt% Lactose and 30wt% HPMC shows zero-order release of diclofenac over the initial 8 hours at a release rate of 9.6mg/hr.

3DP™ Pharmaceutical Materials

All of the materials used in fabricating drug delivery tablets by 3DP™ in these studies are standard pharmaceutical materials. They include FDA approved excipients, drug compounds, and other additives.

A.1 Powders

Pharmaceutical excipients in the form of powders form the powder build bed into which binding solutions, active materials, and other additives are printed. As-received solid material or powders are first sifted through stainless steel sieves and separated into respective particle size classes. If necessary, material is ground into fine powder and then sifted to achieve the desired size ranges. The powder can then be mixed with other components to make up the composition of the powder build bed.

Often different powders are combined to achieve several physical attributes. Qualitative and quantitative features include flowability, migration inhibition, plasticity (for pressing), diffusivity, permeability, etc.

Spray-Dried Lactose Monohydrate (Pharmatose DCL 11)

Lactose is a common water-soluble excipient material used for the fabrication of 3DP™ tablets. As-received powder is spherical in shape with a median particle size of 100μm. This spray-dried form of lactose makes it flow easily which makes it an ideal candidate for spreading into thin layers at tap density. The sponge-like granules have central pockets and many smaller (~7micron) interconnected pores as determined by low pressure powder mercury poresimetry and SEM.

Microcrystalline Cellulose (Avicel PH301, FMC Corporation)

Microcrystalline cellulose is a naturally occurring water-insoluble polymer and has many applications as a pharmaceutical excipient. It is classified as a disintegrant as it promotes the disintegration of conventional pressed tablets by swelling in body fluids and causing the rapid bulk erosion of the form. The as-received powder is irregularly shaped and slightly acicular.

Hydropropyl Methylcellulose (HPMC, Methocel K4M, Dow Chemical Co.)

Hydropropyl Methylcellulose, or HPMC, is a water-soluble polymer derived from cellulose. It is typically used to form a hydrophilic matrix in sustained release applications as it forms a diffusive gel layer through which drug compound is released slowly. The backbone of HPMC is the same as cellulose, a natural carbohydrate that contains a basic repeating structure of anhydroglucose units. During manufacturing of HPMC, cellulose fibers are heated with caustic solution that is in turn treated with methyl chloride and propylene oxide. This substitutes hydroxypropyl and methyl units for anhydroglucose units. The amount of substitute groups on the anhydroglucose units of cellulose can be designated by weight percentage or by the average number of substitute groups attached to the ring, or the "degree of substitution". The number of substitute groups on the ring and the types of groups determine the properties of the product, such as water solubility and thermal gelation temperature. The methocel HPMC K series has a methoxyl degree of substitution of 1.4, or 22% methoxyl substitution, and a hydroxypropyl molar substitution of 0.21, or 8% hydroxypropyl substitution. The fibrous product of the above substitution reaction is purified and ground to a fine uniform powder.

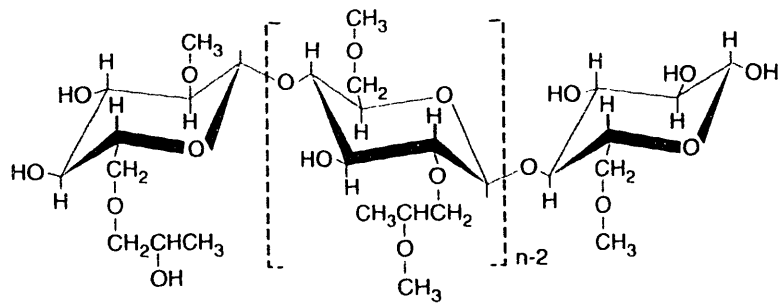

Figure A.1 Chemical Structure of HPMC (Methocel Technical Handbook)

Table A.1 Degree of Substitution for Methocel HPMC K series

Methoxyl degree of substitution	Methoxyl %	Hydroxypropyl molar substitution	Hydroxypropyl %
1.4	22	0.21	8.1

The methocel HPMC "K4M" product is a high viscosity grade of the K series. This adds to its low water permeability and slower release kinetics. Another methocel K series HPMC is the K100LV. This can be used for accelerated release kinetics.

Table A.2 HPMC Viscosity Grades

DOW Methocel Product	Viscosity of 2wt% in H_2O, 20°C
HPMC K4M	4000 millipascal-seconds
HPMC K100LV	100 millipascal-seconds

A.2 Solutes for Printed Binder Solutions

The solutes used in 3DP are generally dissolved in water or organic solvents to make the binder solution to be printed into the powder bed. The materials used in this research are discussed below with respect to their function in drug delivery forms.

A.2.1 Eudragit Polymers for pH dependent Controlled Drug Delivery

Eudragit acrylic polymers from RÖhm America Inc. are a complete line of copolymers specially designed for oral drug delivery with pH sensitive control. These copolymers are readily dissolved, and are conveniently incorporated into the printing of 3DP oral drug delivery tablets. Figure A.2 shows the basic chemical backbone of this class of polymers.

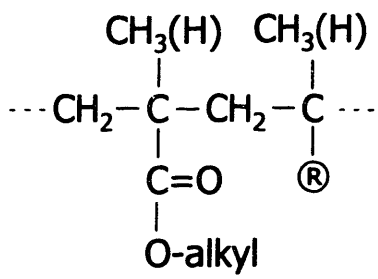

Figure A.2 Backbone of pH-Dependent Eudragit Polymers[63]

Eudragit E100 ®= -CO-OCH$_2$CH$_2$N(CH$_3$)$_2$

Eudragit E100 is a cationic polymer based on dimethylaminoethyl methacrylate and neutral methacrylates. It becomes water soluble by salt formation with acids, and therefore is gastrosoluble.[63]

Eudragit L100 and S100 ®= -COOH

Eudragit L100 and S100 are grades of anionic polymers based on methacrylic acid and methacrylic acid esters. The difference between the two

materials is the ratio of carboxyl groups to ester units: This ratio is about 1:1 in L100 and 1:2 in S100. The two enteric materials are insoluble below pH 5 and can therefore resist gastric fluid. The pH of the stomach is in the range of pH 1 to 3. [12] The two materials dissolve step-wise in higher pH mediums by salt formation in the neutral to weakly alkaline intestinal fluid: L100 undergoes dissolution from pH 6, and S100 undergoes dissolution from pH 7. For comparison purposes, the pH range of the duodenum is 5.5 – 6.0, and the pH increases gradually to about pH 6.5-7.0 near the colon.[64]

Figure A.3 illustrates the dissolution profiles for the above three Eudragit materials vs. pH in the gastro-intestinal tract. These materials can be printed selectively to engineer complex delivery forms. Such complex tablets are introduced in chapter 5.

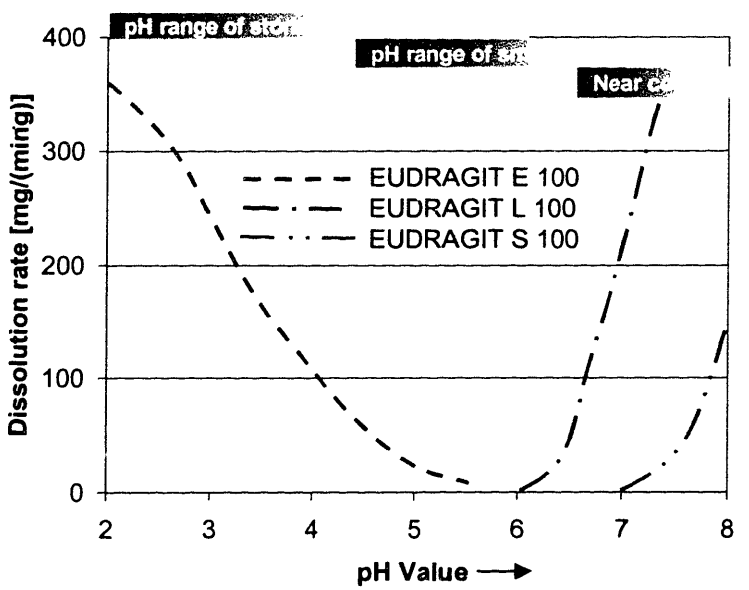

Figure A.3 Dissolution Profiles for E100, L100, and S100[64]

A.2.2 pH Independent Drug Delivery Solutes

Eudragit RL/RS PO ®= -CO-$OCH_2CH_2N^+(CH_3)_3$ -

Eudragit RLPO and RSPO are polymers used in extended release applications. These polymers are not soluble, nor do they exhibit pH sensitive behavior. Drug is released from the matrices formed with these polymers by diffusion, independent of the medium pH. The permeability of the matrix is based on NH^{+4} groups.

Polyvinylpyrrolidone PVP K25 (International Specialty Products)

PVP is a commonly used water soluble pharmaceutical excipient for a variety of applications. It is used to help modify the viscosity of printed solutions.

Fluorescein Disodium Salt, Uranine (Sigma Chemical Co.)

Fluorescein is a water soluble compound that has an intense green fluorescence. It has been used in several studies to trace 3DP droplet placement because of this strong fluorescence which persists even when diluted to extremely small concentrations. Fluorescein can be viewed well under UV light for qualitative purposes. It can also be used in quantitative fluorimetry measurements at an excitation wavelength of 491nm with peak maximum emmision at 513nm. Fluorescein has a low detection limit of approximately 0.1 nanomolarity.

Other fluid additives

Other materials used as solutes include sucrose, sodium chloride, and colorants.

A.3 3DP Actives and Drug Substances

Diclofenac Sodium (Sigma Chemical Co.)

- Solubility limit in D.I. water at 25°C is ~50mg/mL
- Solubility limit in methanol at 25°C is ~33wt%
- Non-Steroidal Anti-Inflammatory Drug substance

Chlorpheniramine Maleate (Sigma Chemical Co.)

- Solubility Limit in D.I. water at 25°C is ~100mg/mL
- Anti-histamine

APPENDIX TWO

CJ/CD OSP Drawings and Electronics

This Appendix is a specific description of the current construction of the Continuous Jet Charge and Deflect Organic Solvent Printhead (CJ/CD OSP). The printhead is equipped with 4 charging and deflection cells to print and recycle 4 different materials in a single build. Included in this Appendix are complete circuit diagrams and schematic drawings of the printhead assembly. Sections of this Appendix have been reproduced with the permission of Therics Inc.[65]

Figure A.1 is a schematic drawing of the CJ/CD OSP printhead. Both the electronics block and the nozzle clip are shown. The electronics block of the printhead contains the charging cells, deflection cells and LEDs. The removable nozzle clip holds the jewel tube orifices in the proper alignment with respect to the other printhead components, and allows for front-to-back nozzle positioning and easy removal of individual nozzles for cleaning.

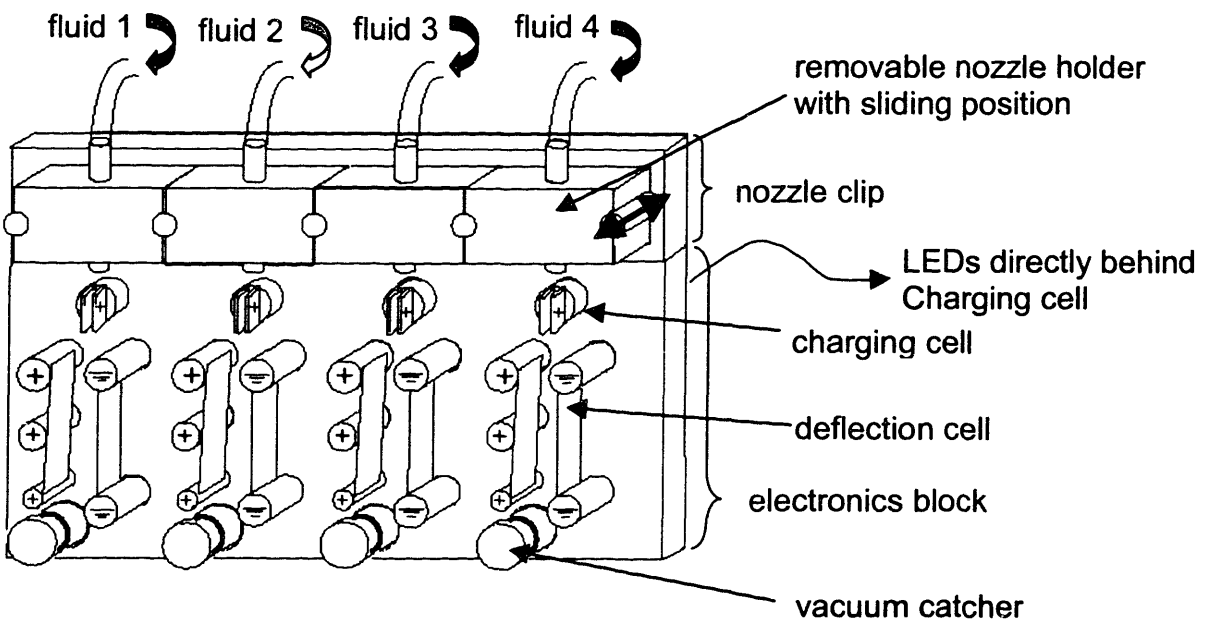

Figure A.1 Schematic of the CJ/CD OSP

The electronics block and the nozzle clip have both been machined from Teflon™ for ease of machining, low weight, and material compatibility. Teflon is also chosen for the electronic block because of the need for a dielectric material to separate the charging and deflection cell components, and for its low wettability.

The two printhead components are mounted on an aluminum plate that attaches to the fast-axis air slide carriage. Also attached to this plate are the fluid delivery lines and the ribbon cable connector. The fluid delivery lines are attached to the aluminum plate to provide an electrical ground for the fluid stream to allow droplet charging.

Electronic Block Components

The printhead electronics block carries the charging cells, LED strobes, deflection cells, and vacuum catcher ports.

The LED strobes are mounted in the back of the electronics block. Their function is to provide a strobe flash synchronized with the piezo crystal signal to allow imaging of droplet breakoff.

The charging cells are each constructed from stainless steel tubing aligned with the LED strobes. This allows the droplet stream to be imaged with the strobe flash from the front of the printhead. The stainless steel tube is used to make the electrical connection on the back of the printhead. On the front the tube ends in a pair of flat vertical plates. The droplet stream falls between these plates during breakoff.

The charging cells are operated at a maximum voltage of +110V. When the voltage is off, the droplets are uncharged and will be printed. When the voltage is on, the positive charging field induces a surface negative charge on the droplets, assuming the fluid stream is properly grounded. If the droplets

break off in the charging field, they retain this charge and will be deflected to the vacuum catcher and will not be printed. It is important that droplet breakoff occurs near the middle of the plates to ensure consistent droplet charging.

The deflection cells consist of paired stainless steel plates, one at ground, and the other plate at +300V to +1100V. The positive plates attract the negatively charged droplets, leading them to the vacuum catcher port. The plates are mounted on stainless steel tubes that run through the electronics block to the electrical connections in the back.

The vacuum catcher port is a cylinder that fits into the vacuum catcher tube. The catcher tube is a hole machined through the electronics block. At the back side of the printhead a stainless steel tube is inserted to make the connection to the Tygon™ vacuum catcher line. This line leads to a peristaltic pump which pulls the unprinted droplets through the vacuum catcher port to a waste container. One vacuum catcher port is allotted to each nozzle , allowing for recycling of individual fluids with no cross-contamination.

The vacuum catcher port insert contains a groove midway along the length. This groove is the target area for the droplet stream to hit the catcher. The walls of the groove prevent the stream from wetting out along the entire length of the catcher port. The insert is not permanently mounted, but is allowed to slide to correct for any front to back stream misalignment. At the bottom of the catcher port insert is a hole for the droplet stream to enter the vacuum catcher line.

Orifice Assembly

The orifices used for the MIT 4 jet printhead are based on sapphire jewel tubes used at Therics, and generally range between 45 and 55μm. The jewel tube is fitted into the nozzle clip, described above. The jewel tube is supplied with fluid by an attached Teflon fluid line (0.034" OD, 0.022" ID). This fluid line is

attached to the piezoelectric crystal (Morgan Matroc, Inc., Bedford, OH. Product code PZT-5H), a ceramic of lead zirconate titanate. It is an extruded tube 0.050 OD x 0.030 ID, electroless nickel plated on inner and outer surfaces. It is cut to 4 mm lengths and interference fit it to the outside of the Teflon tube.

A minimum distance between the piezo and the orifice must be maintained to allow the Teflon to absorb the acoustic wave that propagates in the Teflon material while passing the peristaltic wave. The acoustic wave attenuates much faster than the expansion pulse. It also travels three times as fast; therefore, the two waves positively and negatively reinforce as they travel down the line. Shorter tubing distances cause variation in the breakoff length of the stream as the operating frequency varies above and below the Rayleigh frequency. Longer distances decrease the overall signal strength of the breakoff, so a compromise between signal strength and minimum variation in breakoff length must be achieved. The distance typically used for aqueous fluids is 43 mm measured between the end of the piezo and the point where the Teflon meets the nozzle. This distance has been shortened to 18mm for organic solvents due to the smaller surface tensions of these solvents. This distance has been found to optimize the breakoff energy and decrease stream threading in viscoelastic fluids based on organic solvents for a 45-50 μm orifice and 35-50 kHz frequency input. Such fluids include polymers dissolved in ethanol, methanol, acetone, and chloroform.

Leads are soldered onto the nickel plating on the piezo crystal. Care must be taken to minimize the heat input to the piezo crystal to prevent loss of piezoelectric properties. The leads are attached to connectors mounted on the aluminum plate to interface with the ribbon cable. Finally, there is an additional length of Teflon tubing that attaches to the grounding assembly. This length of tubing can be any convenient length determined by printhead geometry.

Control Electronics

The CJ/CD OSP printhead uses a 26 wire ribbon cable to transmit electronic signals. The ribbon cable leads back to a control box that collects the signals from various external components and passes them to the appropriate wire in the ribbon cable. Figure A.2 is a schematic of the electronics system supporting the printhead. Table A.1 lists the components needed and the input/output specifications for each component.

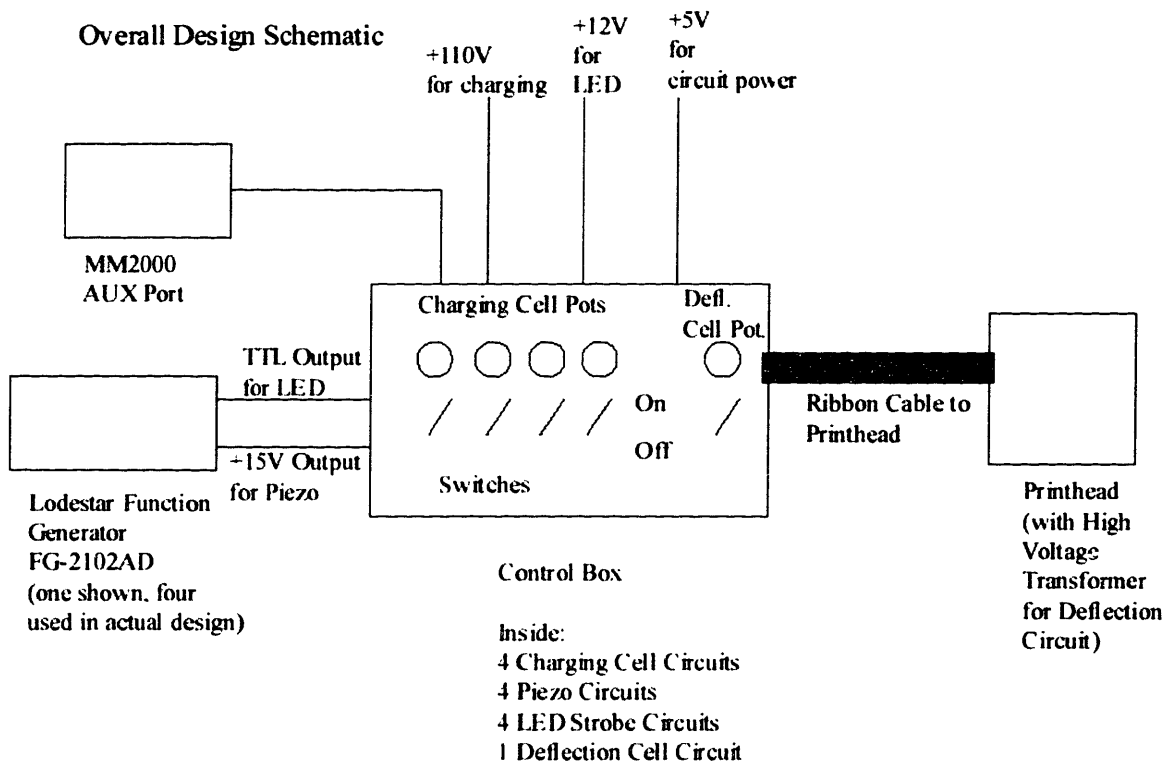

Figure A.2 Schematic of the electronics system supporting the printhead

Table A.1 Electronic Components

Quantity	Name	Specifications
1	Printhead Electronics Block	Teflon, with stainless steel deflection cells, stainless steel charging cells.
2	Vacuum Catcher Port Inserts	Stainless Steel
4	LED's for Strobe	Gilway Technical Lamp, Woburn, MA. Part #E197
1	Nozzle Block	Teflon
1	High Voltage Amplifier for Deflection Circuit	Q15
1	Resistor on printhead for deflection circuit	1.1 MOhm
4	Piezo Connectors	
4	Sapphire/Ruby orifice assemblies with piezo crystal	Assembled by Jim Serdy
1	Aluminum Mounting Plate for printhead components	
1	Ribbon cable and Connectors	26 wire
1	Electronics Box to house circuits boards and connectors	
3	DC power supply	1 Each: +110V, +12V, +5V
5	On-off switches (four for charging cells, one for deflection cell)	
4	Potentiometers for charging cells	10 kOhm
1	Potentiometer for deflection cell	10 kOhm
4	HCPL-2212 Optocoupler chips for charging circuits	
12	Resistors for charging circuits	1 kOhm
8	Capacitors for charging circuits	0.1 μF
8	Schottky diodes for charging circuits	60V
4	Transistors for Charging circuits	NPN,2N4401
8	Resistors for Strobe circuits	220 Ohm
4	Resistors for Strobe circuits	15 kOhm
4	Capacitors for Strobe circuits	100 pF
4	LS221 Chips for Strobe circuits	
4	Transistors for Strobe circuits	NPN,2N4401
1	Resistor for deflection circuit	220 Ohm
1	Voltage Regulator for deflection circuit	LM317T
4	Amplifiers for Piezo Circuits	SM-33
4	Function Generators	Lodestar FG-2102AD, +15V Output, TTL output
12	Coax Cable with BNC connectors to connect: -MM2000 to electronics box (4x for charging circuits) -Function Generators to electronics box (4x for piezo circuits, 4x for strobe circuits)	50 Ohm

Piezo Circuit

The piezo circuit, shown in Figure A.3, is the simplest circuit of the four major printhead circuits. It consists of the +15V main output from the function generator, passed through an amplifier to increase the voltage to +60V (with slight frequency dependence). This signal is then routed to the ribbon cable and the piezo connectors on the printhead.

Piezo Circuit

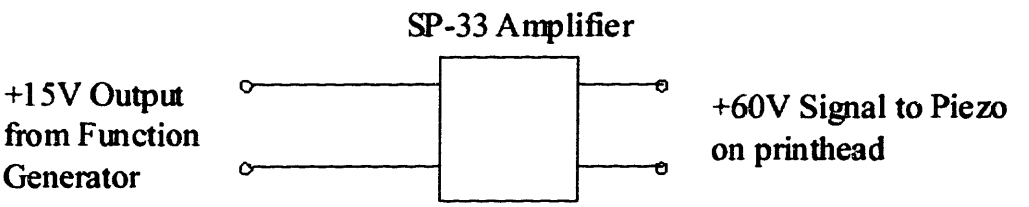

Figure A.3 Piezoelectric Circuit[66]

The piezo is operated by activating the function generator, which outputs a square wave function at the appropriate frequency. Frequency and amplitude of the vibrations are tuned on the function generator front panel. Typical operating frequencies of the piezo are 22-50 kHz, though values of 10-60 kHz are occasionally used.

Four function generators are used to provide the signals for the four nozzles, one function generator per nozzle. Each piezo circuit uses a pair of wires on the ribbon cable, accounting for eight wires out of the 26 on the cable.

Strobe Circuit

The LED strobe circuit, shown in Figure A.4, is based around a LS221 chip to convert the function generator TTL square wave output into a pulse width suitable for driving the LED. The chip is a dual monostable multivibrator with

schmitt-trigger inputs. Although each chip has two vibrator circuits, only one was used for each circuit because the two vibrators provide opposite output given identical input.

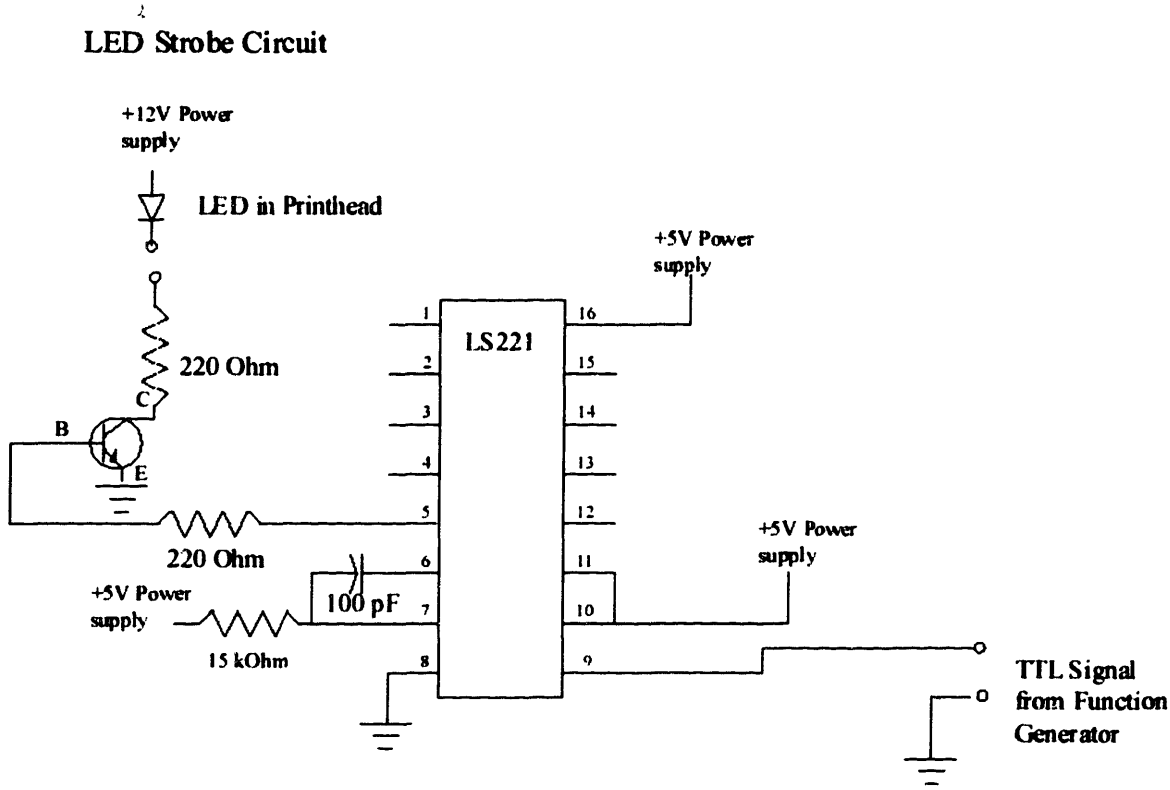

Figure A.4 LED strobe circuit[66]

The chip receives the +5V TTL input from the TTL port on the function generator on pin 9. +5V DC power is supplied at pins 10,11, and 16 and grounded at pin 8. An additional +5V DC supply is used, along with a resistor and capacitor connected to pins 6 and 7. The combination of the resistor and the capacitor determine the pulse width applied to the LED according to the formula:

Pulse Width = 0.7RC = (0.7)(15000 Ohm)($1x10^{-10}$ F) = $1.05x10^{-6}$ sec = 1.05 μsec

The output pulse from the chip, pin 5, is directed to the NPN transistor. The voltage at the transistor collector modulates the flow of current from the +12V DC source driving the LED. The +12V DC source is connected through the

ribbon cable to the LED, and then a second ribbon cable wire back to a 220 ohm resistor and the transistor base. The transistor emitter is connected to ground. The 220 ohm resistor controls the flow of current, and therefore controls the brightness of the LED strobe.

Charging Cell Circuit

The charging cell circuit, shown in Figure A.5, converts the output from the MM2000 AUX port into high or low values of the charging voltage, as directed by the program run by the MM2000. The MM2000 command structure allows 8 bits (numbered 1-8) to be used as input or output bits. The values of bits 1-7 are available on the MM2000 AUX port as a +5V DC signal.

Charging Cell Circuit

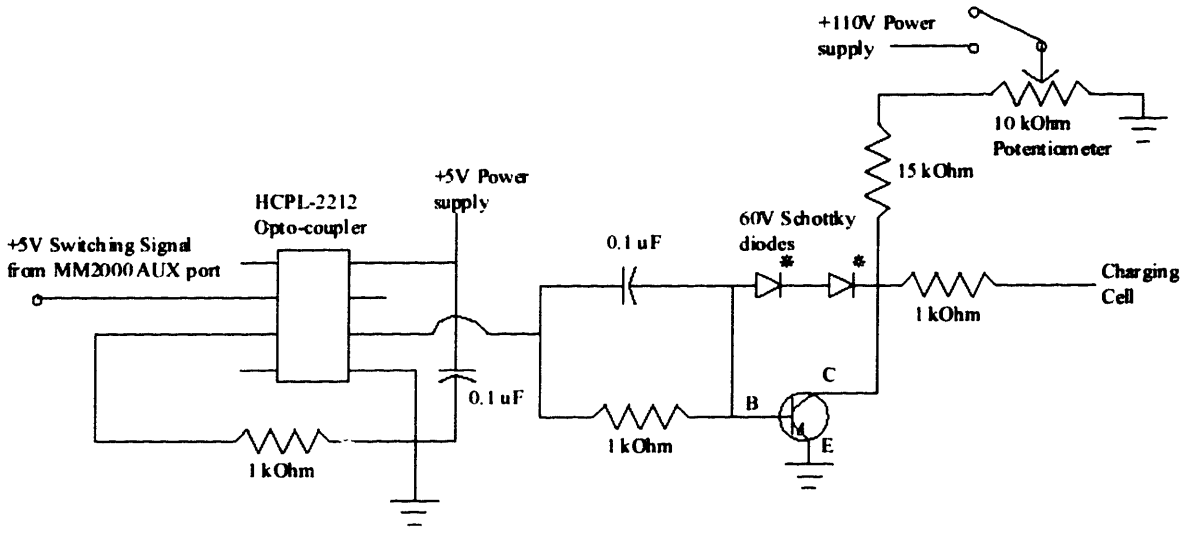

Figure A.5 Charging cell circuit[66]

The four +5V DC outputs from the MM2000 are directed to four identical charging circuits, one for each charging cell. The MM2000 signal is directed to pin 2 of a HCPL-2212 Optocoupler. +5V DC Power is supplied to the chip at pin 8, and the output voltage is connected at pin 6. This output voltage is passed though a resistor and capacitor to a transistor that modulates the +110V DC

power supply for the charging cell. A pair of 60V Schottky diodes, connected in series is used to increase the speed with which the charging voltage can be switched from high to low.

When the MM2000 bit is set, the +5V signal is high and the chip output is high, allowing current to flow through the transistor. This leaves the charging cell at ground voltage, and no droplet charging occurs. If the MM2000 bit is then cleared, the +5V signal drops to zero and the chip output drops as well, inhibiting flow of current through the transistor and raising the charging cell voltage. The magnitude of this voltage is determined by the 10 kOhm potentiometer connected between the +110V DC power supply and the charging circuit.

Each charging circuit uses a single wire in the ribbon cable. No separate ground wire is necessary.

Deflection Cell Circuit

The deflection cell circuit, shown in Figure A.6, uses an LM317T voltage regulator to modulate a +5V DC power supply. A potentiometer is used to adjust the output voltage of the regulator from +1.2V to +4.0V. This voltage is passed through the ribbon cable to a Q15 amplifier mounted on the printhead. The voltage output by the amplifier is +300V to +1100V and is connected to the deflection cell plates.

Deflection Cell Circuit

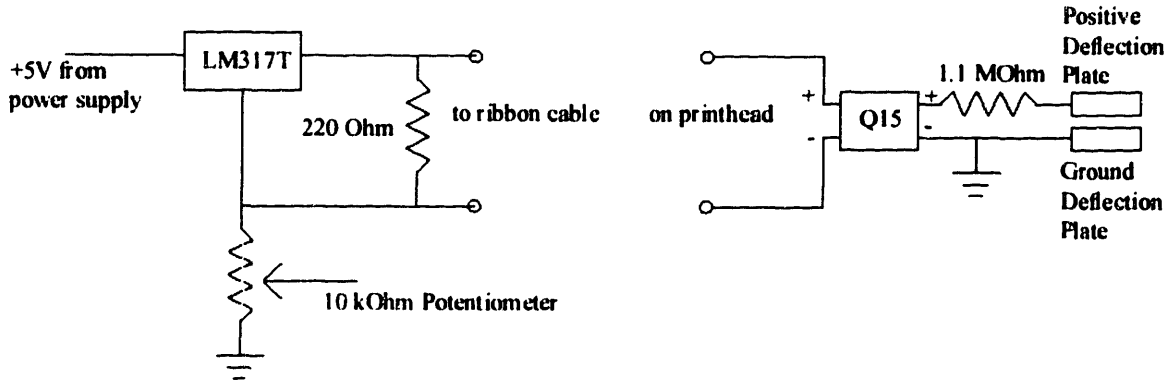

Figure A.6 Deflection cell circuit[66]

The reason that the deflection circuit includes the transformer on the printhead is that the ribbon cable is not capable of carrying the high voltages associated with the deflection circuit. The ribbon cable is only required to carry the +5V signal to the transformer, which is then amplified directly on the printhead. It is for this reason, that only one deflection circuit and voltage is used for all four fluid streams.

Printing Conditions for Chapter 6

Appendix 3a Tablets printed for observation in glass slide assembly

PRINTING PARAMETER	
Powder System	70wt% HPMC K4M 30wt% Lactose Monohydrate
Powder Size (μm)	53-74
Layer Thickness (μm)	300
Packing Fraction	0.412
BINDER	
Binder Solution Solutes	N/A
Binder solution solvent	-
Solution density g/cc	-
Weight fraction	-
Line Spacing (um)	-
Nozzle Orifice (um)	-
Flow Rate (g/min)	-
Modulation Frequency (KHz)	-
ACTIVE	Diclofenac Sodium
Drug Solution Solutes	18wt% diclofenac, 1wt% PVP, 0.05wt% fluorescein
Drug Solution Solvent	Methanol
Solution density g/cc	0.90
Line Spacing (um)	120
Nozzle Orifice (um)	50.4
Flow Rate (g/min)	0.97
Modulation Frequency (KHz)	42
SATURATION (% of void space filled per pass)	0.566
Overall number of passes	3
Drug Volume Fraction	0.15
DOSAGE	
Total mgs printed per tablet	101.8
COMPRESSION (yes/no)	Yes
Compression Force (psi)	15000
% Vertical compression	N/A
Dosage per unit tablet volume δ mg/cc	325

Appendix 3b Printing Parameters for Diclofenac Dual Release Tablets

PRINTING PARAMETER	
Powder System	70wt% HPMC K4M 30wt% Lactose Monohydrate
Powder Size (μm)	53-74
Layer Thickness (μm)	200
Packing Fraction	0.412
BINDER	
Binder Solution Solutes	Eudragit™ L100
Binder solution solvent	Ethanol
Solution density g/cc	0.82
Weight fraction	5wt% L100
Line Spacing (um)	120
Nozzle Orifice (um)	50.4
Flow Rate (g/min)	0.97
Modulation Frequency (KHz)	42.8
ACTIVE	Diclofenac Sodium
Drug Solution Solutes	18wt% diclofenac,1wt% PVP,0.05wt% fluorescein
Drug Solution Solvent	Methanol
Solution density g/cc	0.90
Line Spacing (um)	120
Nozzle Orifice (um)	50.4
Flow Rate (g/min)	0.92
Modulation Frequency (KHz)	48
Apparent Saturation	1.86
DOSAGE	
Total mgs printed per tablet	25.8
COMPRESSION (yes/no)	Yes
Compression Force (psi)	15000
% Vertical compression	55.0
Dosage per unit tablet volume δ mg/cc	312

Appendix 3c Printing Parameters for Chlorpheniramine Maleate Dual Release Tablets

PRINTING PARAMETER	
Powder System	70wt% HPMC K4M 30wt% Lactose Monohydrate
Powder Size (μm)	53-74
Layer Thickness (μm)	200
Packing Fraction	0.412
BINDER	
Binder Solution Solutes	Eudragit™ L100
Binder solution solvent	Ethanol
Solution density g/cc	0.82
Weight fraction	5wt% L100
Line Spacing (um)	120
Nozzle Orifice (um)	50.4
Flow Rate (g/min)	0.93
Modulation Frequency (KHz)	48.4
Binder Saturation	
ACTIVE	Chlorpheniramine Maleate
Drug Solution Solutes	20wt% Chlorpheniramine Maleate
Drug Solution Solvent	80% ethanol 20% D.I. water
Solution density g/cc	1.15
Line Spacing (um)	120
Nozzle Orifice (um)	50.4
Flow Rate (g/min)	0.98
Modulation Frequency (KHz)	45.7
Apparent Saturation	1.46
DOSAGE (Total mgs printed per tablet)	23.0
COMPRESSION (yes/no)	Yes
Compression Force (psi)	15000
% Vertical compression	55.0
Dosage per unit tablet volume δ mg/cc	277

Appendix 3d Constant *Uniform* Diclofenac Distribution Tablets

PRINTING PARAMETER	
Powder System	70wt% HPMC K4M 30wt% Lactose Monohydrate
Powder Size (μm)	53-74
Layer Thickness (μm)	300
Packing Fraction	0.412
BINDER	N/A
Binder Solution Solutes	-
Binder solution solvent	-
Solution density g/cc	-
Weight fraction	-
Line Spacing (um)	-
Nozzle Orifice (um)	-
Flow Rate (g/min)	-
Modulation Frequency (KHz)	-
ACTIVE	Diclofenac Sodium
Drug Solution Solutes	18wt% diclofenac, 1wt% PVP, 0.05wt% fluorescein
Drug Solution Solvent	Methanol
Solution density g/cc	0.90
Line Spacing (um)	120
Nozzle Orifice (um)	50.4
Flow Rate (g/min)	0.97
Modulation Frequency (KHz)	42
SATURATION (% of void space filled per pass)	0.56
Overall number of passes	1
Polymer Volume Fraction	N/A
DOSAGE	
Total mgs printed per tablet	44.1
COMPRESSION (yes/no)	Yes
Compression Force (psi)	15000
% Vertical compression	50.0
Dosage per unit tablet volume δ mg/cc	107

Appendix 3e Printing Parameters for 80%Lactose 20%HPMC Radial-Release Zero-order Tablets

PRINTING PARAMETER					
Powder System	80wt% HPMC K4M 20wt% Lactose Monohydrate				
Powder Size (μm)	53-74				
Layer Thickness (μm)	300				
Packing Fraction	0.425				
BINDER	N/A				
Binder Solution Solutes	-				
Binder solution solvent	-				
Solution density g/cc	-				
Weight fraction	-				
Line Spacing (um)	-				
Nozzle Orifice (um)	-				
Flow Rate (g/min)	-				
Modulation Frequency (KHz)	-				
ACTIVE	Diclofenac Sodium				
Drug Solution Solutes	18wt% diclofenac, 1wt% PVP, 0.05wt% fluorescein				
Drug Solution Solvent	Methanol				
Solution density g/cc	0.90				
Line Spacing (um)	120				
Nozzle Orifice (um)	50.4				
Flow Rate (g/min)	0.98				
Modulation Frequency (KHz)	45.7				
Fast axis speed cm/sec	150				
SATURATION (% of void space filled per pass)	0.584				
	Zone 1	**Zone 2**	**Zone 3**	**Zone 4**	**Zone 5**
Overall number of passes	1	2	3	4	5
DOSAGE per zone in mgs	22.34	14.72	11.08	9.09	44.58
Total mgs printed per tablet	101.8				
COMPRESSION (yes/no)	Yes				
Compression Force (psi)	15000				
% Vertical compression	50.0				
Dosage per unit tablet volume δ mg/cc	108	217	325	434	542

Appendix 3f Printing Parameters for 70%Lactose 30%HPMC Radial-Release Zero-order Tablets

PRINTING PARAMETER					
Powder System	70wt% HPMC K4M 30wt% Lactose Monohydrate				
Powder Size (μm)	53-74				
Layer Thickness (μm)	300				
Packing Fraction	0.412				
BINDER	N/A				
Binder Solution Solutes	-				
Binder solution solvent	-				
Solution density g/cc	-				
Weight fraction	-				
Line Spacing (um)	-				
Nozzle Orifice (um)	-				
Flow Rate (g/min)	-				
Modulation Frequency (KHz)	-				
ACTIVE	Diclofenac Sodium				
Drug Solution Solutes	18wt% diclofenac, 1wt% PVP, 0.05wt% fluorescein				
Drug Solution Solvent	Methanol				
Solution density g/cc	0.90				
Line Spacing (um)	120				
Nozzle Orifice (um)	50.4				
Flow Rate (g/min)	0.97				
Modulation Frequency (KHz)	42				
Fast axis speed cm/sec	150				
SATURATION (% of void space filled per pass)	0.566				
	Zone 1	**Zone 2**	**Zone 3**	**Zone 4**	**Zone 5**
Overall number of passes	1	2	3	4	5
DOSAGE per zone in mgs	22.1	14.56	10.96	8.99	44.10
Total mgs printed per tablet	100.7				
COMPRESSION (yes/no)	Yes				
Compression Force (psi)	15000				
% Vertical compression	50.0				
Dosage per unit tablet volume δ mg/cc	107	215	322	429	536

Appendix 3g Printing Parameters for 70%Lactose 30%HPMC 3D-Release Zero-order Tablets

PRINTING PARAMETER					
Powder System	70wt% HPMC K4M 30wt% Lactose Monohydrate				
Powder Size (μm)	53-74				
Layer Thickness (μm)	305				
Packing Fraction	0.412				
BINDER	N/A				
Binder Solution Solutes	-				
Binder solution solvent	-				
Solution density g/cc	-				
Weight fraction	-				
Line Spacing (um)	-				
Nozzle Orifice (um)	-				
Flow Rate (g/min)	-				
Modulation Frequency (KHz)	-				
ACTIVE	Diclofenac Sodium				
Drug Solution Solutes	18wt% diclofenac, 1wt% PVP				
Drug Solution Solvent	Methanol				
Solution density g/cc	0.90				
Line Spacing (um)	120				
Nozzle Orifice (um)	50.4				
Flow Rate (g/min)	0.96				
Modulation Frequency (KHz)	45.6				
Fast axis speed cm/sec	150				
SATURATION (% of void space filled per pass)	0.573				
	Section 1	**Section 2**	**Section 3**	**Section 4**	**Section 5**
Overall number of passes	1	2	3	4	5
DOSAGE per zone in mgs	28.19	13.34	6.99	5.75	17.38
Total mgs printed per tablet	71.65				
COMPRESSION (yes/no)	Yes				
Compression Force (psi)	15000				
% Vertical compression	47.7				
Dosage per unit tablet volume δ mg/cc	110	220	330	440	550

References

1. Wu, B. "Microstructural Control During Three Dimensional Printing of Polymeric Medical Devices." Ph.D. Thesis, Massachusetts Institute of Technology, Jan. 1997.

2. Uhland, S. "Fabrication of Advanced Ceramic Components Using Slurry-Based Three Dimensional Printing" Ph.D. Thesis, Massachusetts Institute of Technology, June, 2000.

3. Bakken, E.E., Heruth, K. "Temporal control of drugs, an engineering perspective", *Ann. New York Acad. Sci.* **618** pp.422-427, 1991.

4. Zaffaroni, A. "Overview and Evolution of Therapeutic Systems", *Ann. New York Acad. Sci.*, **618** pg. 406, 1991.

5. Kerc, J., Kofler, B., and Mohar, M. "Three-Phase Pharmaceutical Form (Threeform) for Nifedipine Zero Order Release", *Proceed. Int'l Symp. Control. Rel. Bioact, Mater.*, Controlled Release Society, Inc., **25** pp 912-913, 1998.

6. Theeuwes, F., Yum, S.I., Haak, R., Wong, P., "Systems for Triggered, Pulsed, and Programmed Drug Delivery", *Ann. New York Acad. Sci.*, **618** pp. 435-437, 1991.

7. Smolensky, M.H, and D'Alonzo, G.E., "Investigative Protocols for Chronotherapeutics", *Ann. New York Acad. Sci.*, **618** pp 465 – 479, 1991.

8. Kohno I., *et al.* "Effect of Imidapril in Dipper and Nondipper Hypertensive Patients: Comparison between Morning and Evening Administration", *Chronobiology International* **17**(2) pp. 209-219, 2000.

9. Hrushesky, W.J.M, "Automatic Chronotherapy: An Integral part of the Future of Medicine", www.rpi.edu/~hrushw/AutomaticChronotherapy.html

10. Hanna, L. "A New Approach to Initial Antiretroviral Therapy: Protease-Sparing Combination Regimens", *Bulletin of Experimental Treatment for AIDS*, Oct. 1998.

11. Lantz, R.J., and Schwartz, J.B. Pharmaceutical Dosage Forms: Tablets, Volume 2, ed. H.A. Lieberman, and L. Lachman, Marcel Dekker, pp.1-52, 1991.

12. McGinity, Stavchansky, and Martin. Pharmaceutical Dosage Forms: Tablets, Volume 2, ed. H.A. Lieberman, and L. Lachman, Marcel Dekker, pp.270-271, 1991.

13. Fonner, Anderson, and Banker, Pharmaceutical Dosage Forms:Tablets, Volume 2, ed. H.A. Lieberman, and L. Lachman, Marcel Dekker, pp.252-254, 1991.

14. Spiroflow Systems Inc., "Dust Containment and Static Control in Bulk Bag Handling", *Pharmaceutical Processing Online*, www.pharmpro.com.

15. Yoo, J. *et al.* "Content Uniformity Study of Microdose Tablets Fabricated by the Theriform™ Process", AAPS Annual Meeting, Boston, MA Nov. 2-6, 1997.

16. Rogers, A.R., and Clements, J.A. "The examination of Segregation of Granular Materials in a Tumbling Mixer", *Powder Technology* **5**(72) pp. 167-178, 1971.

17. C.K. Lai, D. Holt, J.C. Leung, G.K. Raju, P. Hansen, and C.L. Cooney "Real Time and Non-Invasive Monitoring of Blend Homogeneity of Dry Pharmaceutical Powders using Laser Induced Fluorescence", *AIChE Journal*, submitted 2000.

18. Massachusetts Institute of Technology : Three Dimensional Printing web site: http://web.mit.edu/afs/athena.mit.edu/org/t/tdp/www/

19. Yoo, J. *et al.* "Transformation-Toughened Ceramic Multilayers with Compositional Gradients", *J. Am. Ceram. Soc.*, **81**(1), pp. 21-32, 1998.

20. Therics Incorporated, Princeton, New Jersey.

21. Katstra, W.E., Palazzolo, R.D., Rowe, C.W., Giritlioglu, B., Teung, P. and Cima, M.J. "Oral Dosage Forms Fabricated by Three Dimensional Printing", *J. Controlled Release*, **66** pp. 1-9, 2000.

22. Grau, J.E. "Fabrication of Engineered Ceramic Components by the Slurry-Based Three Dimensional Printing Process", Ph.D. Thesis, Massachusetts Institute of Technology, June, 1998.

23. DeBear, B. "Slurry Deposition of High Quality Layers for 3D Printing", M.S. Thesis, Massachusetts Institute of Technology, 1999.

24. Teung, P. "Evaluation of Lee Microvalve Jets for Use in Drop on Demand Three Dimensional Printing", M.S. Thesis, Massachusetts Institute of Technology, 2001.

25. Enokido, Y., TDK Corporation, *personal communication*

26. Savart, F. "Memoire sur la constitution des veines liquids lancees par des orifices circulaires en mince paroi", Ann. Chim. Phus. **53** pp. 337-345, 1833.

27. Rayleigh, F. R. S. "On the Stability of Jets", *Proc. London Math. Soc.* **10**(4) pp. 4-13, 1878.

28. Milner, J. "Time of Flight Controller and Stream Position Compensation System for the Three Dimensional Printing Process", M.S. Thesis, Massachusetts Institute of Technology, May, 1990.

29. Goldin, M. *et al.* "Breakup of a Laminar Capillary Jet of a Viscoelastic Fluid", *J. Fluid Mech.* **38**(4) pp.689-711, 1969.

30. Bredt, J. F. "Binder Stability and Powder/Binder Interaction in Three Dimensional Printing", Ph.D. Thesis, Massachusetts Institute of Technology, Jan. 1995.

31. Palazzolo, R. "Formulation of Oral Dosage Forms by Three Dimensional Printing" M.S. Thesis, Massachusetts Institute of Technology, 1999.

32. Fan, T.L. "Droplet-Powder Impact Interaction in Three Dimensional Printing", Ph.D. Thesis, Massachusetts Institute of Technology, 1995.

33. Cima, M.J. 3.63: Ceramics Processing, Massachusetts Institute of Technology, *lecture notes.*

34. Nikolakis, V., et al. "Zeolite Growth by Addition of Submicron Particles", Chem. Mater. **12** pp. 845-53, 2000.

35. Lauder, A.J. "Microstructure and Particle Arrangement in Three Dimensional Printing", M.S. Thesis, Massachusetts Institute of Technology, 1992.

36. Teung, P. *Private communication*

37. Arthur, T. "Factors Limiting the Surface Finish of Three Dimensional Printed Parts", M.S. Thesis, Massachusetts Institute of Technology, 1996.

38. Lenormand, R. "Flow Through Porous Media: Limits of Fractal Patterns" *AIP Conf. Proc.* **154** Physics and Chemistry of Porous Materials II, American Institute of Physics, 1987.

39. Bear, J. Dynamics of Fluid in Porous Media, American Elsevier Pub. Co., 1972

40. Kissa, E. "Capillary Sorption in Fibrous Assemblies", *J. Colloid and Interface Sci.* **83** pp.265-272, 1981.

41. Gillespie, T. "The Spreading of Low Vapor Pressure Liquids in Paper", *J. Colloid and Interface Sci.* **13** pp.32-50, 1958.

42. Borham, A., Rungha K.K., "An Experimental Study of the Radial Penetration of Liquids in Thin Porous Substrates", *J. Colloid and Interface Sci.* **158** pp. 403-411.

43. Marmur, A. "The Radial Capillary", *J. Colloid and Interface Sci.* **124**(1) pp. 301-308, 1988.

44. DeGennes, P.G. "Dynamics of Entangled Polymer Solution – I. The Rouse Model", *Macromolecules* **9** pp. 587-593, 1976.

45. Doi, M., Edwards, S.F., The Theory of Polymer Dynamics, Oxford University Press, 1986.

46. Devotta, I., et al. "The Life of a Dissolving Polymeric Particle", *Chemical Engineering Science* **49**(5) pp.645-54, 1994.

47. LabView™ software by C.W. Rowe, Therics Inc.

48. CRS Handbook of Chemistry and Physics, 74th Addition, CRC Press, NY, 1993.

49. Ingham, D., Pop, I., Transport Phenomena in Porous Media, Elsevier Science Publishers, 1998.

50. Reed, J.S. Introduction to the Principals of Ceramic Processing, Wiley-Interscience Publications, NY 1988, pp. 415-417.

51. Rowe, C.W. *personal communication*

52. Yoo, J., E.R.N Bornancini, D. Monkhouse, D.C, Yang, A., and Shanahan, G., "Content Uniformity Study of Microdose Tablets Fabricated by the TheriForm™ Process", AAPS Annual Meeting, Boston, MA Nov. 2-6, 1997.

53. Mukesh C. Gohel, Maulik K. Panchal, and Viral V. Jogani. "Novel Mathematical Method for Quantitative Expression of Deviation from the Higuchi Model." *AAPS PharmSciTech*; 1(4) No.31, 2000. (http://www.pharmscitech.com/).

54. Rowe, C.W., Katstra, W.E., Palazolo, R.D., Giritlioglu, B., Teung, P., and Cima, M.J. "Multimechanism Oral Dosage Forms Fabricated by Three Dimensional Printing", *J. Controlled Release*, **66** pp. 11-17, 2000.

55. Reynolds, T.D. et. al. "Polymer Erosion of Hydrophilic Matrices", *Proceed. Int'l Symp. Control. Rel. Bioact, Mater.*, **25**(1998), Controlled Release Society, Inc., pp 928-29, 1998.

56. Bettini, R. et.al., "Polymer Relaxation in Swellable Matrices Contributes to Drug Release", *Proceed. Int'l Symp. Control. Rel. Bioact, Mater.*, **25**(1998), Controlled Release Society, Inc., pp 36-37, 1998.

57. Rajabi-Siahboomi, A.R., "Slow Release Hydrophillic Matrix Systems: Investigation of the Interactions between Water and Hydroxypropylmethylcellulose", *Proceed. Int'l Symp. Control. Rel. Bioact, Mater.*, **25**(1998), Controlled Release Society, Inc., pp 52-53, 1998.

58. Reynolds, T.D., et.al. "Investigation of the Effect of Surface Area/Volume on Drug Release from HPMC Controlled Release Tablets", The Dow Chemical Company, Midland, MI, Oct. 2000.

59. Katzhendler, I. et. al., "Modeling of Drug Release from Erodible Tablets", *J. Pharm. Sci.*, **86**(1), 1997.

60. Hopfenberg, H.B. "Controlled Release from Erodible Slabs, Cylinders, and Spheres." American Chemical Society Sympsosium Series, **33**, *eds:* D.R. Paul and F.W. Harris, American Chemical Society, p. 26-32.

61. OROS technology, Alza Corp. www.alza.com

62. Langer, R., "1994 Whitaker Lecture: Polymers for Drug Delivery and Tissue Engineering," *Annals of Biomedical Engineering* **23** pp. 101-111, 1995.

63. Rohm Pharma Polymers, "Protective and Insulating Coatings", Eudgragit product manual, pg. 4.

64. Rohm Pharma Polymers, "Enteric Coatings for pH Control", Eugragit product manual, pg. 4.

65. Rowe, C.W., Therics Inc. *Internal document*

66. Brancazio, D., and Serdy, J. *Personal communication*

THESIS PROCESSING SLIP

FIXED FIELD: ill. _____ name _____

index _____ biblio _____

► **COPIES:** Archives Aero Dewey Barker Hum

Lindgren Music Rotch Science Sche-Plough

TITLE VARIES: ► ☐ _____

_____

_____

NAME VARIES: ► ☐ _____

_____

IMPRINT: **(COPYRIGHT)** _____

_____

► **COLLATION:** _____

_____

► **ADD: DEGREE:** _____ ► **DEPT.:** _____

► **ADD: DEGREE:** _____ ► **DEPT.:** _____

SUPERVISORS: _____

_____

NOTES:

cat'r: date:

page:

► **DEPT:** _____

► **YEAR:** _____ ► **DEGREE:** _____

► **NAME:** _____

_____